DOKUZ EYLUL UNIVERSITY
GRADUATE SCHOOL OF NATURAL AND APPLIED SCIENCES

PRODUCTION AND CORROSION BEHAVIOUR OF MICRO-ARC COATED MAGNESIUM ALLOYS

by
Emrah ÇAKMAK

September, 2009
İZMİR

PRODUCTION AND CORROSION BEHAVIOUR OF MICRO-ARC COATED MAGNESIUM ALLOYS

A Thesis Submitted to the
Graduate School of Natural and Applied Sciences of Dokuz Eylul University
In Partial Fulfillment of the Requirements for the Degree of Master of Science
in Metallurgical and Materials Engineering, Metallurgical and Materials Program

by
Emrah ÇAKMAK

September, 2009
İZMİR

M. Sc. THESIS EXAMINATION RESULT FORM

We have read the thesis entitled **"PRODUCTION AND CORROSION BEHAVIOUR OF MICRO-ARC COATED MAGNESIUM ALLOYS"** completed by **EMRAH ÇAKMAK** under revision of **ASSIST. PROF. DR. UĞUR MALAYOĞLU** and we certitfy that in our opinion it is fully adequate, in scope and in quality, as a thesis for the degree of Master of Science.

Assist. Prof.Dr. Uğur MALAYOĞLU

Supervisor

Prof.Dr. Rasim İPEK

(Jury Member)

Prof.Dr. Ahmet ÇAKIR

(Jury Member)

Prof.Dr. Cahit HELVACI

Director

Graduate School of Natural and Applied Science

ACKNOWLEDGEMENTS

I would like to express my most sincere appreciation to Assist. Prof. Dr. Uğur MALAYOĞLU for his supervision, support and advice in this work. His knowledge and expertise has been of immeasurable assistance throughout my graduate studies. Thanks are also due to him for the provision of office, laboratory and workshop facilities in the department.

My sincere thanks go to Prof. Dr. Ahmet ÇAKIR and Assist. Prof. Dr. Ufuk MALAYOĞLU for technical discussions and providing access to the corrosion testing equipment.

Special thanks also go to my colleagues Mr. Kadir TEKİN, Ms. Esra DOKUMACI, Mr. Osman ÇULHA for their technical assistance and friendship. In addition I should thank other technical and academic staff in the department, without whom I could have achieved very little.

Finally, thanks to my parents, Engin and Nermin ÇAKMAK, my dear sister, Emral ÇAKMAK and my adorable friend Ms. Selcen AKKUŞ, for all their support, encouragement and patient over the last two years.

This innovation was carried out within research project named as, "Improving the corrosion and wear properties of magnesium alloys by micro-arc oxidation method" which numbered 107M495 and I gratefully acknowledge to Scientific & Technological Research Council of Turkey (TUBITAK) for the financial assistance of this project.

Emrah ÇAKMAK

PRODUCTION AND CORROSION BEHAVIOUR OF MICRO-ARC COATED MAGNESIUM ALLOYS

ABSTRACT

The current study is composed of two stages. In the first stage, in order to investigate the effect of alloying elements and treatment time, the thickness of 10 micrometer (K10) and 25 micrometer (K25) ceramic coatings were fabricated on different chemical composition having AZ91D, AZ31B, AM60B and AM50B magnesium alloys in alkaline phosphate based electrolyte by micro-arc oxidation method using with a pulsed bipolar direct current (DC) power supply.

In the second stage, the effect of different sealant post-treatments on corrosion resistance of micro-arc oxidation (MAO) coated AM60B and AM50B magnesium alloys were investigated.

The surface morphology and elemental composition of produced MAO coatings was determined using Scanning Electron Microscope (SEM) equipped with Energy Dispersive X-ray Spectrometer (EDS). The crystallographic phase analysis and identification of MAO coatings was carried out by X-ray diffraction (XRD). High resolution surface profilometer was used for mapping of the 3-Dimensional surface features and roughness. Electrochemical tests conducted using potentiodynamic polarization technique in 3.5 percent NaCl solution at room temperature in order to evaluate the efficiency of sealed and unsealed MAO coatings on the corrosion resistance of magnesium alloys.

The results displayed that enhanced corrosion protectiveness was provided by MAO coatings formed on different magnesium alloys. It is observed that the microstructure and chemical composition of magnesium alloys is crucially effective on the formation, structural and corrosion properties of MAO coatings. Further corrosion protection is achieved by applying alkaline post treatment processes.

Keywords: Corrosion, micro-arc oxidation, magnesium, post-treatment

MİKRO-ARK KAPLI MAGNEZYUM ALAŞIMLARININ ÜRETİMİ VE KOROZYON DAVRANIŞI

ÖZ

Bu çalışma iki aşamadan oluşmaktadır. İlk aşamada alaşım elementi ve işlem süresinin incelenmesi amacıyla fosfat esaslı bazik bir elektrolit banyosu içerisindeki farklı kimyasal kompozisyonlara sahip AZ91D, AZ31B, AM60B ve AM50B magnezyum alaşımları yüzeylerinde darbeli iki kutuplu doğru akım güç kaynağı kullanarak mikro-ark oksitleme metodu (MAO) ile 10 mikrometre (K10) ve 25 mikrometre (K25) kalınlığında seramik kaplamalar üretilmiştir.

İkinci aşamada MAO yöntemiyle kaplanmış magnezyum alaşımlarının korozyon direnci üzerine son işlemin etkisi incelenmiştir

Üretilen MAO kaplamaların yüzey morfolojisi ve elementel kompozisyonu Enerji Dağılımı X-ışını Spektroskopisi (EDS) bağlantılı Taramalı Elektron Mikroskobu (SEM) ile belirlenmiştir. MAO kaplamaların kristalografik faz analizleri ve tanımlamaları X-Işını Difraksiyonu(XRD) ile gerçekleştirilmiştir. Yüzey pürüzlülüğü ve üç boyutlu yüzey haritası ve için yüksek çözünürlüklü yüzey profilometresi kullanılmıştır. MAO kaplamaların magnezyum alaşımlarının korozyon direnci üzerine olan etkinliklerinin belirlenebilmesi için yapılan elektrokimyasal testler, yüzde 3,5 NaCl çözeltisi içinde oda sıcaklığında potansiyodinamik polariazyon tekniği uygulanarak gerçekleştirilmiştir.

Sonuçlar farklı magnezyum alaşımları üzerine kaplanan MAO kaplamaların gelişmiş korozyon koruyuculuğu sağladığını göstermektedir. Magnezyum alaşımlarının mikroyapıları ve kimyasal kompozisyonları MAO kaplamaların oluşumu, yapıları ve korozyon özellikleri üzerine önemli etkide bulunduğu gözlemlenmiştir. Alkali son işlem proseslerinin uygulanmasıyla daha da ileri korozyon koruması başarılmıştır.

Anahtar kelimeler*:* Korozyon, Mikro-ark oksitleme, magnezyum, son-işlem

CONTENTS

Page

M. Sc. THESIS EXAMINATION RESULT FORM ii
ACKNOWLEDGEMENTS iii
ABSTRACT iv
ÖZ v

CHAPTER ONE – INTRODUCTION AND MOTIVATION 1

CHAPTER TWO – MAGNESIUM AND ITS ALLOYS 7

2.1 Introduction 7

2.2 Characteristic Profile of Magnesium 14

2.3 Alloying Systems of Magnesium 18
2.3.1 Alloying Elements 18
2.3.2 Casting Alloys 23
2.3.3 Wrought Alloys 27

2.4 Heat Treatment of Magnesium Alloys 29
2.4.1 Annealing 31
2.4.2 Stress Relieving 31
2.4.3 Solution Treatment and Aging 31

2.5 Applications 32

CHAPTER THREE – CORROSION AND SURFACE PROTECTION OF MAGNESIUM ALLOYS 37

3.1 Introduction. 37

3.2 Corrosion Characteristics of Pure Magnesium 39
3.2.1 Environmental Effects 39
3.2.1.1 General Corrosion in Aqueous Solution 39
3.2.1.2 Corrosion in the Solutions Containing Specific Ions 41
3.2.1.3 Corrosion Caused by Organic Compounds 42
3.2.1.4 Corrosion in the Air 43
3.2.2 Metallurgical Effects 44

3.3 Corrosion Characteristics of Magnesium Alloys 45
3.3.1 Influences of Environment 46
3.3.2 Influences of Metallurgical Factors 46
3.3.2.1 Impurity Elements 46
3.3.2.2 Important Alloying Elements for Corrosion Aspect 50
3.3.2.3 Role of β Phase 52
3.3.2.4 Microstructure 53

3.4 Corrosion Types of Magnesium Alloys 53
3.4.1 Galvanic Corrosion 53
3.4.2 Stress Corrosion Cracking(SCC) 56
3.4.3 Corrosion Fatigue 57
3.4.4 Pitting Corrosion 58
3.4.5 Crevice Corrosion 59
3.4.6 Filiform Corrosion 60

3.5 Corrosion Protection of Magnesium Alloys 60
3.5.1 High Purity(HP) Magnesium Alloys 60
3.5.2 Surface Modification 61
3.5.3 Microstructure Refinement 61
3.5.4 Effect of Heat Treatment.. 62

3.6 Protective Coatings and Films 62
3.6.1 Electrochemical Plating 62
3.6.1.1 Pre-treatment Proceses. 64
3.6.2 Conversion Coatings 65
3.6.3 Anodizing 68
3.6.4 Gas-Phase Depositon Processes 70
3.6.5 Organic/Polymer Coatings 72
3.6.6 Micro-Arc Oxidation (MAO).. 74

CHAPTER FOUR – MICRO-ARC OXIDATION 76

4.1 Background 76

4.2 Development of the MAO Process 77

4.3 MAO Processing 79
4.3.1 Coating Formation 81
4.3.2 Electrochemical Characteristics of MAO Process. 81
4.3.3 Discharge Characteristics 84
4.3.4 Phase Formation During Film Growth 85

4.4 Effect of Process Parameters 87

4.5 Corrosion Protection of MAO Coatings 91

4.6 Applications of MAO 93

4.7 Industrial Processes.. 94
4.7.1 Magoxid-Coat Process. 94
4.7.2 Tagnite Process. 95
4.7.3 Keronite Process. 96

CHAPTER FIVE – EXPERIMENTAL STUDIES.....97

5.1 Purpose.....97

5.2 Materials 98
5.2.1 Substrates.....98
5.2.2 Chemicals 98

5.3 Preprocessing 99
5.3.1 Substrate Preparation.....99
5.3.2 Pre-treatment.....100
5.3.3 Electrolyte Preparation. 100

5.4 Preparation of MAO Coatings 101

5.5 Post-Treatment Processing.....105

5.6 Material Characterization 106
5.6.1 Scanning Electron Microscopy (SEM)/Energy Dispersive Spectroscopy (EDS).....106
5.6.2 Optical Microscopy Analyses. 106
5.6.3. X-Ray Diffractions (XRD) 106
5.6.4 Three-Dimensional (3D) Surface Roughness Analyses.....107

5.7 Electrochemical Corrosion Testing 107

CHAPTER SIX –RESULTS AND DISCUSSION.....112

6.1 Substrate Characterization 112
6.1.1 Microstructure of Mg Alloy Substrates.....112
6.1.2 XRD Analyses of Mg Alloy Substrates. 115

6.2 Characterization of MAO coatings.....116
6.2.1 Surface Morphology and Structure of MAO Coatings 116
6.2.2 Cross-Sectional Structure of MAO Coatings 123

6.2.3 XRD Analyses of MAO Coatings..... 130
6.2.4 Three Dimensional Surface Profile (3D) and Roughness Measurements of MAO Coatings..... 133

6.3 Characterization of Sealed MAO Coatings..... 137
6.3.1 Surface Morphology of Sealed MAO Coatings..... 137
6.3.2 XRD Analyses of Sealed MAO Coatings..... 145
6.3.3 Surface Profile (3D) and Roughness Measurements of Sealed MAO Coatings 147

6.4 Electrochemical Corrosion Behaviour of MAO Coated Mg Alloys 152
6.4.1 Potentiodynamic Polarization Behaviour of MAO Coatings 152
6.4.2 Potentiodynamic Polarization Behaviour of Sealed MAO Coatings 161

CHAPTER SEVEN- CONCLUSION 166

7.1 General Results 166

7.2 Future Plans 168

REFERENCES 170

CHAPTER ONE
INTRODUCTION

Magnesium is the lightest construction metal, which makes it one of the favoured material to minimize vehicle weight in order to reduce exhaust gas emissions and transportation costs. Due to limited fossil fuel stores and environmental problems associated with fuel emission products; there is a push in the automotive industry to make cars lighter in order to decrease fuel consumption. The use of magnesium alloys can significantly decrease the weight of automobiles without sacrificing structural strength (Mordike et al., 2001). Magnesium alloys have high strength to weight ratio with a density that is only 2/3 that of aluminium and 1/4 that of iron. Magnesium also has high thermal conductivity, high dimensional stability, good electromagnetic shielding and damping characteristics, good machinability and is easily recycled. These properties make it valuable in a number of applications including defence, biotechnology, automobile and computer parts aerospace components, mobile phones, sporting goods handheld tools and household equipment (Gray et al., 2002). In addition to that magnesium has been suggested for use as an implant metal due to its low weight and inherent biocompatibility (Staiger et al., 2006).

Unfortunately, magnesium has a number of undesirable properties including poor corrosion and wear resistance, poor creep resistance and high chemical reactivity that have hindered its widespread use in many engineering applications especially in acidic environments and salt-water conditions. Magnesium and its alloys are extremely susceptible to galvanic corrosion because the most other metals have a more noble electrochemical potential. Electrolytic contact with another metal can cause the formation of local corrosion cells on the surface leading to pitting which can cause decreased mechanical stability and an unattractive appearance (Song et al., 2003).

One of the problems with magnesium is its chemical reactivity. As soon as it comes in contact with air or water an oxide /hydroxide layer forms on the surface which can have a detrimental effect on coating adhesion and uniformity. This passive oxide layer on magnesium surface must be removed prior to metal plating. Thus, the precleaning process plays a critical role in the development of a good protective coating on magnesium and its alloys (Gray et al., 2002). Another challenge in the plating of magnesium is that the quality of the metal coating depends on the alloy being plated. Alloys are especially difficult to plate because intermetallic species such as $Mg_{17}Al_{12}$ (β phase) are formed at the grain boundaries, resulting in a non-uniform surface potential across the substrate, and therefore further complicating the plating process.

In order to improve the corrosion resistance of the Mg alloy, many surface modification techniques have been employed in literature, in order to provide corrosion protection of magnesium alloys including electrochemical plating, conversion coatings (chromating, phosphating), anodic oxidation (anodizing), chemical or physical gas-phase deposition process (CVD, PVD), thermal spray (thermal oxidation), laser surface alloying, sol–gel method. Each of the techniques has its own merits and limitations. Most of these methods involve high temperatures during processing (PVD, CVD and thermal spray) or post-treatment (sol-gel) which may degrade the coating and/or substrate. In addition, sol-gel processing has been of limited use due to poor interfacial adhesion, shrinkage and oxidation of the substrate. The conversion coating process and anodizing are the most popular methods. One of the main disadvantages of conversion coatings is the toxicity of the treatment solutions. The conventional conversion coatings are based on chromium compounds that have been shown to be highly toxic carcinogens (Hagans & Haas, 1994). DOW 9, DOW 17, HAE and Cr 22 are well-known anodizing processes that formulated acidic solutions such as phosphoric acid, chromate or chromic acid, and/or hydrofluoric acid. Anodizing usually offers a relatively simple and cost-effective way; however, the coatings are rather thin, porous and cannot satisfied the corrosion resistance reqirements in aggressive service conditions (Blawert et al., 2006).

The acid-based electrolytes for magnesium anodizing are currently being phased out because of environmental concerns. Chromic acid is regulated as a known carcinogen and fluorides are regulated by Occupational Safety and Health Administration (OSHA) (Blawert et al., 2006).

The development of an environmentally friendly process is a necessity due to the more stringent environmental protection laws currently in effect or being proposed.

The term “micro-arc oxidation” (MAO), refers to the same process as historical name plasma electrolytic oxidation (PEO), electrolytic plasma oxidation (EPO), microplasmic oxidation (MPO) anodic spark deposition (ASD), in german Anodishe Oxidation an Funkenanladung (ANOF), plasma anodizing and spark anodizing which is a relatively new, cost-effective promising, unique and environmentally friendly surface engineering method based on plasma assisted anodic oxidation to form a protective, thick, hard, dense and well adhered ceramic coating on valve metals surface such as Mg, Al, Ti, Zr, Ta and Hf whose metal oxides easily form on the surface when contact to air or aqueous environment that exhibit insulating behaviour with increasing potential until a critical breakdown of electrical field strength during MAO process. When, the barrier film is broken and visible sparks occur. If this higher voltage is held, many tiny sparks cover the whole surface of samples, and the spark spots move on the surface rapidly (Markov et al., 1997).

The modern MAO process is based on a conventional anodising process. MAO process differs from conventional anodizing with respect to its high operating voltages which cause dielectric breakdown of a passive film formed on the component surface. When dielectric breakdown takes place due to high electrical field reached in the passive film, micro-discharges appear as lighting dots moving on the surface. Local temperatures in discharge regions can reach up to 10^4 K (Klapkiv, 1995).

Metal atoms ionize in discharge channel via thermal ionization mechanisms to form metal oxides which then erupt into the electrolyte due to high pressure and solidify on the surface (Yerokhin et al., 1999).

The plasma electrolytic oxidation baths generally consists of of low concentration alkaline solutions such as alkali hydroxide, silicate, borate, phosphate, aluminate, tungstate species and all variants of this process are considered to be environmentally friendly. The process results in the formation of a ceramic layer that offers protection to the base alloy in terms of corrosion, wear and offers other functional characteristics including thermo-optical, dielectric, thermal barrier, low friction coefficient and also can be used as pre-treatment for topcoat paints and other metal/ceramics to create composite coatings. The process has demonstrated significant interest in offering improved surface treatment to Mg and Al alloys and as a replacement for conventional acid based processes such as HAE and DOW 17 and other chemical processes that contain hexavalent chrome, and including anodising processes.

Although certain properties of these coatings have been evaluated, both by academic researchers and in industrial trials, such investigations have usually had specific applications in mind, or have been concerned with empirical optimisation of a particular processing parameter. Few structure-property relations have been established, possibly because the coating structure has never been established in detail. The structural investigation allows structure-property relationships to be established, and also helps to elucidate the mechanism of coating formation and corrosion resistance.

Many researchers have tried to explain growth mechanism of MAO process with their developed model conceptions. Various researchers have found that the chemical / phase composition and corrosion behaviour of ceramic coating on magnesium alloys basically depend on the process parameters (discharge characterisation, voltage regime, frequency, current density, duration) and the electrolytes (pH, temperature, conductivity).

In the last decade, micro-arc oxidation has become a well-developed technology, with commercial variants such as those produced by Magoxid, Tagnite and Keronite achieving wide acceptance in industry. Their development, however, has been largely empirical and understanding of the coatings remains at a very early stage. The effect of post-treatment on the corrosion resistance of MAO coatings has been overlooked. In addition to that 3-Dimensional surface topography of coatings has not been characterised yet and more detailed investigations are required for improving corrosion properties.

The objectives of this study are summarized below:

1. Produce protective MAO coatings on AZ31, AZ91, AM50, AM60 magnesium alloys;

2. Characterize the crystallographic, morphological structure and elemental composition of produced MAO coatings;

3. Determine the electrochemical behaviour and corrosion resistance of MAO coatings formed on four magnesium alloys having different chemical composition

4. Analyze of the effect of alloying elements, surface roughness and post treatments on the corrosion resistance of MAO coatings;

This thesis contains seven chapters. Chapter 1 provides introductory information about magnesium and its alloy and surface modification techniques that have been used in literature due to improve their poor corrosion resistance. The advantages and limitations of these techniques also discussed. Moreover, chapter 1 gives a preface to micro-arc oxidation, including an overview, description and development of process. Chapter 2 reviews the general properties of magnesium and its alloys. Chapter 3 demonstrates the corrosion characteristics, and surface protection techniques of

magnesium and its alloys. Chapter 4 gives detailed information about the MAO process such as historical background, principles, equipments, applications and summary of literature. Chapter 5 introduces the experimental techniques used in the present study. These include specimen preparation, microscopy, X-ray diffraction and electrochemical corrosion measurement. The results and interpretations of experimental studies which help to clarify corrosion behaviour of MAO coatings were given in Chapter 6. The surface morphology, roughness and phase composition of coatings were characterized. The pore sealing capability of post treatments and optimization of process parameters were investigated in this chapter. The effect of key alloying elements of magnesium alloys on corrosion behaviour of MAO coating was also determined. Chapter 7 is the final chapter of this study where concludes arrived judgements with respect to logical thinking.

CHAPTER TWO
MAGNESIUM AND ITS ALLOYS

2.1 Introduction

High-technology companies increasingly rely on the technical and economic potential of innovative materials. Additionally, politics and the public are demanding a more economical use of scarce primary energy sources.

One of the key goals for the next decades will be the further reduction of emissions to lower the growing environmental impact. Taking this into consideration, the use of light metals as construction materials is generally viewed as becoming of key importance in the future.

Although magnesium alloys are fulfilling the demands for low specific weight materials with excellent machining abilities and good recycling potential, they are still not used to the same extent as the competing materials aluminium and plastics. One of the reasons is the fairly high priced base material, coupled with the partial absence of recycling possibilities. On the other hand, the variety of magnesium available to the consumer is still limited to a few technical alloys. Unfortunately, there is a lack of know-how in the use of magnesium, not least within the companies dealing with the machining and application of construction materials. As a result, the industry still tends to use “conventional” materials instead of magnesium alloys.

Magnesium is found to be the 6^{th} most abundant element, constituting 2% of the total mass of the Earth’s crust which discovered in 1774 and named after the ancient city Magnesia (Greek). It belongs to the second main group in the periodic table of elements (group of alkaline earth metals) and is therefore not found in elemental form in nature, but only in chemical combinations. The silicates olivine, serpentine, and talc do not play any role in refining magnesium, although they represent the most commonly occurring natural magnesium compounds. More important are the mineral

forms magnesite $MgCO_3$ (28% Mg), dolomite $MgCO_3 \cdot CaCO_3$ (13% Mg), and carnallite $KCl \cdot MgCl_2 \cdot 6H_2O$ (8% Mg), as well as sea water, which contains 0.13% Mg or 1.1 kg Mg per m^3 (3rd most abundant among the dissolved minerals in sea water). Magnesium is recovered by electrolysis of molten anhydrous $MgCl_2$, by thermal reduction of dolomite, or by extraction of magnesium oxide from sea water. The global production of roughly 436,000 t (1997) is covered by melt electrolysis to 75% and by thermal reduction to 25% (Byron, 1997).

Considering the total energy needed to produce magnesium from its various raw materials, it consumes a relative large amount of energy compared to other metals as long as the calculation is based on the mass. Referring it to the volume of the gained primary material magnesium shows a contrary effect: in this case, magnesium uses much less energy than e.g. aluminium or zinc and even competes with polymers. In addition, it is assumed that the present electrical energy of 40–80 MJ/kg (25 MJ/kg would be possible in theory) need for electrolysis can be reduced to 40 MJ/kg or less by all the big producers in the near future. This would mean that the corresponding values for producing aluminium (electrolysis of Al_2O_3 to yield aluminium consumes 47 MJ/kg) could be undercut. Optimization or improvement of existing production methods and the establishment of a secondary recirculation could open new perspectives for reducing the cost of primary magnesium production (Cahn et al., 1996).

The inherent advantages of magnesium include a unique blend of low density, high specific strength, stiffness, electrical conductivity, heat dissipation and absorption of vibration. When combined with easy machining, casting, forming and recycling, magnesium is seen as a very attractive material for a large volume of applications. In recent years the interest in magnesium has grown dramatically, which has spurred academic research and industrial trials to identify more efficient ways of manufacturing the primary metal, as well as a search for new alloys and extending areas of their application.

The magnesium industry in its early stages was turbulent, driven by military applications and wars. A periodically volatile market was also recorded through later history but over the last quarter of the twentieth century a tremendous growth was achieved. The historical development milestones of magnesium are given in Table 2.1.

Table 2.1 The key milestones of magnesium discovery and early development (Czerwinski, 2007)

Year	Name	Country	Milestone
1754	Joseph Black	England	Discovery of magnesia during decomposition of calcium and magnesium carbonates
1808	Humphrey Davy	England	Establishing that magnesia represents the oxide of new metal magnesium
1828	Antoine-Alexander Bussy	France	Isolation of magnesium metal by fusion of anhydrous magnesium chloride with metallic potassium
1833	J. von Liebling & Michael Faraday	England	Production of magnesium metal by electrolytic reduction of the chloride
1852	Robert Bunsen	Germany	Production of magnesium metal from anhydrous magnesium chloride
1853	St. Claire Deville & Caron	France	Production of magnesium from anhydrous magnesium chloride by reduction with potassium in a heated closed container
1860	Johnson Matthey & Co	England	Commercial production based on Deville-Caron process
1886	IG Farbenidustry	Germany	Commercial production of magnesium by electrolysis of molten carnallite (Bunsen's cell)
1896	Chemische Fabrik Griesheim Elektron & Aluminium und Magnesium Fabrik	Germany	Full scale commercial production based on Bunsen's cell

In 1852, Robert Bunsen produced anhydrous magnesium employing ammonium chloride and improved electrolysis to permanently separate magnesium from chlorine. In the late 1920's, K. Pistor and W. Moschel produced magnesium by a reduction of magnesium anhydrous chloride obtained by carbo-chlorination of magnesite:

$$MgO + C + Cl_2 = MgCl_2 + CO_2 \quad (2.1)$$

$$2MgO + C + 2Cl_2 = 2MgCl_2 + CO_2 \quad (2.2)$$

The above technology, then owned by I.G. Farbenindustry, along with its subsequent modifications, affect the worldwide manufacturing of magnesium until today.

The remarkable emergence of China as the world's largest source of magnesium continues to have a significant impact on the industry. The share of global supply from China grew from 5% in 1994 to over 65% in 2004. In 2005 the production grew by 8%, as compared to 2004, reaching 468,000 tonnes. While adding this potential to Western suppliers, along with the secondary metal production, the world's present capacity exceeds 900,000 tonnes, predicted as the consumption level by 2010. The major manufacturing centers of the primary metal in 2004 are listed in Table 2.2. As compared to the year 2000, a number of western companies abandoned the market, including North West Alloys, the USA (43,000 tonnes); Pechiney, France (18,000 tonnes); and Norsk Hydro, Norway (43,000 tonnes) (Czerwinski, 2007). The structure of world consumption of magnesium is given in Figure 2.1

Table 2.2 The major manufacturing centers of the primary magnesium metal

Country	Manufacturer	Capacity in tonnes per year as of 2004	Process type	Feed/Process features
Brazil	Rima	11,000	Thermal	Based on own reserves of dolomite which is reduced in a sillico-thermal processing under vacuum
Canada	Timminco Metals, Haley Station, Ontario	7,000	Thermal	Pidgeon process, calcined dolomite is reduced by ferrosilicon in a vacuum retort
Canada	Norsk Hydro, Becancour, Quebec	48,000	Electrolytic	Based on imported magnesite which is transformed to magnesium chloride then dehydrated and subjected to electrolysis
China	Shanxi Province, approx 70 plants Ningxia Province, approx 15 plants Henan Province, approx 50 plants	600,000+	Thermal	Pidgeon process with pilot-scale vertical retorts
Israel	Dead Sea Magnesium	33,000	Electrolytic	Electrolytic decomposition of carnallite hexahydrate
Kazakhstan	Ust-Kamenogorsk, Titanium Magnesium Works	14,000	Electrolytic	Process based on natural carnallite and magnesium chloride with top anode entry cell
Russia	Solikamsk Magnesium Works,	23,000	Electrolytic	Based on natural carnallite from Verhokamsk
Russia	Avisma, Berezniki Titanium Magnesium Works	30,000	Electrolytic	Bottom anode entry cell
USA	US Magnesium, Great Salt Lake, Utah	43,000	Electrolytic	Carbo chlorination and electrolytic decomposition in open or closed cells

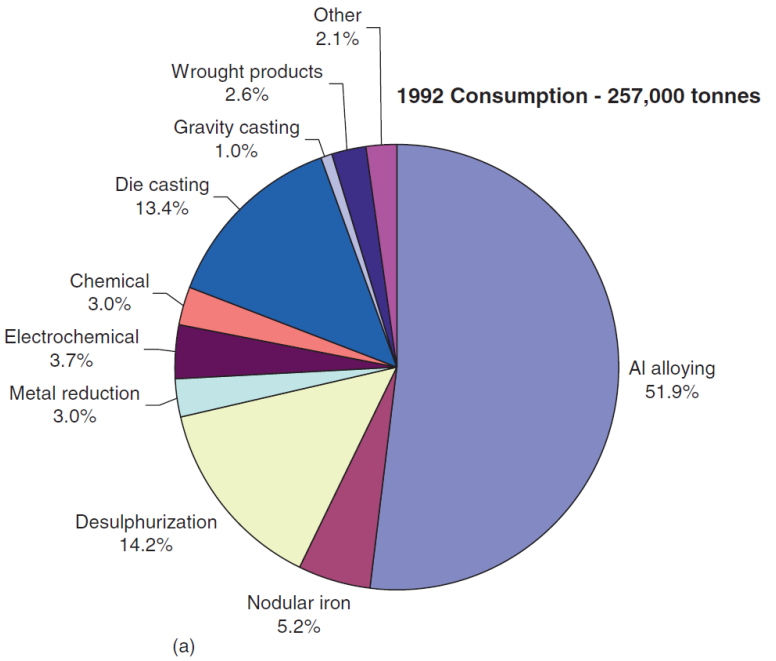
1992 Consumption - 257,000 tonnes
Other
2.1%
Wrought products
2.6%
Gravity casting
1.0%
Die casting
13.4%
Chemical
3.0%
Electrochemical
3.7%
Metal reduction
3.0%
Desulphurization
14.2%
Nodular iron
5.2%
Al alloying
51.9%

(a)

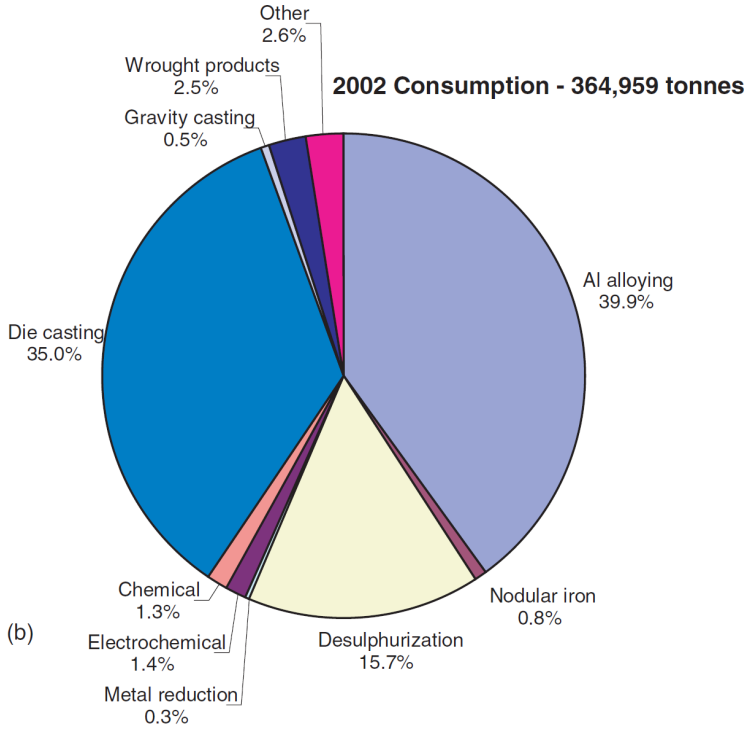
2002 Consumption - 364,959 tonnes
Other
2.6%
Wrought products
2.5%
Gravity casting
0.5%
Die casting
35.0%
Chemical
1.3%
Electrochemical
1.4%
Metal reduction
0.3%
Desulphurization
15.7%
Nodular iron
0.8%
Al alloying
39.9%

(b)

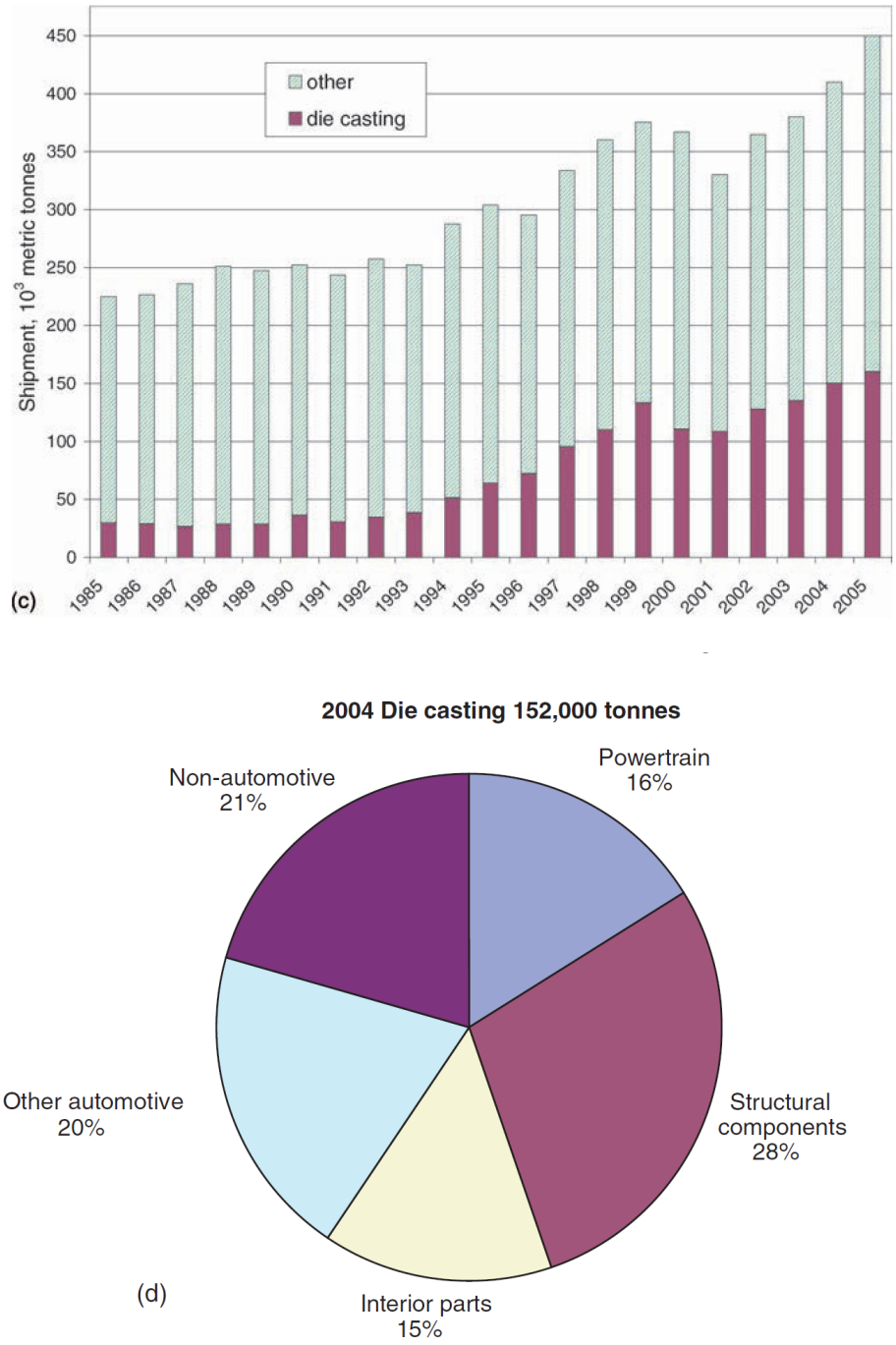

Figure 2.1 The structure of world consumption of magnesium: (**a**) 1992; (**b**) 2002; (**c**) growth of die casting segment over last two decades; (**d**) Structure of die casting segment in 2004(Czerwinski, 2007)

2.2 Characteristic Profile Of Magnesium

Magnesium crystallizes in the hexagonal closest packed structure and is therefore not amenable to cold forming. Below 225 °C, only {0001} <1120> basal plane slipping is possible, along with pyramidal {1012} <1011> twinning. Pure magnesium and conventionally cast alloys show a tendency for brittleness due to intercrystalline failure and local transcrystalline fracture at twin zones or {0001} basal planes with big grains. Above 225 °C, new {1011} basal planes are formed and magnesium suddenly shows good deformation behaviour, suggesting that extensive deformation only occurs above this temperature (Staroselsky et al, 2003). Table 2.3 shows the most important properties of pure magnesium.

Most magnesium alloys show very good machinability and processability, and even the most complicated die-cast parts can be easily produced. Cast, moulded, and forged parts made of magnesium alloys are also inert gas weldable and machinable. Another aspect is the good damping behaviour, which makes the use of these alloys even more attractive for increasing the life cycle of machines and equipment or for the reduction of sonic emission. Pure magnesium shows even higher damping properties than cast-iron, although these properties are highly dependent on the prior heat treatment (Kainer, 2003).

Along with the excellent properties, there are some disadvantages to the application of these alloys. As already mentioned, the cold working abilities are very poor and the corrosion resistance of magnesium alloys is very low. Besides, magnesium is very reactive. When cast, magnesium has a high mould shrinkage of approximately 4% when solidifying and of about 5% during cooling. This high degree of shrinkage leads to microporosity, low toughness, and high notch sensitivity that cannot be ignored. This behaviour, as well as the high thermal expansion coefficient (10% above the corresponding value for aluminium), is often put forward as an argument against the use of magnesium alloys.

Table 2.3 Properties of Pure Magnesium (Avedesian & Baker, 1999)

Property class	Specific property	Values	Unit	Remarks
Crystallography	Crystal structure	Hexagonal close-packed		20 °C
		a = 0.32092	nm	
		c = 0.52105	nm	
	Atomic volume	13.97	cm^3/mol	
	Burger's vector	0.321	nm	
Mass	Density-Solid phase	1.738	g/cm^3	20 °C
		1.650	g/cm^3	650 °C
	Volume change on solidification	4.2 volumetric, 1.5 linear	%	
	Volume change on cooling	5 volumetric, 1.7 linear	%	Cooling from 650 °C to 20 °C.
Mechanical	Young's modulus	45	GPa	
	Shear modulus	17.2	GPa	
	Ultimate tensile strength	80-180	MPa	
	Fracture elongation	1-12	%	
	Hardness	30-47	HB	
	Poisson's ratio	0.35		
	Viscosity	1.23	mPa s	650 °C
		1.13	mPa s	700 °C
	Surface tension	0.56	N/m	650 °C
	Solid-liquid interfacial free energy γ_{SL}	0.115	J/m^2	650 °C
Electrical	Resistivity	45.3	nΩ m	a axis
		37.8	nΩ m	c axis
Thermal	Melting point	650 ± 1	°C	
	Boiling point	1090	°C	
	Thermal expansion	26.1	µm°C	20-100 °C
		29.9		20-500 °C
	Thermal conductivity (solid phase)	156	W/m K	27 °C
		149		327 °C
		130		650 °C
	Thermal conductivity (liquid phase)	78	W/m K	650 °C
	Latent heat of fusion per mol	8.954	kJ/mol	
	Latent heat of fusion per unit volume	5.90	J/m^3	
	Heat of vaporization	127.4	kJ/mol	
	Specific heat capacity	1.025	kJ/kg K	20 °C
	Lattice diffusion $D_L = D_{oL}\exp\left(-\frac{Q_L}{RT}\right)$	$D_{oL}=1.0\times10^{-4}$ $Q_L=135$	m^2/s kJ/mol	

The negative properties mentioned above deter construction engineers from accepting magnesium alloys as a competitive replacement for aluminium or steel. Therefore, attempts have been made to improve the characteristic profile of magnesium alloys by employing different alloying elements so as to achieve better precipitation and solid-solution hardening. In this way, all the advantageous properties listed below have been realized:

- lowest density of all construction metals at 1.8 g/cm^3
- high specific strength (strength/density ratio)
- excellent casting ability,
- good machining ability (milling, turning, sawing)
- improved corrosion resistance with high-purity (HP) alloys
- high damping properties
- good weldability under inert

The static and dynamic mechanical properties are inferior to the corresponding values for the competing aluminium, e.g. the Young's modulus. Nevertheless, magnesium is found in all places where weight saving takes priority over the other properties, mainly because the specific strength can reach and even exceed the values for aluminium and steel. Densities and specific strengths of different materials are compared in Figure 2.2.

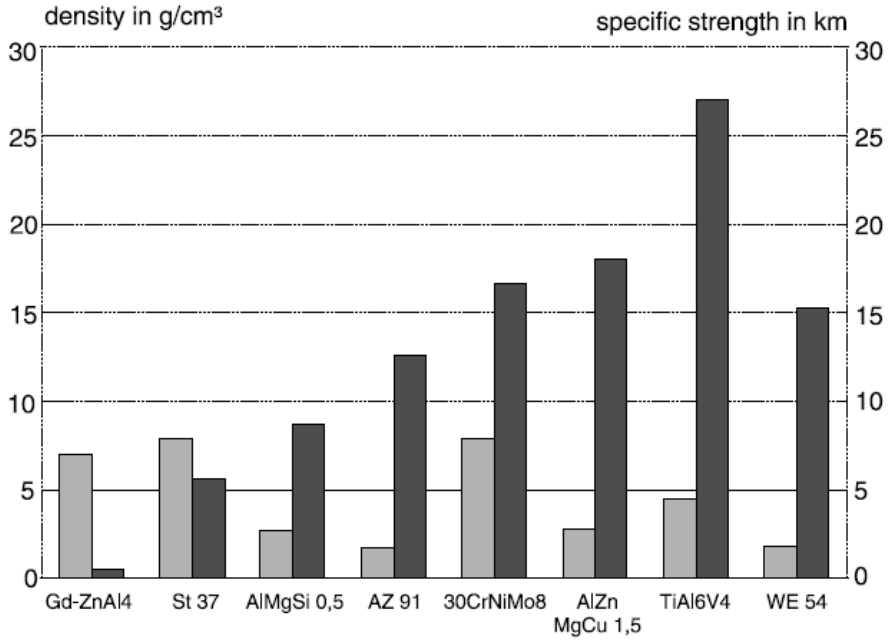

Figure 2.2 Densities and specific strengths of selected materials (Kainer, 2003)

The strength to weight ratio and Young's modulus for two magnesium alloys and several other materials are compared in Figure 2.3.

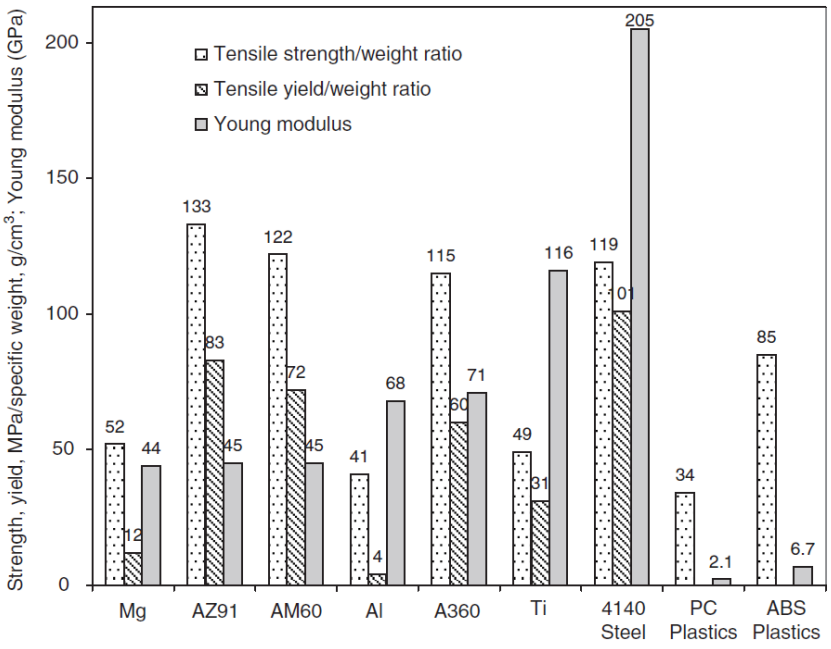

Figure 2.3 A comparison of the strength to weight ratio and Young's modulus for two magnesium alloys and several other materials (Czerwinski, 2007)

2.3 Alloying Systems of Magnesium

The identification of magnesium alloys is standardized worldwide in the ASTM norm; each alloy is marked with letters indicating the main alloy elements, followed by the rounded figures of each (usually two) weight in percentage terms. Table 2.4 shows the key letters for every available alloying element. The last letter in each identification number indicates the stage of development of the alloy (A, B, C,...). In most cases, these letters show the degree of purity. The alloy AZ91D, for example, is an alloy with a rated content of 9% aluminium (A) and 1% zinc (Z). Its development stage is 4 (D). The corresponding DIN specification would be MgAl9Zn1. ASTM dictates the following composition (all values weight-%): Al 8.3–9.7; Zn 0.35–1.0; Si max. 0.10; Mn max. 0.15; Cu max. 0.30; Fe max. 0.005; Ni max. 0.002; others max. 0.02. Iron, nickel, and copper have tremendous negative effects on the corrosion resistance and hence these values are strictly limited.

Table 2.4 ASTM codes for magnesium's alloying elements (Avedesian & Baker, 1999)

Abbreviation letter	Alloying element	Abbreviation letter	Alloying element
A	aluminium	N	nickel
B	bismuth	P	lead
C	copper	Q	silver
D	cadmium	R	chromium
E	rare earths	S	silicon
F	iron	T	tin
H	thorium	W	yttrium
K	zirconium	Y	antimony
L	lithium	Z	zinc
M	manganese		

2.3.1 Alloying Elements

Since the advent of magnesium alloys, there has been a lot of effort to influence the properties of pure magnesium with different alloying elements. The main mechanism for improving the mechanical properties is precipitation hardening and/or solid-solution hardening. While solid-solution hardening is determined by the

differences in the atomic radii of the elements involved, the effectiveness of precipitation hardening mainly depends on a reduced solubility at low temperatures, the magnesium content of the intermetallic phase, and its stability at application temperature. Magnesium forms intermetallic phases with most alloying elements, the stability of the phase increasing with the electronegativity of the other element.

By the 1920s, aluminium had already become the most important alloying element for significantly increasing the tensile strength, specifically by forming the intermetallic phase $Mg_{17}Al_{12}$. Figure 2.4 exhibits that the influence of Al content on mechanical properties of Mg–Al alloys. Similar effects can be achieved with zinc and manganese, while the addition of silver leads to improved high-temperature strength. The Mg–Al, Mg-Zn and Mg-Mn equilibrium phase diagrams are given Figure 2.5, Figure 2.6 and Figure 2.7 respectively. High percentages of silicon reduce the castability and lead to brittleness, whereas the inclusion of zirconium forms oxides due to its affinity for oxygen, which are active as structure-forming nuclei. Because of this, the physical properties are enhanced by fine grain hardening. The use of rare earth elements (e.g. Y, Nd, Ce) has become more and more popular since they impart a significant increase in strength through precipitation hardening. Copper, nickel, and iron are very rarely used. All these elements increase susceptibility to corrosion, as established by the precipitation of cathodic compounds when they solidify. In contrast to regular cases, where a magnesium oxide or -hydride layer protects the metal and lowers corrosion rate, these elements increase the corrosion rate. This is one of the reasons why alloy development has been directed towards “high-purity” (HP) alloys with very little use of iron, nickel, or copper. The properties of HP alloys and the detrimental effect of heavy metals on corrosion behaviour of magnesium and its alloys will be discussed in next chapter.

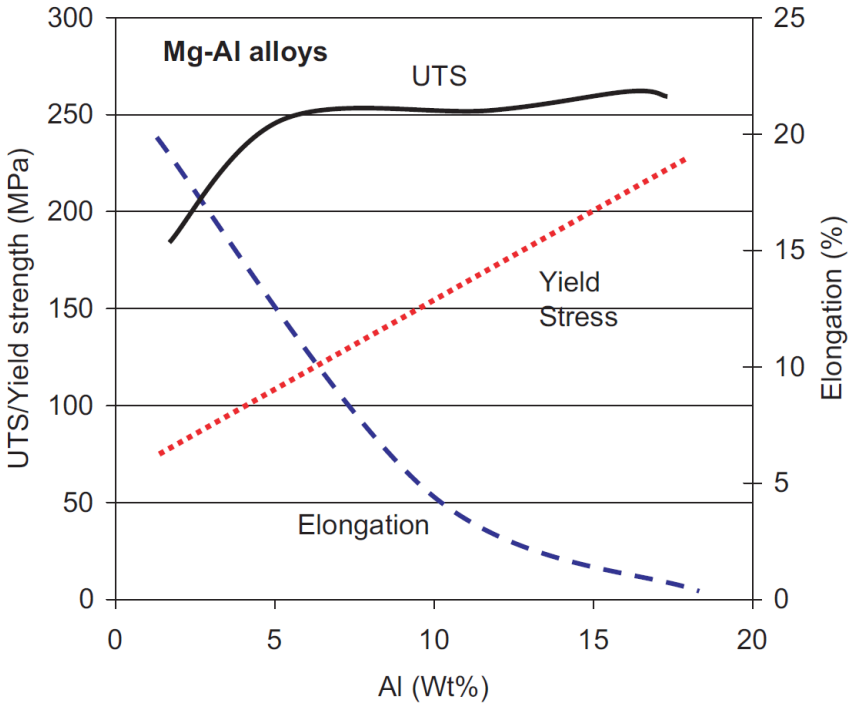

Figure 2.4 The influence of Al content on mechanical properties of Mg–Al alloys (Westengen et al, 2005

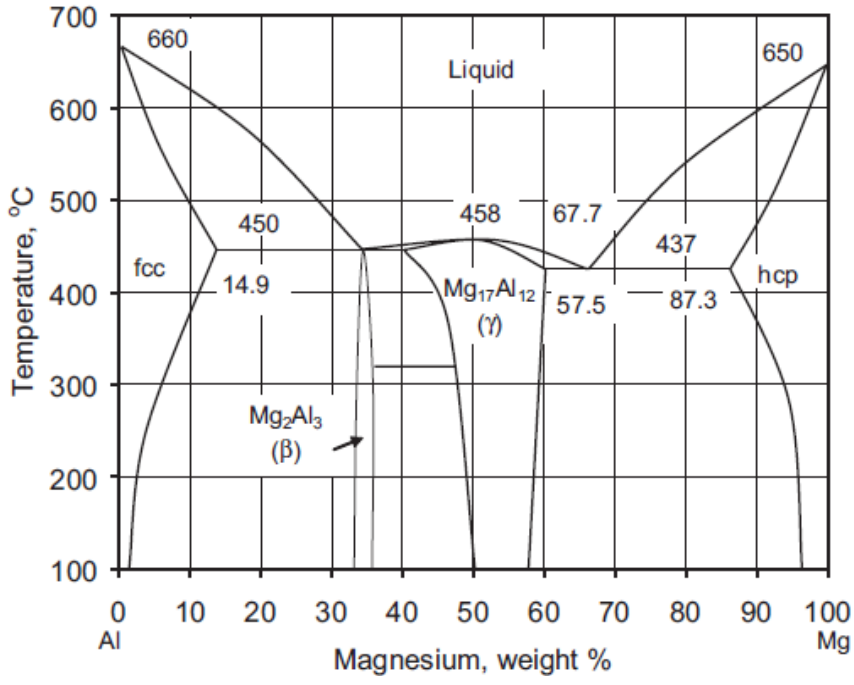

Figure 2.5 The Mg–Al equilibrium phase diagram (Nayeb-Hashemi & Clark, 1988)

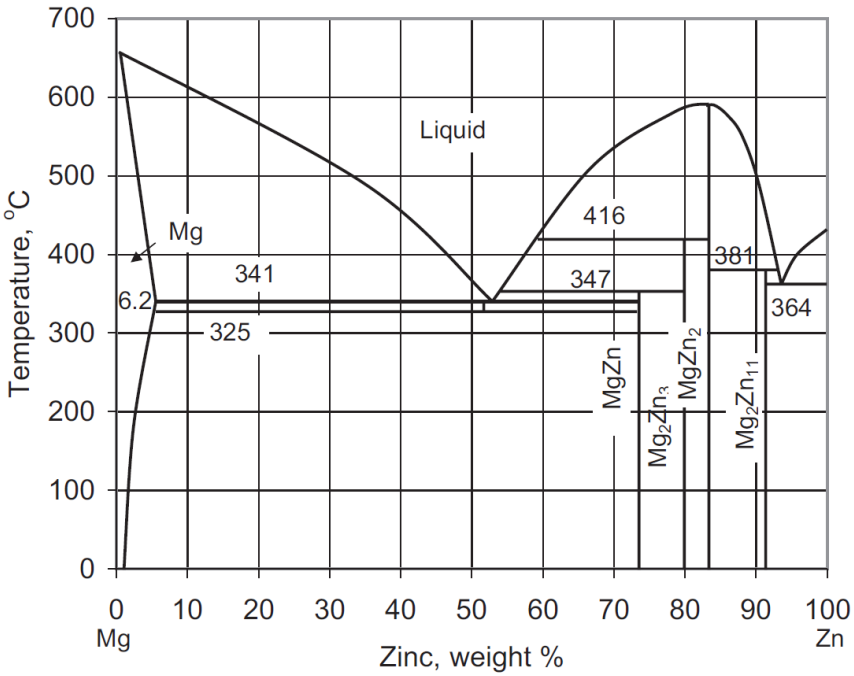

Figure 2.6 The Mg–Zn equilibrium phase diagram (Nayeb-Hashemi & Clark, 1988)

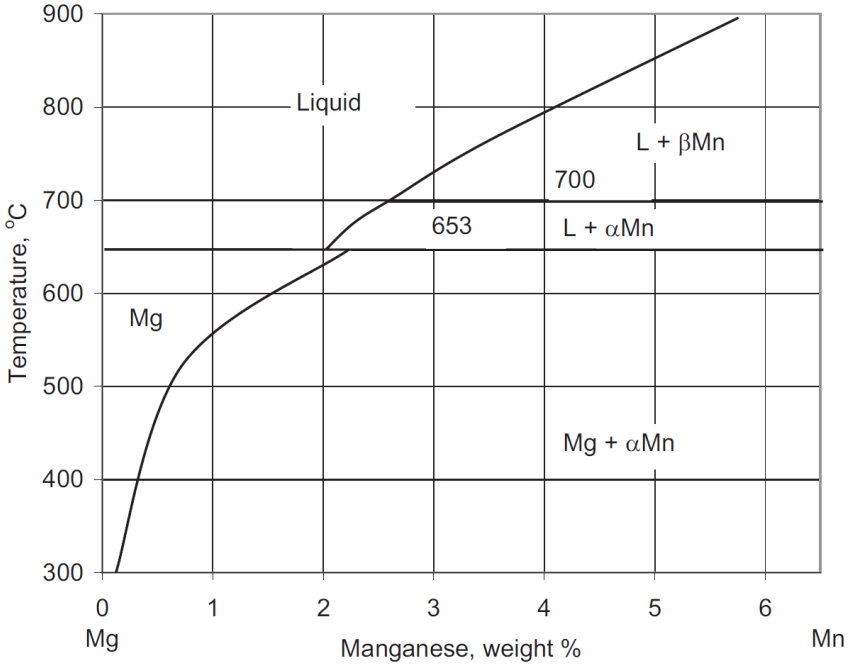

Figure 2.7 The Mg–Mn equilibrium phase diagram (Nayeb-Hashemi & Clark, 1988)

The solubility of intermetallic phases in binary magnesium alloys are shown in Table 2.5.

Table 2.5 Solubility data and intermetallic phases in binary magnesium alloys (Polmear, 1995)

Solute element	Maximum solubility (wt%)	(at%)	Adjacent intermetallic phase	Melting point of intermetallic phase (°C)	Type of equilibrium
Lithium	5.5	17.0	–	–	Eutectic
Aluminium	12.7	11.8	$Mg_{17}Al_{12}$	402	Eutectic
Silver	15.0	3.8	Mg_3Ag	492	Eutectic
Yttrium	12.5	3.75	$Mg_{24}Y_5$	620	Eutectic
Zinc	6.2	2.4	MgZn	347	Eutectic
Neodymium	≈ 3	≈ 1	$Mg_{41}Nd_5$	560	Eutectic
Zirconium	3.8	1.0	Zr	1855	Peritectic
Manganese	2.2	1.0	Mn	1245	Peritectic
Thorium	4.75	0.52	$Mg_{23}Th_6$	772	Eutectic
Cerium	0.5	0.1	$Mg_{12}Ge$	611	Eutectic
Indium	53.2	19.4	Mg_3In	484	Peritectic
Thallium	60.5	15.4	Mg_5Tl_2	413	Eutectic
Scandium	≈ 24.5	≈ 15	MgSc	–	Peritectic
Lead	41.9	7.75	Mg_2Pb	538	Eutectic
Thulium	31.8	6.3	$Mg_{24}Tm_6$	645	Eutectic
Terbium	24.0	4.6	$Mg_{24}Tb_5$	–	Eutectic
Tin	14.5	3.35	Mg_2Sn	770	Eutectic
Gallium	8.4	3.1	Mg_5Ga_2	456	Eutectic
Bismuth	8.9	1.1	Mg_3Bi_2	821	Eutectic
Calcium	1.35	0.82	Mg_2Ca	714	Eutectic
Samarium	≈ 6.4	≈ 1.0	$Mg_{6.2}Sm$	–	Eutectic

General properties of alloying elements on magnesium alloys were summerized in Table 2.6.

Table 2.6 General effects of alloying elements in magnesium materials (Cahn et al, 1996)

Al	The improvement of the physical properties with aluminium was already established in the 1920s. These alloys containing Al were sold as "Elektron". Aluminium increases the tensile strength and the hardness, although the hardness effect caused by the precipitated phase $Mg_{17}Al_{12}$ is only observed up to 120 °C. These alloys are usually heat treated (T6), except under die-cast conditions, which hardly allow for heat treatment. Besides these improvements of the mechanical properties, there is the big advantage of better castability (eutectic system, T_E = 437 °C). This is the main reason why most technical alloys – especially casting alloys (mainly AZ91) – contain a high percentage of aluminium. The disadvantage is a higher tendency for microporosity.
Be	Beryllium is only supplied to the melt in small amounts (<30 ppm); the melt oxidation can be reduced dramatically.
Ca	Calcium has a positive effect on grain refining and aids creep resistance. On the other hand, calcium can lead to sticking to the tool during casting and to hot cracking [9].
Li	Lithium leads to solid-solution hardening at ambient temperatures, reduces density, and increases ductility. However, it has strong negative effects on the burning and vapour behaviour of the melt. Corrosion behaviour gets worse. Above 30% Li-content, the lattice structure changes to fcc.
Mn	Above 1.5 weight-% manganese, the tensile strength is increased. Alloying with manganese results in better corrosion resistance (Fe content is controlled by lowering the solubility), grain refinement, and weldability.
RE	All rare earth elements (including yttrium) form eutectic systems of limited solubility with magnesium. Therefore, precipitation hardening is possible and makes sense. The precipitates are very stable and raise the creep resistance, corrosion resistance, and high-temperature strength. Technical alloying elements are yttrium, neodymium, and cerium. Due to the high costs, these elements are mainly used in high-tech alloys.
Si	Silicon lowers the castability, but the creep resistance can be raised by stable silazide formation.
Ag	Silver, together with the rare earth metals, strongly increases the high-temperature strength and creep resistance, but also leads to low corrosion resistance.
Th	Thorium is the most effective element for increasing high-temperature strength and creep resistance of magnesium alloys. Unfortunately, however, it is radioactive and is therefore substituted by other elements.
Zn	Zinc induces the same behaviour as Al in terms of castability and strengthening. By adding up to 3% zinc, shrinkage can be compensated and tensile strength is raised. As with aluminium, there is a tendency towards microporosity, and on adding more than 2% hot cracking can also occur.
Zr	Addition of zirconium leads to an increase in tensile strength without a loss of ductility, because of its affinity for oxygen. The formed oxides are structure-forming nuclei and aid grain refining. Zirconium cannot be added to melts containing aluminium or silicon.

2.3.2 Casting Alloys

The first group consists of eleven major systems with over twenty commercial chemistries. Three systems containing thorium are obsolete due to its hazardous radiation features. The major challenges include development of alloys well suited to the permanent mold process using a steel mold since even alloys designed for sand casting create problems. Moreover, non-reactive mold coatings are required to

reduce a corrosive attack of molten magnesium alloy. According to recent experiments, low-pressure permanent mold casting can accelerate structural magnesium market growth since it allows casting magnesium components not feasible by other manufacturing techniques. While applying AM50 alloy to the front cradle of an automobile, high mechanical properties were achieved due to controlled solidification and tranquil mold fill (Weiss & Robison, 2005). The technique can incorporate internal cores allowing the casting of complex shapes. A gravity filling permanent mold casting exhibited an influence of the grain refinement on castability of alloys AZ91 and AM50 (Loughanne, 2005).

The commercial die casting alloys consist of five major systems with over fifteen individual chemistries. The three traditional systems of AZ, AM and AS were extended by AE and A–Sr groups. Two first systems of AZ and AM represent over 60% and 35% consumption, respectively, with the AS, AE and A–Sr together having around 5% of the market. The application of HK group (Mg–Th–Zn–Zr), with stable properties up to 350 °C, has to be stopped due to the radioactivity of Th. Table 2.7 gives a short overview of available alloying systems for pressure die-casting.

Table 2.7 Overview of all available casting alloys (Kainer, 2003)

The most important die-casting alloy groups:
AZ alloys
- good room temperature properties
- low heat resistance and creep resistance
- limited ductility

AM alloys
- lower Al content and elimination of zinc improves ductility
- limited room temperature properties and castability

AS alloys
- significantly higher heat and creep resistance through Mg-RE precipitations
- only casting is possible
- limited castability

Consumption of the European automobile industry:

2004	AZ: 61%	AM: 32%	AS/AE: 7%
1999	AZ: 67%	AM: 29%	AS/AE: 4%

Thin wall applications, representing the majority of present injection molding, require alloys with high fluidity. The die casting alloy AZ91D is the present workhorse, representing the predominant volume of consumption by the thin-wall market. Since the alloy was designed a long time ago for general purposes, its application for thinner and lighter components, combined with a high quality surface finish, may not be optimal, causing surface defects and reducing the yield of production. There is a quest, therefore, for alloys that better suit this specific niche market. At present, the three major groups of alloys are promoted worldwide:

(i) Mg–Al–Zn alloys with increased content of Al;

(ii) Mg–Al–Zn–Sn alloys with increased contents of Al and Zn;

(iii) Mg–Zn–Al alloys with increased content of Zn.

Aluminium is, as already described above, the most frequently used alloying element for magnesium, with contents varying between 3 and 9 weight-percent. These alloys have good mechanical properties and excellent corrosion resistance. The more aluminium the melt contains (eutectic system, $T_{Eutetic}$ = 437 °C; Al content ~33%), the better the castability. The most widely used of magnesium die-casting alloys is AZ91 because of its superb castability even for the most complex and thin-walled parts.

As mentioned above, the negative effect of a high aluminium content is the formation of the interdentritic grain boundary phase $Mg_{17}Al_{12}$. It lowers the strength within the finegrained crystal structure and leads to limited ductility of the alloy, as is also found for zinc components. Nominal compositions of well-known cast magnesium alloys according to ASTM standarts were given in Table 2.8.

Table 2.8 Nominal composition of selected cast Mg alloys (Avedesian & Baker, 1999)

ASTM designation	Nominal composition (wt%) Al	Zn	Mn	Si	Cu	Zr	RE (MM)	RE (Nd)	Th	Y	Ag
AZ63	6	3	0.3								
AZ81	8	0.5	0.3								
AZ91	9.5	0.5	0.3								
AM50	5		0.3								
AM20	2		0.5								
AS41	4		0.3	1							
AS21	2		0.4	1							
ZK51		4.5				0.7					
ZK61		6				0.7					
ZE41		4.2				0.7	1.3				
ZC63		6	0.5		3						
EZ33		2.7				0.7	3.2				
HK31						0.7			3.2		
HZ32		2.2				0.7			3.2		
QE22						0.7		2.5			2.5
QH21						0.7		1	1		2.5
WE54						0.5		3.25		5.1	
WE43						0.5		3.25		4	

To improve the deformation behaviour of magnesium alloys, the Al content is decreased, the alloying with zinc is completely abandoned, and manganese is added instead. These alloys of the magnesium–aluminium–manganese family, e.g. AM20, AM50, AM60 (Mn contents between 0.2 and 0.4%) show lower strength at ambient temperature, but they are less brittle than the Al/Zn-based alloys. AMx alloys exhibit better deformation behaviour, but the low aluminium content limits their castability.

One of the most important criteria for magnesium alloys is the high-temperature and creep behaviour. For this reason, in earlier years attempts were made to reduce the aluminium content in the melt and to use different materials for alloying. During production of the VW-Beetle, the addition of silicon had already been established (Schumann & Friedrich, 2006). The resulting alloys, AS21 and AS41, were found to possess much greater high-temperature strength and creep resistance than AZ91. The mechanism whereby high-temperature and creep behaviour is improved is based on a reduction of the aluminium content and the formation of the intermetallic phase Mg_2Si (T_m = 1085 °C), which shows good stability even at high temperatures. In this context, the AE alloys have to be taken into consideration, although they cannot be produced by die-casting because very stable Al-RE precipitates are formed on slow cooling. An overview of the tensile strength as a function of temperature for the most frequently used alloying systems is given in Figure 2:8.

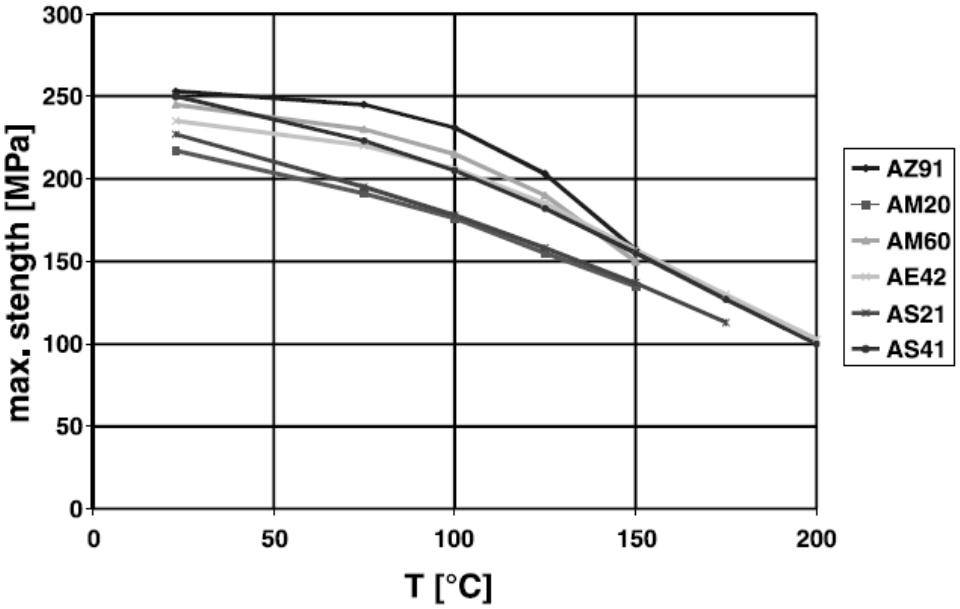

Figure 2.8 Tensile strengths of the most important Mg die-casting alloys as a function of temperature (Norks Hydro Databank, 1996)

Applications at temperatures beyond 200 °C demand properties that can only be served by alloys containing silver and/or rare earths. Specifically, this means the QE alloy group, which exhibit remarkable high-temperature properties, and the high-tech alloys WE-x, which allow applications up to 300 °C. The disadvantage of both series of alloys is their low castability; the production method is limited to sand and gravity casting. Additionally, the high costs have to be considered as a reason for many not to use them (e.g. 13 €/kg for QE22, 25 €/kg for WE54; compared to 2–3 €/kg for an AZ or AM alloy). For this reason, these alloys are mainly used in special applications such as in the aircraft and spacecraft industries. The falling prices for rare earths in the international markets may lead to a change in this trend in the future.

2.3.3 Wrought alloys

Wrought alloys account for 10-15% of all magnesium alloys. The poor cold workability of the hexagonal lattice structure and the formation of twins have resulted in a very limited usage of magnesium as a wrought material. Therefore, the range of available wrought alloys is still limited. The hot forming processes include

rolling, extrusion and forging and are conducted at temperatures higher than 300 °C–350 °C but below 500 °C. The following cold work forming is limited to prevent cracking. There are seven commercial systems with approximately fifteen individual chemistries. Two systems containing thorium are obsolete. Typical extrusion grades include AZ80, ZK21, ZK60, ZC71, ZM21, ZM61 and AZ21X1. Grades such as AZ31, ZE10, M1A, ZM21, HM21, HK31 or ZK31 are used for rolling. For forging, AZ80, ZK60, AZ61 and HM21 are mainly used. Due to higher cost of wrought alloys compared to die cast grades the use of the former is limited. Tables 2.9 and Table 2.10 give an overview of the compositions and properties of selected alloys respectively. The Mg/Al series of alloys (AZ31, AZ61 and AZ80) plays the most important role, being used on a scale comparable to that of the casting alloys.

Table 2.9 Summary of available magnesium wrought alloys (Cahn et al, 1996)

alloy	Al	Ca	Zn	Mn	Cu	Zr	Y	Nd	Th
AZ21X1	1,6-2,5	0,1-0,25	0,8-1,6	0,15 max.	0,05				
AZ31	3,0		1,0	0,3					
AZ31B	2,5-3,5	0,04 max.	0,7-1,3	0,20-1,0	0,05				
AZ61A	5,8-7,2		0,40-1,5	0,15-0,5	0,05				
AZ80	8,5		0,5	0,12					
AZCOML	2,0-3,6	0,04 max.	0,3-1,5	0,15 min	0,10				
AZM	6,0		1,0	0,3					
ZC71			6,5	0,7	1,2				
ZK40			3,5-4,5			0,45 min			
ZK60A			4,8-6,2			0,45 min			
ZM21			2,0	1,0					
ZW3			3,0			0,6			
HM21				0,8					2,0
HM31						0,7			2,0
WE43						0,5	4,0	4,0	
WE54						0,5	5,25	3,5	

Table 2.10 Mechanical properties of various magnesium wrought alloys (Cahn et al, 1996)

Alloy/condition	Tensile Strength [MPa]	0,2%-Yield Strength [MPa]	Fracture Elongation [%]	0,2%-Compression Strength [MPa]
Solid Profile				
AZ31B-F	262	193	14	103
AZ61A-F	317	228	17	131
AZ80-T5	379	276	7	241
HM31A-T5	303	269	10	172
ZK60A-T5	365	303	11	248
Tubes/Hollow Profiles				
AZ31B-F	248	165	16	83
AZ61A-F	283	165	14	110
ZK60A-T5	345	276	11	200
Sheets/Bands				
AZ31B-H24	290	221	15	179
AZ31B-0	255	152	21	110
HK31A-H24	262	207	9	159
HK31A-0	228	200	23	97
HM21A-T8	248	193	11	145

Alloys such as ZC71, ZW3, and ZM21 are available, but are not used to any great extent. Wrought alloys are hot-worked by rolling, extrusion and forging at temperatures above 350 °C. Additional cold-working procedures can be applied afterwards with low deformation rates to prevent the formation of cracks (Cahn et al, 1996). Since magnesium is envisaged for use in parts with high safety concerns, there has been a noticeable increase in interest in wrought alloys.

2.4 Heat Treatment of Magnesium Alloys

The purpose of heat treatment of magnesium alloys is to improve mechanical properties of a final product or modify properties required at a certain stage of processing. The major temper designations and heat treatments applied to magnesium alloy are given in Table 2.11 and Table 2.12 respectively. The most frequently implemented heat treatments are described below.

Table 2.11 Temper designations of magnesium alloys

General divisions	
F	As fabricated
O	Annealed recrystallised (wrought products only)
H	Strain hardened
T	Thermally treated to produce stable tempers. Other than F, O or H
W	Solution heat treated (unstable temper)
Subdivisions of H	
H1, plus one or more digits	Strain hardened only
H2, plus one or more digits	Strain hardened and then partially annealed
H3 , plus one or more digits	Strain hardened and then stabilised
Subdivisions of T	
T1	Cooled and naturally aged
T2	Annealed (cast products only
T3	Solution heat treated and then cold worked
T4	Solution heat treated
T5	Cooled and artificially aged
T6	Solution heat treated and artificially aged
T7	Solution heated and stabilised
T8	Solution heat treated, cold worked, and artificially aged
T9	Solution heat treated , artificially aged and cold worked
T10	Cooled, artificially aged, and cold worked

Table 2.12 Heat treatments applied to magnesium alloys

Alloy	Heat Treatment			
Cast Alloy	**F**	**T4**	**T5**	**T6**
AM100A		×	×	×
AZ63A		×	×	×
AZ81A		×		
AZ91C		×		×
AZ92A		×		×
EZ33A			×	
EQ21A				×
QE22A				×
WE43A				×
WE54A				×
ZC63A				×
ZE41A			×	
ZE63A				×
ZK51A			×	
ZK61A		×		×
Wrought Alloys				
AZ80A			×	
ZC71A	×		×	×
ZK60A			×	

2.4.1 Annealing

Annealing is applied to restore the alloy's structure after cold deformation. Thus it is conducted on wrought alloys. The temperature required depends on the alloy grade and values may range from 290 °C to 450 °C. After holding at temperature for a period depending on the component size, slow cooling follows.

2.4.2 Stress Relieving

As opposed to annealing, which is used mainly with wrought alloys, stress relieving applies to both cast and wrought alloys. For wrought alloys the purpose is to remove stress generated during forming, straightening or welding. For castings, this heat treatment is performed to remove stress from casting to provide dimensional stability during machining or to avoid stress corrosion cracking during further service. The temperature–time parameters depend on the alloy chemistry and its state. The typical values are between 150 °C and 340 °C and a time period from several minutes to several hours.

2.4.3 Solution Treatment and Aging

This is a treatment which leads to precipitation hardening and consists of two stages:
(i) solution annealing, when alloy is heated to temperatures above the solvus line;
(ii) aging, when the solution annealed alloy is re-heated to cause precipitation of certain compounds.

The temperature-time parameters depend on the alloy chemistry and values for several typical alloys are listed in Table 2.13. The time and temperature are interdependent, and better effect is frequently achieved by lowering temperature and increasing time. The effect of strengthening due to precipitation hardening depends on the alloy chemistry. While for Mg–9Al alloy it is approximately 20%, for rare earth metals it is higher, and for Mg–5%Zn it is around 70%. The age hardening

response of Mg–Al based alloys is, however, poor compared with age hardenable Al alloys.

Table 2.13 The recommended parameters of solution treating and aging for magnesium castings and wrought products (Avedesian & Baker, 1999)

		Solution treatment			Aging	
Alloy	Temper	Temp., °C	Time, h	Max temp. °C	Temp., °C	Time, h
AZ91	T4	413	16–24	418		
	T5				168	16
	T6	413	16–24	418	168	16
AZ63	T4	385	10–14	391		
	T5				260	4
	T6	385	10–14	391	218	5
AM100	T4	424	16–24	432		
	T5				232	5
	T6	424	16–24	432	232	5
WE43	T6	525	4–8	535	250	16
ZE63	T6	480	10–72	491	141	48
ZK61	T5				149	48
	T6	499	2	502	129	48
ZK60	T5				150	24
AZ80	T5				177	16–24

2.5 Applications

In the past, the driving force behind the development of magnesium alloys was the potential for lightweight construction in military applications. Nowadays, the emphasis has shifted towards saving weight in automobile applications in order to meet the demands for more economic use of fuel and lower emissions in a time of growing environmental impact. It is interesting to note that the use of magnesium in cars is by no means a recent innovation. As early as the 1930s, it was common to include magnesium cast parts in automobiles, with the VW-Beetle as the most famous example. Since the start of its production in 1939, more and more parts, such as the crank case, camshaft sprocket, gearbox housing, several covers, and the arm of an electric generator, were added until the total magnesium weight reached 17 kg in 1962, which meant a reduction of 50 kg in total mass compared to steel. The production of the VW-Beetle used almost 21,000 t of magnesium alloys in 1960 and

the Volkswagen Group reached a total consumption of 42,000 t of magnesium alloys in 1972, until the change from air-cooled to watercooled engines dramatically reduced the use of magnesium alloys (Schumann & Friedrich, 2006).

Other manufacturers used magnesium in their technical applications, as well as in complex parts such as tractor hoods made of die-castings (dimensions: 1250 mm × 725 mm × 480 mm; weight 7.6 kg), main gear boxes for helicopters (casting weight 400 kg, machined 200 kg), crank cases for zeppelin engines, air intake cases for propjet engines (weight 42 kg), frames, rims, instrument panels, fan blades for cooling towers (weight 169 kg), etc. Figure 2.9 depicts the production of light weight materials in the 20th century.

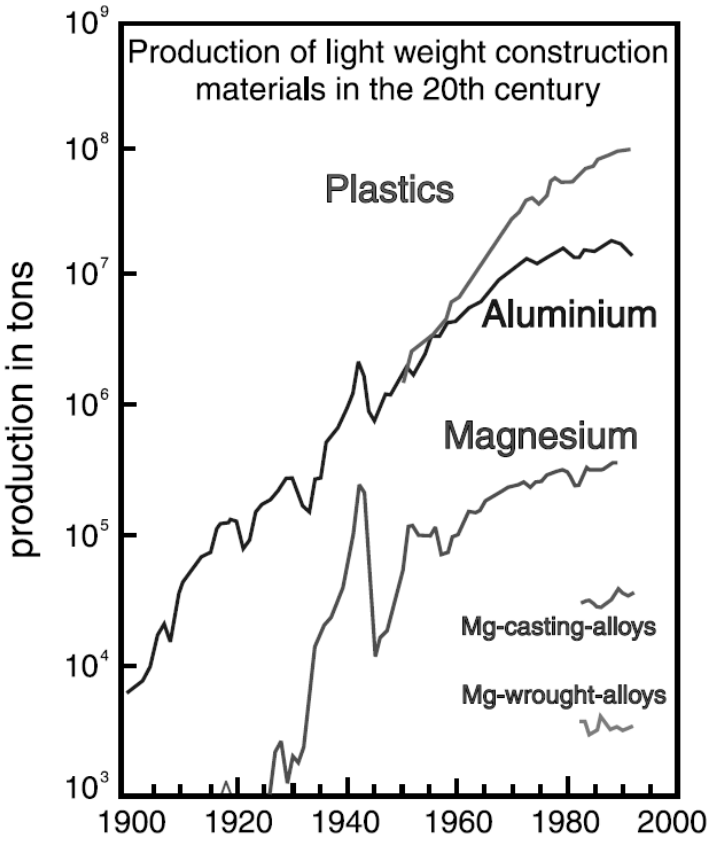

Figure 2.9 Production of materials with low density in the 20th century (Mordike & Ebert, 2001)

Why the trend of utilizing magnesium alloys did not continue in a straightforward manner is hard to explain today. A main factor was certainly the limited capacity of the few magnesium producers, as a result of which a low and constant price on the world market was not attained.

A further factor favouring magnesium use is that it counts as a substitute for polymers for which no satisfactory recycling solution has yet been found.

Besides the specific properties of magnesium mentioned above, further favourable factors are its low casting temperature (650–680 °C, depending on the alloy) and the relatively low energy needed for melting. The energy needed for AZ91 (2 kJ/cm^3) is about 77% of that required to melt the aluminium alloy AlSi12CuFe. The high price of magnesium usually refers to its mass not its volume, and the lower density coupled with other factors can actually make it cheaper in real terms. Thus, the low thermal content allows the casting process to be 50% faster than with aluminium; a high clock cycle of parts is possible, maintaining high precision and good surface quality.

On freezing, the crystal structure is very fine grained, which results in good mechanical properties at room temperature but also leads to poor creep resistance. Moreover, the microstructure can be porous due to turbulences at high mould-filling speeds; subsequent heat treatments are useless since the pores would break apart. Magnesium does not attack iron moulds as much as aluminium does; the moulds can have steeper walls and the potential savings in terms of tools can be as much as 50% compared with the use of aluminium (Luo et al, 1995).

The automotive industry is by far the major user of magnesium alloys on a large scale, due to the possibility of mass-producing series parts by pressure die-casting with high quality at reasonable costs. Examples of magnesium parts in vehicles include:

- gearbox housing, e.g. in the VW Passat, Audi A4
- the inner tailgate in the Lupo (“3-liter car”), which is made of AM50 (3.2 kg)

- tank cover in the Mercedes-Benz SLK
- cylinder head caps, e.g. made of AZ91HP by cold-chamber casting, and having a weight of 1.4 kg
- dashboard, e.g. in the Audi A8 and in the Buick Park Avenue/Le Sabre
- seat-frames
- steering wheels, e.g. in the Toyota Lexus, Celica, Carina, and Corolla
- rims, e.g. in the Porsche Carrera RS (9.8 kg AM70 HP; low-pressure ingot casting) (Kainer & Von Buch, 2003)

The use of magnesium in the gearbox housing in the VW Passat is also primarily based on the weight savings achieved on replacing aluminium alloys. The use of the AZ91 alloy instead of aluminium led to a total weight reduction of almost 25%, and the geometry and production equipment remained identical (Davis, 1991).

Magnesium's low density, its shielding against electromagnetic radiation, and the possibility of producing thin-walled parts has led to further use of die-cast parts in the computer industry, in mobile phones, and in hand tools (e.g. chainsaws) (Anon 1984). Lightweighting and downsizing are challenges for mobile electronic /communications equipment. Firstly, for the same fuel and energy savings during shipping, whether land-based or aerospace-based. Secondly, light and small laptop computers, cameras, cell phones and hand-held devices are desirable for many other reasons: human ergonomics (low mass/thinner walls, down to 0.4 mm), EMI/EMF shielding (both from inside and outside fields), vibration and noise reduction, thermal management to reduce internal heat loads on electronic components, rigid and impact resistance, low inertia for moving components such as actuator arms, and metallic look and feel compared to polymers. Electronic/communication systems that currently use magnesium are laptop computers, cellular phones, digital cameras, digital projectors, TVs, hand-held devices and electronic enclosures.

To reduce fatigue and increase safety for workers, the hand tool industry has incorporated many lightweight parts into their assembled devices. Examples are chain saws, drills, handsaws, impact nailers and garden tools.

The sport equipment industry is characterized by high interest in new materials for speed and performance. Net shape lightweight parts are now used in bicycles, fishing reels, sunglass frames, archery bows, and snow boards (Ito et al., 2000)

Military uses for magnesium are extensive and include radar equipment, portable ground equipment, helicopter transmission, rotor housing and in torpedos.

Aerspace industry has been wary of lightweight cast alloys because of concerns with porosity and corrosion.Yet savings by lightweighting could be as high as US $300 per pound of weight saved for commercial aircraft or US $30,000 for spacecraft. A power boost of 30% can be gained by a mass reduction of 40%. Thus the incentives are high to upgrade structure/processing/properties (Cole, 2006).Table 2.14 compares to value of a pound in weight saved in aerospace industry.

Table 2.14 Value of a pound in weight saved in various industrial segments (Cole, 2006)

Aerospace segment	Value of a pound in weight saved (US $)
Commercial/transport	300
Fighter	3,000
Space	30,000

CHAPTER THREE
CORROSION AND SURFACE PROTECTION OF MAGNESIUM ALLOYS

3.1 Introduction

Magnesium and its alloys are the lightest, but also the most basic construction material. Table 3.1 lists the corresponding data in this respect. The standard electrode potential of magnesium is -2.37 V, but in 3% sodium chloride the electrode potential is -1.63 V (vs. SCE) (Maker & Kruger, 1993).

Table 3.1 Light alloys (symbol, crystalline structure, density, reaction and standard reduction potential) (Kurze, 2006)

Light alloy	Symbol crystalline structure	Density [g/cm^2]	Reaction	Standard reduction potential E° [V] taken from [1]
Magnesium	Mg (2)	1.7	$Mg^{2+} + 2\ e \Leftrightarrow Mg$	−2.37
Beryllium	Be (2)	1.85	$Be^{2+} + 2\ e \Leftrightarrow Be$	−1.85
Aluminium	Al (1)	2.7	$Al^{3+} + 3\ e \Leftrightarrow Al$	−1.66
Titanium	Ti (2)	4.5	$Ti^{2+} + 2\ e \Leftrightarrow Ti$	−1.63

(1) cubic, (2) hexagonal.

The use of magnesium-based materials delivers, on one hand, the important advantages of reduced mass, while offering improved mechanical and physical properties. However, the characteristics of magnesium-based materials also make them highly susceptible to corrosion. Indeed, the existence of unfavourable ambient conditions (such as those caused by the spreading of salt on the roads during the cold months of the year), and the effect of airborne pollutants such as SO_2, mean that the use of magnesium-based materials continues to be regarded with a great degree of scepticism.

In the past 20 years, numerous effort have been made toward improving the corrosion properties of magnesium and magnesium alloys to make them more suitable material for use in engineering design. However, room temperature

corrosion in various environments, including the atmospheric one, is still a major disadvantage of magnesium, which leads to eliminate a number of its engineering applications. The elimination of bad design, flux, inclusions, surface contamination, galvanic couples and inadequate or incorrectly applied surface protection can significantly decrease the corrosion rate its of magnesium alloys in service

The poor corrosion resistance of magnesium is associated with two issues:
(i) low protective behaviour of the quasi-passive hydroxide film;
(ii) susceptibility to galvanic corrosion due to very low electronegative potential.

At room temperature, magnesium in air develops a thin gray oxide film (<1μm) on its surface. When combined with moisture, this film converts to magnesium hydroxide (Brucite; $Mg(OH)_2$) and hydrated oxidic component of the alloying elements which is unstable in neutral or acidic ranges. In neutral or low pH environments, magnesium dissolves as Mg^+ and Mg^{2+} and the evolution of hydrogen accompanies this reaction. As a result the $Mg(OH)_2$ layer does not provide lasting protection. The protective properties are further diminished by certain ions, like: chloride, chlorate, bromide or sulphate, which break down the protective film.

From an engineering perspective, the corrosion resistance of magnesium alloys is of primary concern rather that the behaviour of pure magnesium. Therefore, factors that describe the alloy chemistry and microstructure are of importance: alloying elements, impurities, phase composition, grain size or crystallographic texture.

One of the most effective ways to prevent corrosion is to coat the base material. Coatings can protect a substrate by in providing a barrier between the metal and its environment and/or through the presence of corrosion inhibiting chemicals in them. In order for a coating to provide adequate corrosion protection, the coating must be uniform, well adhered, pore free and self-healing for applications where physical damage to the coating may occur. One of the problems with magnesium is its chemical reactivity. Formed oxide / hydroxide layer as mentioned above forms on the surface which can have a detrimental effect on coating adhesion and uniformity.

There are a number of possible coating technologies available for magnesium and its alloys, each with their own advantages and disadvantages.

3.2 Corrosion Characteristics of Pure Magnesium

Magnesium, like most metals and alloys, relies on a natural surface film to control its corrosion. Good passive films are those that restrict the outward flow of cations, resist the inward flow of damaging anions or oxidants, and rapidly repair themselves in the event of localized breakdown. The structure and composition of the surface films, which depends strongly on environmental and metallurgical factors, such as electrolyte species and impurities in the metal, determine the protective ability of a passive film.

3.2.1 Environmental Effects

No material shows high corrosion resistance in all kinds of environments. The high corrosion resistance of materials always refers to some specific environments. Magnesium has its own preferred service environments. However, there are fewer media that are suitable for the magnesium and magnesium alloys compared with other materials, such as steels and aluminum alloys. For example, magnesium and magnesium alloys are usually stable in basic solutions, but in neutral and acidic media they dissolve at high rates (Fernando, 1989). This is quite different from aluminum alloys that are normally stable in neutral media but are unstable in both basic and acidic solutions.

3.2.1.1 General corrosion in aqueous solutions

With few exceptions, there is no appreciable corrosion of pure magnesium near room temperature unless water is present (Lindstom et al., 2004). Magnesium dissolution in water or aqueous environments generally proceeds by an electrochemical reaction with water to produce magnesium hydroxide and hydrogen gas. Such a mechanism is relatively insensitive to the oxygen concentration, although

the presence of oxygen is an important factor in atmospheric corrosion (Makar & Kruger, 1993). Reaction 3.1 describes the probable overall reaction:

$$Mg + 2H_2O = Mg(OH)_2 + H_2 \quad (3.1)$$

This net reaction can be expressed as the sum of the following partial reactions:

Anodic reaction: $Mg \rightarrow Mg^{2+} + 2e^-$ (3.2)

Cathodic reaction: $2H_2O + 2e^- \rightarrow H_2 + 2OH^-$ (3.3)

Products formation: $Mg^{2+} + 2OH^- \rightarrow Mg(OH)_2$ (3.4)

The reduction process of hydrogen ions and the hydrogen overvoltage of the cathode play an important role in the corrosion of Mg. Low overvoltage cathodes facilitate hydrogen evolution, causing a substantial corrosion rate (Tomashow, 1966).

Figure 3.1 shows the corrosion domains of Mg in the Mg-H_2O system. The region of water stability lies between the dashed lines. As shown in Figure 3.1, the lines separate the regions of corrosion (dissolved cations, e.g. Mg^{2+}), immunity (unreacted metal, Mg), and passivation (corrosion products, $Mg(OH)_2$) (Makar & Kruger, 1993). From Figure 3.1, it can be seen that stable films would be expected to form depending on the values of the potential and pH. In neutral and alkaline environments, the magnesium hydroxide product can form a surface film that offers considerable corrosion protection to the pure magnesium or its common alloys, although this is not as effective as the oxide layer formed on aluminum. As corrosion proceeds, the metal surface experiences a local pH increase because of the formation of $Mg(OH)_2$, whose equilibrium pH is about 11. The protection supplied by this film is therefore highly dependent on the condition of exposure. High purity magnesium is reported to have a corrosion rate of 10^{-2} - 10^{-3} mils per year (mpy) when exposed to 2 normal KOH solutions at 25 °C (Fernando, 1989).

Magnesium's corrosion performance in pure water is strongly dependent on temperature. At elevated temperatures, the resistance to corrosion in water decreases with increasing temperature.

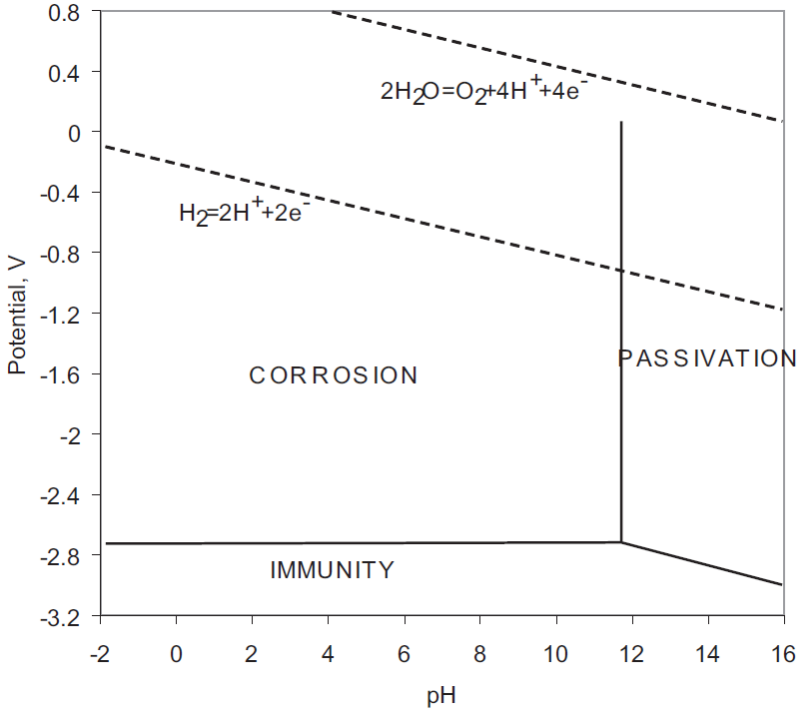

Figure 3.1 Potential-pH diagram (Pourbaix) for magnesium–water system at 25 °C showing ranges of immunity, passivation and corrosion

Magnesium is subject to dissolution by most acids. Even in dilute solutions of strong and moderately weak acids, magnesium dissolves rapidly. There are a few exceptions, such as chromic acid and hydrofluoric acid .Very slow dissolution of magnesium in chromic acid is due to its becoming passive in this acid. An insoluble surface film of MgF_2 is formed which protects against further attack, is the reason why magnesium is resistant to hydrofluoric acid (Tomashov, 1966)

3.2.1.2 Corrosion in the solutions containing specific ions

Salt solutions vary in their corrosivity to magnesium: alkali metal or alkaline-earth metal (chromates, fluorides, phosphates, silicates, vanadates, or nitrates) cause

little or no corrosion (Song et al., 2004). Chromates, fluorides, phosphates, and silicates in particular are frequently used in the chemical treatment and anodize for magnesium surfaces due to their ability to form somewhat protective films (Song et al, 1997). Chlorides, bromides, iodides and sulfates normally accelerate the corrosion of magnesium in aqueous solutions. Practically all heavy metal salts are likely to cause corrosion since magnesium normally displaces heavy metals from solution due to its high chemical activity, except iron phosphate solution.

Oxidizing anions, especially chromâtes, dichromates, and phosphates, which form protective films, can strongly increase the corrosion resistance of magnesium in water or aqueous salt solutions (Tomashov, 1966).

3.2.1.3 Corrosion caused by organic compounds

Baboian et al. (1995) revealed that organic compounds, with a few exceptions, have little effect on magnesium and its alloys. Avedesian & Baker (1999) stated that magnesium is usable in contact with aromatic and aliphatic hydrocarbons, ketones, esters, ethers, glycols, phenols, amines, aldehydes, oils, and higher alcohols. Ethanol causes slight attack, but anhydrous methanol causes severe attack unless significant water content is introduced. Most dry chlorinated hydrocarbons cause little attack on magnesium up to their boiling points. In the presence of water, particularly at high temperatures, chlorinated hydrocarbons may hydrolyze to form hydrochloric acid, causing corrosive attack of the magnesium. Dry fluorinated hydrocarbons, for example, refrigerants, do not attack magnesium at room temperature. When water is present, however, hydrolysis may cause corrosive attack. In acidic food stuffs, such as fruit juices and carbonated beverages, attack of magnesium is slow but measurable. Milk causes attack, particularly when souring.

Some companies are developing new inhibitors for magnesium and magnesium alloys. Song & StJohn (2004) found that the corrosion rate of magnesium in aqueous ethylene glycol depends on the concentration of the solution. A dilute ethylene glycol solution is more corrosive than a concentrated solution at room temperature. An

ethylene glycol solution contaminated by individual contaminants NaCl, $NaHCO_3$ and Na_2SO_4 is more corrosive to pure magnesium. NaCl is the most detrimental contaminate, while in a NaCl contaminated ethylene glycol solution, a small amount of $NaHCO_3$ or Na_2SO_4 has some inhibition effect. Fluorides in ethylene glycol can effectively reduce the corrosion of magnesium due to the formation of a protective fluoride-containing film on the magnesium surface.

3.2.1.4 Corrosion in the air

Humidity plays a major role in the corrosion of magnesium. Corrosion of magnesium increases with relative humidity. At 10% humidity, pure magnesium does not show evidence of surface corrosion after 18 months. However, at 30% humidity, a small amount of visible surface oxide haze and slight corrosion is evident, while at 80% humidity, an amorphous phase is clearly present over about 30% of the surface and the surface exhibits considerable corrosion. Crystalline magnesium hydroxide is formed only when relative humidity is at or above 93%. (McIntyre & Chen, 1998)

Furthermore, the presence of 300 ppm CO_2 and normally 1 ppm of SO_2 in the atmosphere also plays an important role in a formation of the surface films. Lindstom et al (2004) reported that an inhibitive effect of CO_2 in humid air in the atmosphere. Initially, the ambient levels of carbon dioxide enhance the corrosion attack, however, the rate of corrosion in the presence of CO_2 decreases with increased exposure time. The hydroxide ions, generated in the cathodic reaction or dissolved from the film, can form carbonate with carbonic acid. Magnesium hydroxyl carbonate may also form by reaction of solid magnesium hydroxide with CO_2 and water. The presence of the carbonate film, which is thicker than the magnesium hydroxide film, interferes with both the anodic and the cathodic reaction and thus reduces the corrosion rate.

In urban/industrial locations $MgSO_4$-$6H_2O$ and $MgSO_3$-$6H_2O$ can predominate in the surface films. $MgSO_4$-$6H_2O$ and $MgSO_3$-$6H_2O$ are highly soluble and are easily

washed away, re-exposing the surface. Hence, pure magnesium has a poor corrosion resistance in industrial atmospheres (Avedesian & Baker, 1999)

3.2.2 Metallurgical Effects

Magnesium becomes susceptible to accelerated corrosion if there are significant impurity levels present or it is in contact with other metals. Due to the lack of a nature surface film on the impurities, the more positive potential allows impurities to be efficient cathodes for hydrogen discharge, thereby providing significant microgalvanic acceleration of the corrosion rate (Song & Atrens, 1999). Therefore even small amount of impurities in pure magnesium with metals having low hydrogen overvoltages, such as Fe, Ni, Co, or Cu, drastically reduces its corrosion resistance. Metals with higher hydrogen overvoltages, such as lead, zinc, and cadmium, and also strongly electronegative metals, such as manganese and aluminum, are less dangerous in this respect. Figure 3.2 shows effect of impurity and alloying elements on the corrosion of magnesium in a 3% NaCl solution at room temperature. Fe, Cu, Ni can increase the corrosion rate, while Cd, Pb, Sn, and Al can drastically reduce the corrosion resistance of pure magnesium. The effect of various elements on the corrosion of magnesium alloys will be discussed in detail in section 3.3.2.

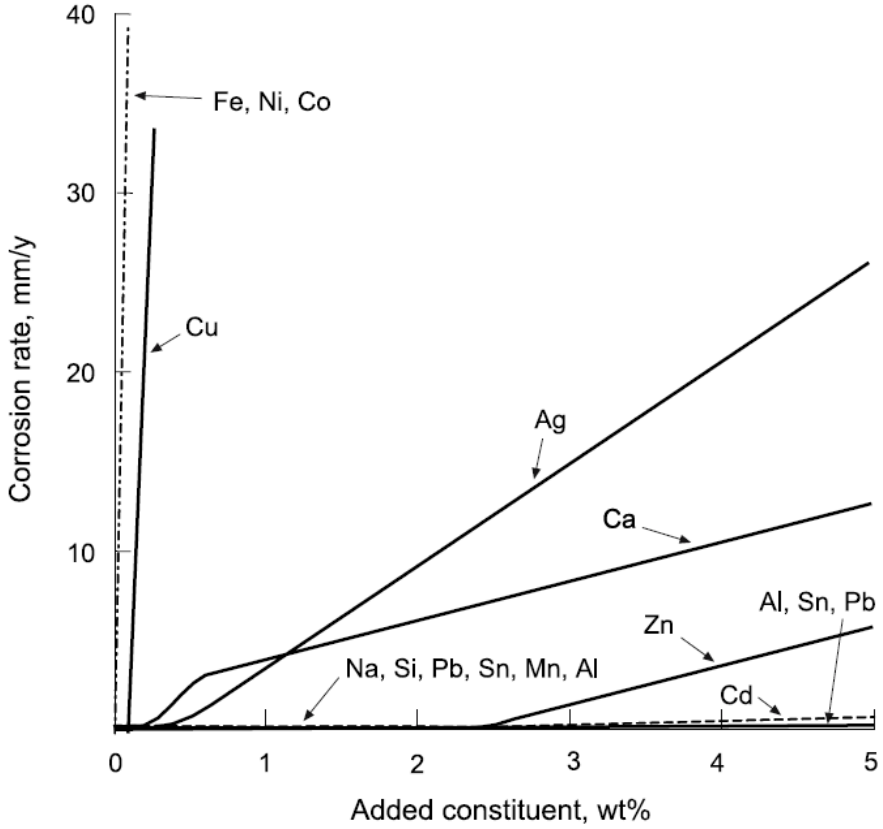

Figure 3.2 Corrosion rates of binary alloys, by alternate immersion in 3% sodium chloride solution (Tomashov, 1966)

3.3 Corrosion Characteristics of Magnesium Alloys

As mentioned in previous, the most widely used magnesium alloys are those with aluminum (to 10%), zinc (to 3%), and manganese (to 2.5%). It is desirable that other metals, particularly Fe, Cu, Ni and Si be present in very small amounts not exceeding a total of 0.4% to 0.6% (Song & Atrens, 1999). Mg alloys corrosion is governed by the characteristics of its surface film. The properties of film on Mg alloys depend on Mg alloys' metallurgy and environmental factors. Magnesium metallurgy includes alloying and impurity elements, phase components and microstructure. Metallurgical manipulation can provide an effective means to improve the corrosion resistance of magnesium alloys.

3.3.1 Influences of Environment

Generally, the corrosion resistance of magnesium alloy is better than that of pure magnesium, because other corrosion resistant phases exist. An analysis of the films formed when magnesium alloys containing Al, Mn, or Zn are exposed to the atmosphere, shows an enrichment of the secondary constituents. It was suggested that the air-formed oxide on Mg-Al alloys has a layered structure composed of MgO/Mg-Al-oxide/substrate, with the Mg-rich oxide becoming thinner with increasing Al content. It is likely that this benefit of Al is related to the strong tendency for Al to form a stable passive film (Song & Atrens, 1999).

Lindstom et al. (2003) studied the influence of NaCl and CO_2 on the atmospheric corrosion of magnesium alloy AZ91. The combination of high humidity and NaCl is very corrosive towards AZ91. However, CO_2 inhibits atmospheric corrosion both in the presence of and in the absence of NaCl. The inhibitive effect of CO_2 was suggested to be due to a combination of pH decrease in the surface electrolyte, stabilizing alumina in the passive film, and the formation of sparingly soluble carbonate-containing corrosion products that slow down the electrochemical reactions.

3.3.2 Influences of Metallurgical Factors

Metallurgical factors include alloying and impurity elements, phase composition and microstructure.

3.3.2.1 Impurity elements

The most critical factor in the corrosion behaviour of Mg and Mg alloys is the metal purity. Iron, nickel, and copper are extremely deleterious because they have low solid-solubility limits and provide active cathodic sites which lead to galvanic corrosion and increase corrosion rates. At the same concentration, the detrimental effect of these elements decreases as follows: Ni>Fe>Cu. When the impurity

concentration exceeds the tolerance limit, the corrosion rate is greatly accelerated, whereas the corrosion rate is low when the impurity concentration is lower than the tolerance limit. The tolerance limits in magnesium alloys are influenced by the presence of other elements. For example, the iron tolerance limit for magnesium-aluminum alloys depends on the Mn or Zn concentration (Makar & Kruger, 1993). Furthermore, impurity limits are different depending on the method of manufacture. For example, die cast AZ91 has higher nickel tolerance than gravity cast AZ91. And the slower solidification rates significantly affect the nickel tolerance, but not Fe and Cu. Different alloys have different tolerance limits as summarized in Table 3.2.

Table 3.2 Tolerance limits for magnesium and magnesium alloys (Makar & Kruger, 1993)

Specimen	Condition	Fe	Ni	Cu
Pure Mg		170 ppm	5 ppm	1000 ppm
Pure Mg		170 ppm	5 ppm	1300 ppm
AZ91		20 ppm	12 ppm	900 ppm
AZ91		0.032 Mn	50 ppm	400 ppm
AZ91	High pressure (F)	0.032 Mn	50 ppm	400 ppm
AZ91	Low pressure (F)	0.032 Mn	10 ppm	400 ppm
AZ91	Low pressure (T4)	0.035 Mn	10 ppm	100 ppm
AZ91	Low pressure (T6)	0.046 Mn	10 ppm	400 ppm
AZ91B			<100ppm	<2500 ppm
AS41	Die casting	0.032 Mn	50 ppm	400 ppm
AZ91	Die casting	50 ppm	50 ppm	700 ppm
AZ91	Die casting	0.032 Mn	50 ppm	700 ppm
AZ91	Gravity casting	0.032 Mn	10 ppm	400 ppm
AM60	Die casting	0.021 Mn	30 ppm	10 ppm
AE42		0.01 Mn	40 ppm	200 ppm

Iron, nickel, copper, and cobalt are the four main elements so far found to have significant detrimental influence on the corrosion resistance of magnesium alloys (Song & Atrens, 1999). Besides these detrimental elements, there is one special element, manganese, which is usually closely related to the detrimental effects of other elements and their tolerance limits.

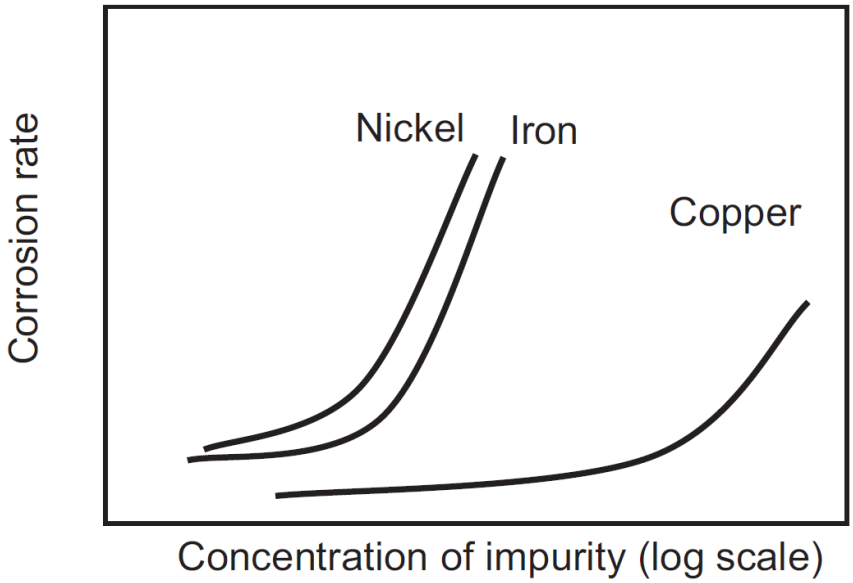

Figure 3.3 The influence of Ni, Fe and Cu impurities on corrosion resistance of magnesium (schematics)

The deleterious effect of iron in pure magnesium is shown in Figure 3.3, and it is suspected to be due to the galvanic coupling between the magnesium matrix and the iron particles scattered in the matrix because Fe has a very low solid solubility in magnesium (about 9.9 ppm) (Song & Atrens, 1999). Due to the low solubility of $FeAl_3$ in magnesium, increasing additions of Al result in increasingly smaller tolerance levels for Fe.

Nickel is more harmful than iron both in pure magnesium and in magnesium alloys, because nickel precipitates in magnesium alloys as Mg_2Ni which is more cathodically active than $FeAl_3$ and Fe, as shown in Figure 3.4. In Figure 3.4, cathodic activity of precipitates phases in magnesium alloys in salt water relative to their alloy matrix were defined.

A small amount of copper has a beneficial effect on the creep strength of magnesium die castings, but strongly accelerates salt water corrosion (Song & Atrens, 1999). Cu is less harmful than iron in magnesium, because copper precipitates in magnesium as Mg_2Cu which has a lower potential than $FeAl_3$ (Hawke & Olsen, 1993). The addition of copper to Mg-Al-Zn alloys has also been shown to

have a detrimental effect on the corrosion resistance. This may be attributed to the incorporation of the copper in the eutectic phase as Mg(Cu, Zn).

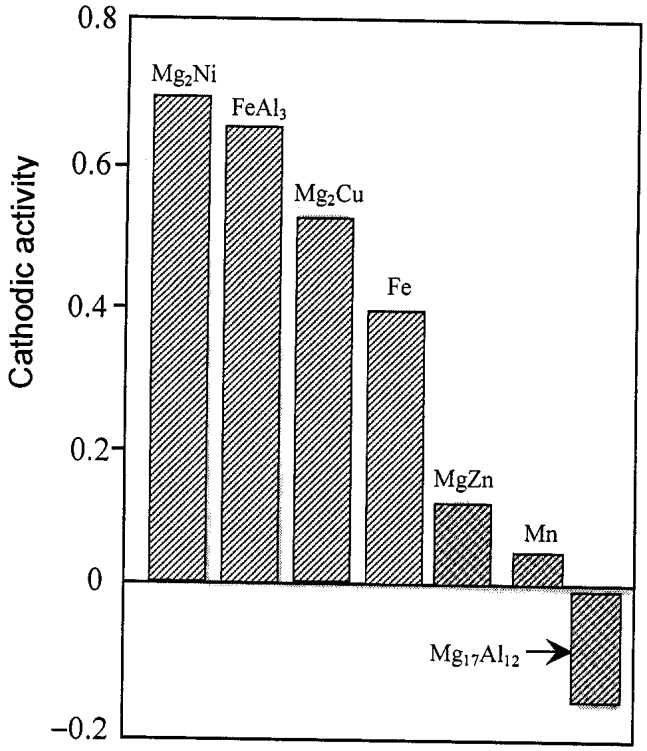

Figure 3.4 Cathodic activity of precipitates phases in magnesium alloys in salt water relative to their alloy matrix (Hawke & Olsen, 1993)

Manganese is added to many commercial alloys, particularly the Mg-Al-Zn alloys (AZ series) to improve corrosion resistance. Manganese itself does not improve the corrosion resistance, it reduces the harmful effect of impurities. For example, manganese increased the Ni tolerance limit. The Fe/Mn ratio seems to control the influence of iron upon the corrosion rate rather than the overall Fe content. Fe tolerance limit was equal to 3.2% of the Mn content regardless of the melt temperature at the time of casting and the type of casting produced (Reichek et al., 1985).

A particle of iron embedded in a particle of manganese is less detrimental to magnesium because the galvanic activity between Mn and Mg is less than that between Mg and Fe. Mn combines with the Fe and precipitates at the bottom of the

crucible, where it reacts with the Fe left in suspension during solidification (Carlson & Jones, 1993).

When Mn and Al are present together, the AlMnFe intermetallic compounds form preferentially relative to $FeAl_3$, which is known to be an active cathodic phase relative to the magnesium matrix. Mn in excess of that needed to render to the Fe content ineffective could be detrimental to corrosion resistance (Carlson & Jones, 1993).

3.3.2.2 Important Alloying Elements for Corrosion Aspect

Alloying elements not only enhance the mechanical properties of Mg but also have a significant impact on the corrosion behaviour of magnesium alloys. Alloying elements can form secondary particles which are noble to the Mg matrix thereby facilitating corrosion or enrich the corrosion product thereby possibly inhibiting corrosion.

Alloying magnesium with aluminium in general improves the corrosion resistance. Lunder et al reported that there is a significant drop in the corrosion rate as the aluminium content is increased from 2 to 4%. Further aluminium additions up to 9% give only a modest further improvement (Lunder et al., 1993).

The aluminium is partly in solid solution, and partly precipitated in the form of $Mg_{17}Al_{12}$. Lefebvre & Nussbaum (1991) discussed that the role of Al in solid solution and role of $Mg_{17}Al_{12}$ in the corrosion process. Both Al in solid solution and $Mg_{17}Al_{12}$ can decrease corrosion rates. The presence of Al in solid solution in the matrix decreases the corrosion rate of Mg alloys in 5% NaCl and $Mg(OH)_2$ solution, which is attributed to a change in the surface microstructures.

However, it has also been found that aluminum can have a negative influence on corrosion. Aluminium reduces the iron tolerance limit from 170 wt. ppm to 20 wt.-ppm. The tolerance limit of iron decreases almost linearly with increasing aluminium

content. This trend in the iron tolerance limit appears to be consistent with the formation of a passive AlMnFe intermetallic phase on solidification(Song & Atrens, 1999).

The presence of Zinc can increase the tolerance limits and reduce the effect of impurities once the tolerance limit has been exceeded. Zinc is believed to improve the tolerance of Mg-Al alloys for all three impurities (Fe, Cu, Ni), but its amount is limited to 1-3%. The addition of 3% Zn raises the tolerance limit to 30 wt.-ppm Fe and greatly reduces the corrosion rate for iron concentrations of up to 180 wt.-ppm for Mg-Al-Mn alloys. For the Mg-Al-Mn -Ni alloys, 3% Zn shifts the tolerance limit from 10 to 20 wt.-ppm Ni and reduces the corrosion rate at higher concentration of nickel (Song & Atrens, 1999).

The zirconium containing magnesium alloys usually have a higher corrosion resistance than zirconium-free magnesium alloys. Song and StJohn (2002) stated that Zr reduces the corrosion rate. Firstly, impurities combine with zirconium and form insoluble precipitates and purify the alloy. Secondly Zr stabilizes the magnesium solid solution making it less soluble in aqueous solutions. The third mechanism is that zirconium combines with some intermetallic precipitates which were originally active cathodic sites, making them less active. Apart from the above mechanisms, the grain refining effect provided by zirconium could be another reason for the higher corrosion resistance of magnesium containing zirconium.

Si is intentionally added only to the Mg-Al-Si alloys (AS series) to combine with Mg and form Mg_2Si which precipitation strengthens the alloy and is relatively innocuous to the corrosion of Mg. Mg_2Si has a steady state corrosion potential of -1.65 V similar to -1.66 V for pure magnesium in 5% NaCl solution (Carlson & Jones, 1993).

It is well known that the addition of rare earth elements (RE) is an effective way to improve the mechanical properties of magnesium alloys at elevated temperatures. The improvement has mainly been attributed to the formation of a metastable RE-

containing phase along the grain boundaries which significantly increases the creep resistance. The beneficial effect of the RE could be similar in nature to that of the Mn additions i.e. the formation of an AlFeMn intermetallic phase which mitigates the harmful effects of Fe. However, no ternary phase was found to form in Mg-Al-RE alloys as the chemical stability of the Al_4RE intermetallic is quite high (Carlson & Jones, 1993).

3.3.2.3 Role of β phase

Phase contents have a pronounced influence on the corrosion of magnesium, because most elements only affect the corrosion resistance of magnesium alloys when they form second phases.

Magnesium-Aluminium alloys contain three main phases: a substitutional solid solution of aluminium in magnesium (α phase) and two intermetallic phases: β ($Mg_{17}Al_{12}$) present in a eutectic phase (α + β) and an intermetallic phase containing Mn, Fe and Al present at a minor level (Song, Atrens and Dargush, 1999).

In general, the β phase present in the alloy is considered more resistant to corrosion than the surrounding matrix alloy. Song et al. (1998) suggested that the role of the β phase in corrosion may be twofold:

(1) The β-phase could have a barrier influence because it is very stable in a NaCl solution;

(2) The β-phase is an efficient cathode for hydrogen evolution.

When the β-phase is present in an alloy, it reduces the reactive surface area, so less area of the alloy is available to be corroded. In this manner, the β-phase might improve the corrosion resistance of the alloy. Unfortunately, in most cases the β-phase is discontinuous and then it does not stop corrosion completely. The cathodic reaction of hydrogen evolution on the β-phase is much easier than on the α-phase. Consequently, if the β-phase is present in a alloy, it acts as an effective cathodic phase to the α-matrix. It causes significant acceleration of the α-phase corrosion by

galvanic coupling. However, the role of β-phase strongly depends on the volume fraction. If β-phase is present in the a-matrix as intergranular precipitates with a small volume fraction, then the β-phase mainly acts as a galvanic cathode, and accelerates the corrosion of the α matrix. If the β fraction is high, then the β phase mainly acts as an anodic barrier to inhibit the overall corrosion performance (Song et al 1998).

3.3.2.4 Microstructure

Microstructural parameters such as composition, porosity, grain size, and amount and distribution of β-phase also play a role in determining the corrosion behaviour. The reduction of grain size increases the overall grain boundary area thereby optimizing the distribution and minimizing the size of any possible detrimental intermetallics such as $FeAl_3$. The microstructure can be controlled by the cooling rate, with more rapid cooling leading to a smaller grain size and a more finely distributed β-phase. Mathieu et al. (2002) found that the casting method strongly influences the corrosion performance through control of the microstructure. The corrosion resistance of semi-solid cast AZ91D alloy is 35% higher than that of the same alloy processed by high pressure die-casting with the impurity level (Cu, Fe) being the same, and the difference in corrosion behaviour is attributed to the distribution, composition and volume fraction of the constituent phases (mainly α and β). Even for the same material, the corrosion resistance is different depending on the location of the material in the casting. Song, Atrens and Dargush (1999) found that the skin of die cast AZ91D shows a corrosion resistance significantly better than its interior in 1 N NaCl at pH 11. This is attributed to a higher β-fraction, and more continuous β-phase around finer α-grains and low porosity.

*3.*4 Corrosion Types of Magnesium Alloys

2.4.1 Galvanic Corrosion

When two dissimilar metals are placed in contact in a corrosive or conductive solution, a potential difference produces electron flow between them. The more

active metal then becomes anodic and is corroded, and the less active metal becomes cathodic and is protected. This kind of corrosion is called galvanic corrosion, or two-metal corrosion. Magnesium and its alloys are highly susceptible to galvanic corrosion, because magnesium has the lowest standard potential of all the engineering metals as illustrated in Table 3.3.

Table 3.3 The standard electrode potentials versus normal hydrogen electrode at 25 °C (Kurze, 2006)

Electrode	Reaction	Potential, V	Remarks
Au, Au^{3+}	$Au^{3+} + e^- \rightarrow Au$	1.50	Noble–cathodic
Pt, Pt^{2+}	$Pt^{2+} + e^- \rightarrow Pt$	1.20	
Ag, Ag^+	$Ag^+ + e^- \rightarrow Ag$	0.80	
Cu, Cu^{2+}	$Cu^{2+} + e^- \rightarrow Cu$	0.34	
H_2, H^+		0.00	Neutral
Sn, Sn^{2+}	$Sn^{2+} + e^- \rightarrow Sn$	−0.14	
Ni, Ni^{2+}	$Ni^{2+} + e^- \rightarrow Ni$	−0.25	
Co, Co^{2+}	$Co^{2+} + e^- \rightarrow Co$	−0.28	
Cd, Cd^{2+}	$Cd^{2+} + e^- \rightarrow Cd$	−0.40	
Fe, Fe^{2+}	$Fe^{2+} + e^- \rightarrow Fe$	−0.44	
Cr, Cr^{2+}	$Cr^{2+} + e^- \rightarrow Cr$	−0.74	
Zn, Zn^{2+}	$Zn^{2+} + e^- \rightarrow Zn$	−0.76	
Al, Al^{3+}	$Al^{3+} + e^- \rightarrow Al$	−0.17	
Mg, Mg^{2+}	$Mg^{2+} + e^- \rightarrow Mg$	−2.37	
Na, Na^+	$Na^+ + e^- \rightarrow Na$	−2.71	
K, K^+	$K^+ + e^- \rightarrow K$	−2.92	
Li, Li^+	$Li^+ + e^- \rightarrow Li$	−3.02	Active–anodic

Galvanic corrosion can also occur between two different phases. When magnesium and its alloys are placed contact with other metals, magnesium and magnesium alloys are corroded, while hydrogen gas is evolved on the other metals. When magnesium and magnesium alloys contain second phases because of impurities or alloying elements, the matrix α-phase is corroded, while the hydrogen gas is evolved on the second phases. Table 3.4 shows typical corrosion potential values for magnesium and common magnesium alloy second phases (Song & Atrens, 2003).

Table 3.4 Typical corrosion potential values for magnesium and for common magnesium second phases (after 2 h in deaerated 5% NaCl solution saturated with $Mg(OH)_2$ (pH 10.5) (Song & Atrens, 2003).

Metal	E_{corr} Vs. SCE
Mg	-1.65
Mg_2Si	-1.65
Al_6Mn	-1.52
Al_4Mn	-1.45
Al_8Mn_5	-1.25
$Mg_{17}Al_{12}(\beta)$	-1.20
$Al_8Mn_5(Fe)$	-1.20
Beta-Mn	-1.17
Al_4Mn	-1.15
$Al_6Mn(Fe)$	-1.10
$Al_6(MnFe)$	-1.00
$Al_3Fe(Mn)$	-0.95
Al_3Fe	-0.74

As can be clearly seen from Table 3.4, the most potent cathodes in Mg-Al alloy are iron-rich phases, in particular the iron-aluminum intermetallic phase $FeAl_3$. As mentioned above, $FeAl_3$ is one of the most detrimental cathodic phases present in Mg-Al alloys on the basis of its potential and its low hydrogen overvoltage. Al-Mn phases are also detrimental, while Mg_2Si have no influence.

The galvanic corrosion rate is increased by the following factors: high conductivity of the medium, large potential difference between anode and cathode, large area ratio of cathode to anode, and small distance from anode to cathode (Fontana, 1996).

High purity magnesium alloys cannot avoid galvanic corrosion if they are coupled with other metals. By proper material selection, proper design and selective use of coatings and insulation materials the risk for galvanic corrosion ban be significantly reduced (Skar, 1999).

2.4.2 Stress Corrosion Cracking (SCC)

Stress corrosion cracking (SCC) is an extremely dangerous type of corrosion damage in engineering service of equipment, vessels etc. which refers to cracking caused by the simultaneously presence of tensile stress and a specific corrosive medium (Fontana, 1996). SCC in magnesium is mainly transgranular. Pure magnesium can be considered immune to stress corrosion cracking in both atmospheric and aqueous environments. Aluminum containing alloys of magnesium are generally considered the most susceptible to SCC, with the tendency increasing with the aluminum content (Baboian, 1995). The alloys AZ61, AZ80, and AZ91 with 6, 8, and 9% aluminum, respectively, can show high susceptibility to SCC in laboratory and atmospheric exposures, while AZ31, a 3% aluminum alloy used in wrought product applications, is considered to show good corrosion resistance. Magnesium-zinc alloys such as ZK60 and ZE41 that are alloyed with zirconium, or zirconium and rare earth elements, are typically considered only mildly susceptible, while magnesium alloys containing no aluminum or zinc are the most SCC-resistant (Song & Atrens, 1999).

The majority of the SCC literature has focused on extruded or rolled magnesium alloys. Die-cast alloys are more susceptible to SCC than rapidly solidification (RS) and semi-solid cast alloys (William & Miller, 1993). SCC of magnesium alloys can occur in moist air, high purity water, $NaCl+K_2CrO_4$ solution, NaBr, Na_2SO_4, NaCl, $NaNO_3$, Na_2CO_3, H_2SO_4, KF, KCl, NaI, $MgCO_3$, NaOH, HNO_3**,** and hydrogen chloride solutions SCC in Mg alloys has been generally attributed to one of two groups of mechanisms: continuous crack propagation by anodic dissolution at the crack tip or discontinuous crack propagation by a series of mechanical fractures at

the crack tip (Winzer et al, 2005). There are two types of models for SCC: the dissolution models and the brittle fracture models. The former includes a preferential attack model, film rupture model, tunnelling theory etc; the later involves cleavage processes and hydrogen embrittlement (HE) theory. Based on the fracture morphology of samples, there exist two kinds of SCC: Transgranular SCC (TGSCC) and intergranular SCC (IGSCC). TGSCC is a major mode of SCC. Most magnesium alloys have HCP crystal structures, which are susceptible to cleavage due to the less slip systems available. For example, pure Mg suffers TGSCC, and Mg alloys suffer TGSCC in distilled water. TGSCC in magnesium alloys is related to hydrogen.

The magnesium hydride theory is proposed due to observations of an approximately 1 μm thick brittle MgH_2 film on a magnesium SCC fracture surface. IGSCC is not the major fracture mode in magnesium. HE may not always be the primary mechanism for SCC crack growth. TGSCC is not related to precipitates of any kind. IGSCC has been related to localize galvanic attack of the matrix when coupled with cathodic $Mg_{17}Al_{12}$ grain-boundary precipitates.

3.4.3 Corrosion Fatigue

A collection of fatigue data of Mg alloys has been gained over the past years. Most of the fatigue data are concerned with fatigue life. There is endurance limit for magnesium alloys in air. Fatigue strength is improved as the grain size decreases (Potzies & Kainer, 2004). The reverse was found to be the case for the fatigue crack propagation resistance (Yue et al., 1995). Many experimental results showed a significant reduction in fatigue strength or fatigue life in sodium chloride solutions, even in tape water or distilled water.

A corrosive medium can more remarkably shorten the fatigue life of extruded magnesium alloys compared with die-cast magnesium alloys. Concerning fatigue testing, especially the test frequency is a very important parameter to be considered in corrosion fatigue, as the corrosion fatigue becomes much more pronounced at lower frequency values in aqueous solution (Ghali et al., 2004).

3.4.4 Pitting Corrosion

Few studies have addressed these forms of localised attack of Mg and Mg alloys because other forms of corrosion such as general, galvanic, or stress corrosion have been the cause of more serious failure of these materials. The studies of pitting of Mg and Mg alloys have been concerned with comparing the pitting behaviour of cast to that of rapidly solidified Mg alloys. Makar & Kruger (1990) showed that rapidly solidified AZ61 exhibited better resistance to pitting than cast AZ61 in a buffered carbonate solution containing various levels of Cl^-. Pit initiation of rapidly solidified AZ61 is found to take place at a higher potential and the pit growth rate was apparently lower than cast AZ61. Heavy metal contamination promotes general pitting attack. In Mg-Al alloys, pits are often formed due to selective attack along $Mg_{17}Al_{12}$ network that is followed by the undercutting and falling out of grains (Song & Atrens, 1999).

By the formation of an electrolytic cell in which the secondary phase particles are the cathode of the type AlMn, AlMnFe, $Mg_{17}Al_{12}$, Mg_2Cu, and the surrounding Mg matrix is the anode. For example, the as-extruded magnesium alloy AM60 was immersed in natural 3.5% NaCl solution, and the corrosion pits occurred on the surrounding of AlMn particles. A model of pitting corrosion mechanism of as-extruded AM60 is given in Figure 3.5 (Zeng et al., 2005).

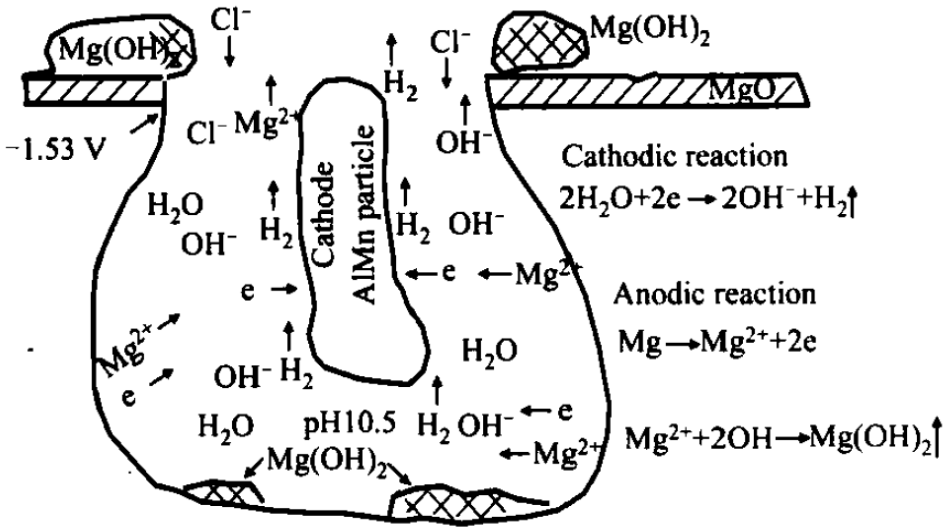

Figure 3.5 Scheme of pitting corrosion mechanism for magnesium alloy AM60 (Zeng et al., 2005)

Firstly, the alloy has a protective oxide film in air. The potential of MgO is - 1 V**.** When it is immersed in a sodium chloride aqueous solution, Cl^- ions will absorb on the α areas bordering on AlMn particles. If the breakdown potential of the oxide film reaches its free corrosion potential ((E_{corr}= -1.53 V for AM60), then the α-matrix as an anode, compared to AlMn particles, starts to dissolve, and a corrosion nucleus may form nearby an AlMn particle. The nucleus develops a corrosion pit, this may result in $Mg(OH)_2$ formation and hydrogen evolution At the end, an occlusion cell or a hemi-spherical corrosion pit will be formed with the corrosion proceeding. The pH value will finally reach and keep at 10.4-10.5. Mg hydroxide precipitates on the bottoms of pits and surfaces of samples (Zeng et al., 2005).

3.4.5 Crevice Corrosion

Crevice corrosion does not occur with the Mg alloys because corrosion is relatively insensitive to oxygen concentration difference. Though a form of attack that occurs at narrow gaps (“crevice”) appears similar to crevice corrosion, it is not true for crevice corrosion. Because the corrosion observed is caused by the retention

of moisture in the crevice which, being unable to evaporate, promotes the corrosion of metal in the narrow recess over extended periods. Ghali et a1. (2004) also suggested that crevice corrosion could be initiated due to the hydrolysis reaction in case of Mg and Mg alloys, at least in certain conditions where it is believed that oxygen does not play a major role in the corrosion mechanism.

3.4.6 Filiform Corrosion

Filiform corrosion often occurs on the metals surface such as steel, Al alloys and Mg alloys. It is caused by active galvanic cells across the metal surface. Its head is anodic, whereas the tail is cathodic. It is typically associated with metal surfaces having an applied protective coating. It does not occur on bare pure Mg (Ghali, 2000). Lunder et a1. (1993) stated that the earlier stage of corrosion for magnesium alloy AZ91 has a characteristic of pitting and filiform corrosion. Filiform corrosion initiates corrosion pits.

3.5 Corrosion Protection of Magnesium Alloys

There are a number of approaches to overcome the corrosion problems of magnesium alloys:

(1) High purity or new alloys: Decrease impurities to below their tolerance limits and develop new alloys with new elements, phases, and microstructure distributions;

(2) Surface modification: this includes ion implantation and laser annealing;

(3) Refinement of the grain size and intermetallic particles: corrosion resistance can be affected through the microstructure;

(4) Protective films and coatings.

3.5.1 High Purity(HP) Magnesium Alloys

Improving corrosion resistance by producing Mg alloys with low concentration of deleterious elements is an often-used strategy. This ensures the highest possible degree of uniform corrosion resistance of the starting material.

3.5.2 Surface Modification

Ion implantation is the technique whereby almost any elemental ions may be implanted into the surface of any solid using a beam of energetic ions accelerated into a target under vacuum conditions. This homogenization is the primary benefit of ion implantation in terms of corrosion resistance. Additional benefits include the ability to alter the surface while retaining the bulk properties, the creation of novel surface alloys, and the elimination of surface adhesion problems associated with coatings. The primary disadvantage is it modifies only a thin film (Hagans, 1984).

Laser annealing technique involves the formation of metastable solid solutions as promoted at metal surfaces by laser annealing, where cooling rates as high as 10^5 K/s are achievable using lasers pulsed in the nanosecond range (Hagans, 1984). It is, therefore, another form of rapid solidification processing, but involves the melting and solidification of surface layers only. Besides the advantages of ion implantation, the advantages include the ability of lasers to treat more complex geometries, the greater depth of treatment, inexpensive operation costs, and greater control of the concentration of the modified layer. The main disadvantage is the extra machining necessary because of dimensional changes during treatment (Hagans, 1984).

3.5.3 Microstructure Refinement

Corrosion resistance can be affected through modification of the microstructure. Reduction of grain size increases the overall grain boundary area thereby optimizing the distribution of detrimental intermetallics and minimizing the size of any possible detrimental intermetallics such as $FeAl_3$. The traditional grain refinement method in sand casting is to add an inoculant which facilitates heterogeneous nucleation during solidification

Rapidly solidified materials show improved corrosion resistance because of a refined microstructure which translates to a more homogeneous composition thereby minimizing the potential of any microgalvanic corrosion cell.

3.5.4 Effect of Heat-Treatment

Heat-treatment can drastically alter the size, amount and distribution of the precipitated β phase Aung & Zhou (2002) studied an AZ91D ingot in the as-cast condition that was homogenized by solution treatment and then aged for various periods of time. The homogenization treatment of an AZ91D ingot at 420 °C for 24h was found to be effective in dissolving the β-precipitates. Artificial ageing at 200°C causes precipitation of the β phase mainly along the grain boundaries. The volume fraction of the β-phase was observed to increase with ageing time. A homogenization treatment improved the corrosion resistance of the AZ91D ingot, but ageing for 8 h, 16 h or 26 h lowered the corrosion resistance. These results support the suggestion that microgalvanic coupling exists between the cathodic β-phase and the anodic α-matrix.

3.6 Protective Coatings and Films

There are a number of technologies available for coating magnesium and its alloys. These include electrochemical plating, conversion coatings, anodizing, organic coatings and vapour-phase processes.

3.6.1 Electrochemical Plating

One of the most cost effective and simple techniques for introducing a metallic coating to a substrate is by electrochemical plating. The electrochemical plating can be subdivided into two types: electroplating and electroless plating. In both cases a metal salt in solution is reduced to its metallic form on the surface of the substrates. In electroplating the electrons for reduction are supplied from an external source. In electroless or chemical plating the reducing electrons are supplied by a chemical reducing agent in solution or, in the case of immersion plating, the substrate itself.

Nickel silver and gold plating on magnesium have both proven useful for space applications such as satellite embarking device. Successful gold plating been achieved using the following sequence on magnesium–lithium alloys (Sharma, 1988)

The capital investment of electrochemical plating process is relatively small. Unfortunately, electroplating process is extremely difficult to achieve uniform coatings on complex shapes due to uneven throwing power. Furthermore, the pre-treatment processes are complicated due to the fact that, in the presence of air, magnesium very quickly forms a passive oxide layer. Cu-Ni-Cr plating has been shown to have good corrosion resistance in interior and mild exterior environments (Innes, 1974) Also, it is necessary to develop non-traditional plating baths since magnesium reacts violently with most acids and dissolves in acidic media. Furthermore, magnesium and its alloys are prone to galvanic corrosion, so the metal coating must be pore free otherwise the corrosion rate will increase. Usually, the coating is at least 40-50 μm thick to ensure pore-free coatings. Furthermore, the alloys are difficult to plate because intermetallic species such as Mg_xAl_y are formed at the grain boundaries, resulting in a non-uniform surface potential across the substrate, and therefore further complicating the plating process.

Electroless plating has good throwing power and can produce a uniform coating thickness on complex objects. It also involves a simple pre-treatment and is suitable for magnesium alloys with high aluminium contents (Gray & Luan, 2002). However, electroless deposited coatings cannot be too thick, the bath life is limited, and deposition rates are slow. In particular, electroless plating requires the use of hydrofluoric acid during the pre-treatment, which increases the danger of the operation and is not environmentally friendly (Gray & Luan, 2002). Research on increasing the bath life and eliminating toxic chemicals is necessary in order to create a green-plating process for coating magnesium. Sharma et al. (1998) studied the properties of an electroless nickel coating on magnesium alloy ZM21. The solution contains nickel carbonate, sodium hypophosphite (metal-reducing agent), citric acid and bifluoride (act as accelerators, complexing agent, and accelerators), thiourea (solution stabilizer and brightening agent) and ammonia solution. No corrosion spots

on the coatings were noticed after 96 hrs of immersion. The formation of corrosion spots initiated only after the fifth day of immersion. Recently, Huo et al. (2004) developed an environmental-friendly combined technique of chemical conversion treatment followed by electroless nickel plating for AZ91D alloy to improve corrosion resistance. The electroless nickel coating containing about 10 wt% phosphorus greatly enhanced the corrosion potential of AZ91D from -1.5V to -0.6V.

3.6.1.1 Pre-treatment processes

The most difficult part of plating magnesium is developing an appropriate pre-treatment process, once a suitable undercoating is in place many desired metals can be plated. To date zinc and nickel have been directly plated onto magnesium, and are used as undercoatings for subsequent metal deposition. The undercoatings must be non-porous since porosity in underlayers promotes porosity in over- layers. A uniform coverage is especially difficult to achieve on magnesium alloys. The existing processes require many steps and are laborious, time consuming and must be precisely controlled to achieve acceptable adhesion and corrosion resistance

The pre-treatment requirements vary for different alloys and different plating baths. There are currently two general processes for treating magnesium prior to plating. These are zinc immersion and electroless nickel plating from a fluoride containing bath. These two general processes are outlined schematically in Figure 3.6.

The etching and plating conditions had a large effect on the adhesion obtained. An insufficient etching or fluoride conditioning resulted in poor adhesion. It was also determined that using hydrofluoric acid for conditioning led to a wide plating window while ammonium bifluoride resulted in a much narrower (pH 5.8–6.0 and temperature 75–77 ^{0}C) window for acceptable adhesion. The chromic acid treatment was found to heavily etch the surface and leave behind a layer of reduced chromium. The fluoride conditioning was found to remove chromium and control the deposition rate by uniform passivating the surface. The passivating effect of fluoride was also exploited in the plating of magnesium alloy MA-8 (Masao, 1986). In this case the nickel plating bath contained fluoride to inhibit corrosion of the substrate during

plating. The authors report strong adhesion of the nickel film however, the bath life is too short to be industrially applicable. The addition of a complexing agent, glycerine, was shown to improve the stability of the plating bath.

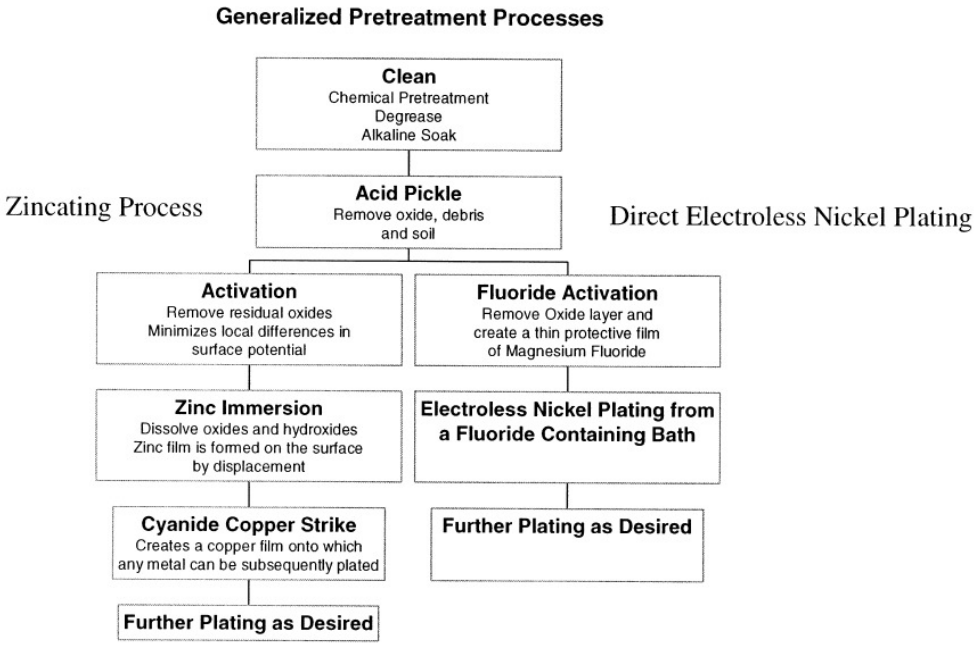

Figure 3.6. Generalised pretreatment processes (Gray & Luan, 2002)

3.6.2 Conversion Coatings

Conversion coatings are produced by chemical or electrochemical treatment of a metal surface to produce a superficial layer of substrate metal oxides, chromâtes, phosphates or other compounds that are chemically bonded to the surface. On magnesium, these coatings are typically used to enhance paint adhesion to the coatings and provide improved corrosion protection to the metal. There are a number of different types of conversion coatings including chromate, permanganate, phosphate, phosphate-permanganate and fluorozirconate treatments.

One of the main disadvantages of conversion coatings is the toxicity of the treatment solutions. The conventional conversion coatings are based on chromium compounds that have been shown to be highly toxic carcinogens. The development of an environmentally friendly process is a necessity due to the more stringent

environmental protection laws currently in effect, or being proposed. The coatings on alloys also represent a significant challenge due to their non-uniform surface composition.

Chromate conversion coatings can be used as pre-treatments prior to a final sealing process or as ‘post-treatments after plating process to improve corrosion resistance, paint or adhesive bonding properties or to provide a decorative finish

The mechanism of formation of chromate conversion coatings is believed to be due to the dissolution of the metal surface, with a corresponding reduction of water or oxygen to form hydroxyl ions, which causes an increase in pH at the liquid–metal interface (Hagans & Haas, 1994). This in turn causes precipitation of a thin complex chromium–metal gel on the surface that contains both hexavalent and trivalent chromium compounds (Sharma, 1989). Pure chromic acid solutions are not used to form conversion coatings because the deposition rate is too slow (Hagans & Haas, 1994). Other anions in solution that can act as a catalyst for deposition are required some of these include acetate, formate, sulfate, chloride, fluoride, nitrate, phosphate and sulfamate ions. The pH of the solution is the most important factor in controlling the formation of chromate films (Eppensteiner & Jenkins, 1992).

The hexavalent chromium is reduced during corrosion to form an insoluble trivalent chromium species that terminates the oxidative attack. The protection afforded by the coating is proportional to the coating thickness (Eppensteiner & Jenkins, 1992). However due to the significant environmental hazards associated with the use of chromate compounds there is a push to find alternative coating process.

Phosphate-permanganate treatments are being explored as an alternative to conventional chromate conversion coatings. These treatments are more environmentally friendly and have been shown to have corrosion resistance comparable to chromate treatments (Gray & Luan, 2002).

Chong & Shih (2003) reported that a conversion coating on magnesium alloys AZ61A, AZ80A and AZ91D prepared from a solution containing permanganate ($KMnO_4$ 20g/l) and phosphate ($MnHPO_4$ 60g/l) showed an equivalent or slightly better passive capability than a conventional chromate-based conversion treatment, but an inferior passive capability for the pure Mg specimen. The manganese is considered to contribute manganese to the coating, and acts as an accelerator without depositing metallic manganese on the magnesium surface. The coatings were shown to have good corrosion resistance and paint adhesion.

It was found that the most important factor in producing the best quality conversion coatings was the control of the pH (Gray & Luan, 2002). Since pH is the most important factor determining conversion coating quality, the research on stabilizing the pH of solutions has gained increasing attention.

A study on stannate treatment of ZC 71 and a metal matrix composite of ZC71+12% SiC particles has been undertaken by Gonzalez-Nunez et al. (1995). After mechanical finishing and pickling, the samples were immersed in a stannate bath for selected periods of time. The treatment resulted in the formation of a 2-3 μm thick, continuous and adherent, crystalline coating of $MgSnO_3$ on both materials. The nucleation and growth of the coating was completed in about 20 minutes. There was an increase in the corrosion potential of the magnesium surfaces as the film formation proceeded indicating that the coating does have a passivating effect on the surface.

The corrosion protection of cerium, lanthanum and praseodymium conversion coatings on magnesium and magnesium alloy WE 43 has been investigated by Rudd et al. (2000). The samples were polished, cleaned in water and methanol and dried prior to immersion in a $Ce(NO_3)_3$, $La(NO_3)_3$ or $Pr(NO_3)_3$ solution. A visible, adherent but easily removed coating was produced on the surface. It has been demonstrated that these coatings provide an increase in corrosion resistance for magnesium and its alloys.

3.6.3 Anodizing

Anodizing is the most widely commercially used coating technology for magnesium and its alloys. This process is technologically more complex than electroplating or conversion coating process. It does involve more capital investment due to the need for cooling systems and high power consumption. Anodizing is an electrolytic process for producing a thick, stable oxide film on metals and alloys. These films may be used to improve paint adhesion to the metal, as a key for dying or as a passivation treatment. The stages for processing include; (1) mechanical pre-treatment, (2) degreasing, cleaning, and pickling, (3) electrobrightening or polishing, (4) anodizing using AC or DC current, (5) dying or post-treatment and (6) sealing (Gray & Luan, 2002).

The films have a thin barrier layer at the metal–coating interface followed by a layer that has a cellular structure. Each cell contains a pore whose size is determined by the type of electrolyte and its concentration, temperature, current density and applied voltage. Their size and density determine the extent and quality of sealing of the anodized film (Mittal, 1995). Colouring of anodized films can be achieved by absorbing organic dyes or inorganic pigments into the film immediately after anodizing, by a second-step electrolytic deposition of inorganic metal oxides and hydroxides into the pores of the film or by a process called integral colour anodizing (Gray & Luan, 2002).

Sealing of the anodized film is necessary in order to achieve an abrasion and corrosion resistant film. This can be accomplished by boiling in hot water, steam treatment, dichromate sealing and lacquer sealing (Gray & Luan, 2002). One of the main challenges for producing adherent, corrosion resistant, anodic coatings on magnesium results from the electrochemical inhomogeneity due to the phase separation in the alloy. Another disadvantage of this technique is that the fatigue strength of the base metal can be affected by localized heating at the surface during the treatment.

DOW 17 process: Chemical treatment no. 17, developed by Dow Chemicals, can be applied to all forms and alloys of magnesium (Hillis, 1994) The anodizing bath employed in this treatment is a strongly alkaline bath consisting of an alkali metal hydroxide and a fluoride or iron salt or a mixture of the two. This process produces a two-phase, two-layer coating. The first layer is deposited at a lower voltage and results in a thin, approximately 5 µm, light green coating, The over layer is formed at a higher voltage. It is a thick dark green, 30.4 µm, layer that has good abrasion resistance, paint base properties and corrosion resistance (Hillis, 1994)

HAE process: named after its discoverer, H.A. Evangelides. This treatment can be applied to all magnesium alloys including the rare-earth magnesium alloys (Evangelides, 1951). The HAE bath is a strongly alkaline and oxidizing solution, consisting of potassium-hydroxide-aluminate-fluoride-manganate and tribasic sodium phosphate (Anonymous, 1957). The treatment produces a two phase coating as in the DOW 17 process At a lower voltage a 5 µm thick, light tan subcoating is produced. At a higher voltage a dark brown, thicker (30 µm) film is produced. Upon sealing the HAE treatment provides excellent corrosion resistance. The corrosion resistance of AZ91D treated with this technique has been tested by a 3-year atmospheric exposure experiment.

ANOMAG process is a proprietary treatment invented by Magnesium Technology Licensing Ltd. The anodizing bath for this process consists of an aqueous solution of ammonia and sodium ammonium hydrogen phosphate (Barton, 1998). The coating produced is a mixed $MgO–Mg(OH)_2$ system with the possibility of additional compounds such as $Mg_3(PO_4)_2$ depending on any additives present in the bath. Due to the presence of ammonia in the system, spark formation is repressed, which eliminates the need for cooling equipment. The coatings produced are semi-transparent to pearl coloured depending on the presence and concentration of certain additives such as fluoride and aluminate.

Guerci et al. (2000) found that the thickness and properties of the oxide layer produced using the Anomag process depend on the bath composition, temperature, current density and treatment time. The coating produced. has a cellular microstructure similar to that observed for other anodizing processes. Further development in the areas of cost reduction, choice of chemicals used in the process and layer thickness optimization was proposed. Another study on coating AZ91 alloy with this process also showed the formation of a porous film with a pore size of about 6 μm and porosity of 13% (Tchevryakov, 2000). Sealing and painting were shown to reduce the pore size and porosity to 3 μm and 4%, respectively. Samples that had been anodized anodized–painted and anodized–sealed all showed a significant reduction in general corrosion rates. The best results occurred for magnesium treated with the Anomag process followed by painting and sealing. These samples showed a 97% reduction in the general corrosion rate compared to the bare metal.

3.6.4 Gas-Phase Deposition Processes

Protective coatings can also be produced from the gas phase. These are typically metallic coatings but can include organic coatings such as thermal spray polymer coatings and diamond like coatings. All of these processes have the advantage that they have little negative environmental impact. However, the capital investment of equipment is really high (Gray & Luan, 2002).

In thermal spray coating process the coating material which can be metal, ceramic, cermet or polymeric is fed to a torch or gun where it is heated to above or near its melting point. The resulting droplets are accelerated in a gas stream onto the substrate and the droplets flow into thin lamellar particles and adhere to the surface (Unger, 1987). There are a number of coating techniques including flame spraying, wire spraying, detonation gun deposition, plasma spray and high velocity oxyfuel.

Some of the advantages of this technique include the ability to create a coating of virtually any material that melts without decomposing, minimal substrate heating

during deposition and the ability to strip and recoat worn or damaged coatings without changing the properties or dimensions of the part (Unger, 1987).

One major disadvantage is that the process is line of sight and small deep cavities cannot be coated, especially if the surface lies parallel to the spray direction. These coatings also require sealing due to their inherent porosity and mechanical finishing to obtain a smooth finishing. One final disadvantage of this technique is the health and safety issues generated by the production of dust, fumes, noise and light radiation during treatment.

Chemical vapour deposition (CVD) can be defined as the deposition of a solid on a heated surface via a chemical reaction from the gas phase. Advantages of this technique include deposition of refractory materials well below their melting points, achievement of near theoretical density, control over grain size, processing at atmospheric pressure and good adhesion (Bunshah, 2001). However, CVD is limited to substrates that are thermally stable at > 600 °C. Efforts are underway to reduce the high temperature requirements and plasma and organometallic CVD processes offset this problem somewhat. A further disadvantage of this process is high-energy cost due to the need for high deposition temperatures and sometimes low efficiency of the process.

Diamond like carbon films (DLC) can be produced using a number of different processes such as physical vapour deposition (PVD), CVD and ion implantation. These coatings are desirable for many applications due to their high hardness, low friction coefficient, electrical insulation, thermal conductivity and inertness. Yamauchi et al. (2005) reported that DLC films were deposited on the AZ31B magnesium alloy substrate by the plasma CVD method using radio frequency. The DLC coating was confirmed to be effective in decreasing the friction coefficient and improving the corrosion resistance in 3 wt% NaCl and 0.05 N NaOH solutions.

Physical vapour deposition processes involves the deposition of atoms or molecules from the vapour phase onto a substrate. There are a few challenges to

overcome in the PVD coating of magnesium substrates. The deposition temperature must be below the temperature stability of magnesium alloys (180°C) and good adhesion must be obtained despite this low temperature. Hoche et al. (2003) developed a new method of plasma anodization to ensure acceptable corrosion resistance, besides excellent wear protection on Mg alloy. The anodizing and PVD-coating can be done in one process. The 0.5 µm plasma anodization layer and 1.5 µm PVD-AI_2O_3 coating was subjected to 120 hours salt spray.

3.6.5 Organic-Polymer Coatings

Organic finishing is typically used in the final stages of a coating process. These coatings can be applied to enhance corrosion resistance, abrasion and wear properties, or for decorative purpose. An appropriate pre-treatment process is required in order to produce coatings with superior adhesion, corrosion resistance and appearance (Gray & Luan, 2002). Many coating processes can be applied to magnesium and magnesium alloys, including painting, powder coating, e-coat, sol-gel process, and polymer plating. But their thicknesses might be limited.

One of the most important steps in painting of magnesium is choosing an appropriate primer. Primers for magnesium should be alkali-resistant and based on resins such as polyvinyl butyral, acrylic, polyurethane, vinyl epoxy and baked phenolic (Hillis, 1994). The addition of zinc chromate or titanium dioxide pigments is commonly used for corrosion prevention.

A study of the corrosion resistance of die cast AZ91D magnesium alloys with paint finishing has been reported by Umehara et al. (1999). Prior to painting, the samples were treated with either a conversion coating or an anodizing process.

Powder coating is a process in which a pigmented resinous coating powder is applied to the substrate and then heated to fuse the polymer together in a uniform, pinhole-free film (Mazia, 1990). Powder coatings can be applied in a number of ways including electrostatic powder spraying, fluidized bed or flame spraying of

thermoplastic powders Powder coating is an excellent alternative to traditional painting processes since it is not detrimental to the environment and uniform thick coatings can be obtained in a single operation even on rough surfaces or edges. There is also little loss of coating material during application and even basic resins that are not readily soluble in organic solvents can be applied. However, there are a few inherent disadvantages to this technique;

1. The powder must be maintained in a very dry, pulverized form.
2. Thin coatings are difficult to obtain.
3. Colour matching and colour uniformity can be difficult to significant amount of oxygen and chrome on the surface maintain.
4. Coating in recessed areas can be difficult.
5. High temperatures required for curing may be unacceptable for some substrates (Mazia, 1990).

E-coat or cathodic epoxy electrocoat is a process for painting metal surfaces by charging the metal part negative and submerging it in a tank that contains positively charged paint. The paint is attracted to the metal to form a uniform coating that is subsequently cured by baking (Jacob, 1992). However, the coating is quite thin therefore it should be combined with a thicker top coat. This process eliminates the environmental hazard posed by using traditional chromate containing conversion or anodized coatings.

Synthesis of gels by the sol-gel process involves the hydrolysis and condensation polymerization of metal alkoxides. One of primary advantages of this technique is the excellent adhesion obtained with a minimum of sample pre-treatment (Gray & Luan, 2002). The metal surfaces are simply degreased, rinsed and dried prior to dip-coating in the sol-gel mixture. A significant advantage is that irregular shapes and larger integral structures can also be coated. However, sol-gel coatings tend to fail if the film thickness exceeds 5 μm because of shrinkage strains during drying, and densification of the as-deposited xerogel film. Phani et al. (2005) reported that sol-gel coatings consisting of ZrO_2 as well as 15 wt% of CeO_2 could be deposited on magnesium alloys AZ91D and AZ31 by the dip coating technique. Coatings

deposited on AZ91D and AZ31 substrates exhibited good corrosion resistance in the salt spray test performed for 96 hr.

Polymer plating is the electrochemical polymerization of a polymer film on the surface of a substrate that functions as one of the electrodes in the electrochemical cell. This process has been used to deposit triazine disulfidemers on the surface of magnesium alloy AZ91D by the electrochemical processing of triazine dithiols at the surface of a magnesium anode (Mori, 2000).

The polymer films produced were found to suppress corrosion by suppressing the transfer of water, oxygen and electrons to the magnesium surface. Corrosion protection was found to depend on the thickness of the film produced and the type of alkyl substituent on the monomer. This process is still in its infancy and will require more study before a marketable process can be developed.

Plasma polymerization can be applied from the gas phase by exposing a substrate to a reactive gas in the presence of glow discharge plasma. The low surface energy coating produced is resistant to atmospheric water, chlorine and oxygen. It is also tough, scratch-resistant and smooth.

3.6.6 Micro-Arc Oxidation (MAO)

As mentioned above, there are many corrosion control techniques have been developed for magnesium alloys. However, it appears that their disadvantages outweigh than their advantages. Therefore, the surface engineering industry needs to new processes which have environmentally friendly and small capital investment. Micro-arc oxidation (MAO), also called Plasma Electrolytic Oxidation (PEO), Electrolytic Plasma Oxidation (EPO) Anodic Plasma Oxidation (ANOF) plasma anodizing which is a promising surface treatment for hexavalent chromium replacement in anti-corrosion protection or in the improvement of the tribological properties of lightweight metal structures. The plasma is discharged by an external power source in a slightly alkaline electrolyte near the surface of the workpiece,

which acts as the anode of the system. This MAO can be distinguished from classical anodizing by the use of voltages above the dielectric breakdown potential of the anodic oxide being formed. The oxygen plasma generated causes partial short-term surface melting and ultimately the formation of an oxide–ceramic layer.

The historical background, development, principles, properties, application areas and summary of the literature review of MAO technique will be discussed in detailed in next Chapter.

CHAPTER FOUR
MICRO-ARC OXIDATION

4.1 Background

The global popularity of Mg alloys is gaining day by day especially in aerospace, automotive, defence, biotechnology, communication industry due to their low densities and high strength/weight ratio. Unfortunately, Mg alloys are extremely vulnerable to corrosion especially in Cl^-, Br^-, SO_4^{2-} containing environments resulting from their high galvanic activity that have hindered its widespread use in many applications. Several surface treatments techniques have been developed in order to provide corrosion protection of magnesium. Each of the techniques has its own merits and limitations. The surface treatment industry is focused on the newer, unique, environmental friendly, functional and cost-effective alternatives.

MAO process differs from conventional anodizing with respect to its high operating voltages in environmentally friendly alkaline electrolyte which refers to the same process as plasma electrolytic oxidation (PEO), electrolytic plasma oxidation (EPO), anodic spark deposition (ASD), Anodishe Oxidation an Funkenanladung (ANOF in German), microplasmic oxidation (MPO), plasma anodizing and spark anodizing which is a cost-effective, environmental friendly surface engineering technique based on plasma - assisted anodic oxidation to form a protective, thick, hard, dense and well adhered ceramic coating on valve metals surface such as Mg, Al, Ti, Nb, Zr, Ta, Hf and their alloys (Shatrov & Samsonov. 2002) whose metal oxides easily form on the surface when contact to air or aqueous environment that exhibit insulating behavior with increasing potential until a critical breakdown of electrical field strength during the initial stage of the MAO process (Rudnev et al, 2006).

Exceeding the critical electrical breakdown potential, the barrier film formed on the surface of valve metals is broken and many tiny sparks cover the whole surface

rapidly. A number of discrete discharge channels form in the oxide layer as a result of dielectric stability loss. Due to strength electric field, anionic compounds draw in to the channel. At the same time, metal atoms ionize in these discharge channels via thermal ionization mechanisms to form metal oxides which then erupt into the electrolyte due to high pressure (Klapkiv, 1995) and solidify on the surface. Lastly, the discharge channels cool and reaction products deposit on its walls. The process repeats itself at a number of discrete localtions over the entire coating surface, leading to an overall increase in the coating thickness. The formation of a ceramic layer that offers protection to the base alloy in terms of corrosion, wear and offers other functional characteristics including thermo-optical, dielectric, thermal barrier, low friction coefficient.

4.2 Development of the MAO process

The first recorded observations of discharges during an electrolysis process were made by Fizeau and Foucault in 1844. They noted luminescence on electrode surfaces during the electrolysis of water. It is likely that this was the result of arc discharges in hydrogen bubbles. Sluginov (1880) became the first person to note a similar discharge phenomenon during the anodising of metals in 1878. Despite the phenomenon having been observed at the very inception of research into electrolysis, no attempts were made to control. The first comprehensive study of “sparking phenomena” during aluminium anodising, published by Gunterschultze & Betz (1937) in 1932, concluded that such discharges were detrimental to the properties of coatings and should be avoided.

Despite the concerns of Gunterschultze & Betz, sparking during anodising soon became an accepted part of the “spark anodising” of magnesium (Evangelides, 1951). And then Evangelides was issued a patent for the electrolytic coating of magnesium and its alloys in 1955 (Evangelides, 1955). His HAE process and similar the DOW 17 process, have since become two of the most favoured anodizing processes for magnesium. These films containing many spherical gas bubbles and porosity, to the detriment of their mechanical properties.

The synthesis of cadmium niobate by McNeill & Nordbloom in 1958 is another early example of the application of micro-arc oxidation. They used a spark discharge to synthesize $Cd_2Nb_2O_7$ on a cadmium anode in an aqueous solution of potassium niobate. It had thus been noted that constituents of the electrolyte could be incorporated into the oxide film to modify its properties and this was soon applied to the spark anodising of magnesium. Films formed in aluminate and silicate solutions were found to consist of a mixture of crystalline MgO and either $MgAl_2O_4$ or Mg_2SiO_4 respectively (McNeill & Nordbloom, 1958). McNeill & Gruss (1966) subsequently filed a wide-ranging patent for "anodic spark reaction processes and reactions". This describes the application of hard alumina, silicate or tungsten trioxide-based coatings to a wide range of metals, including iron and gold.

Significant developments and improvements to the process were subsequently undertaken in the USSR during the 1970s and 1980s. Researchers were particularly interested in the potential benefits of MAO discharges as an enhancement of the conventional anodising of aluminium. They noted that, under certain conditions, discharges provided a mechanism for faster oxide growth, and that the resulting oxide films were very hard. Gradovsky & Bayles (1974) filed the first USSR patent for a "method of coating metals using anodic discharges". Markov & Markova (1976) filed a patent for "AC and pulsed bipolar processes for the production of hard oxide ceramic coatings on Al", heralding the start of Russian research into the process as a competitor for hard anodising. Meanwhile, Van et al (1977), published the first study of the "Mechanism of Anodic Spark Deposition" in USA. This was a major milestone in the development of this process; its potential benefits had finally been recognised, and commercial interest increased markedly.

MagOxid (in Germany), Tagnite (in USA) and Keronite (in UK and USA) are the pionners of MAO technology in 21^{th} century have. These companies have provided a commercial equipment support and had to overcome initial scepticism about the cost-effectiveness of the process and have also made great progress in its efficiency. More recently, great interest has developed in the process as a method of protecting

magnesium as shown in Figure 4.1, which may lead to more widespread use of this lightweight metal.

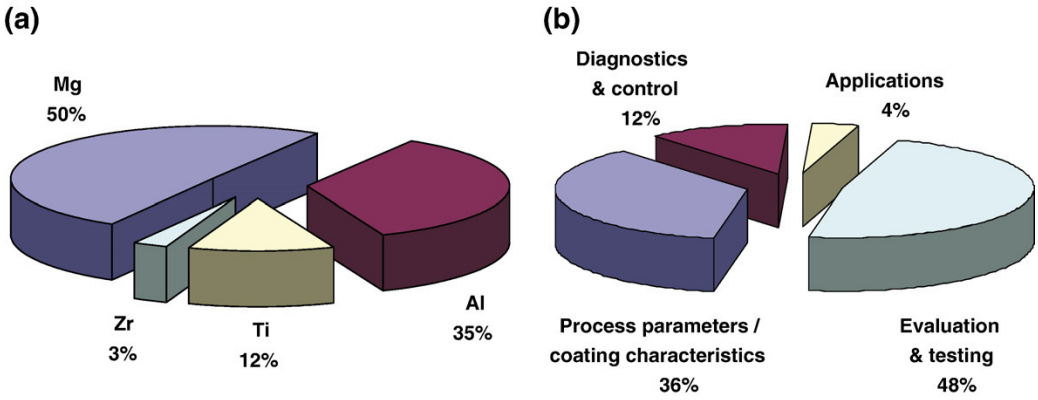

Figure 4.1 Structure of publications in MAO (2001–2006) showing (a) breakdown on materials and (b) breakdown on subjects (Yerokhin, 2007)

4.3 MAO Processing

Magnesium alloys can be subjected to anodic oxidisation however it is not possible to obtain the same level of protection as with aluminium-based materials, as the degree of coverage for MgO is 0.81 (i.e., the Pilling-Bedworth ratio is less than 1). For this reason, anodic oxide coatings applied to magnesium are porous and rough with a coarse surface structure. The anodic layer that is formed from the metal adopts oxidic hexagonal cell structures. Each cell has a pore at its centre. The schematic depiction of anodized aluminium originally published by Keller, Hunter and Robinson, as given in Figure 4.2. For theoretical reasons, it is suitable to suppose that magnesium alloys. They stated that the cell diameter of the porous section of the anodic layer on magnesium (anodised to DOW 17 standard) is 15 nm.

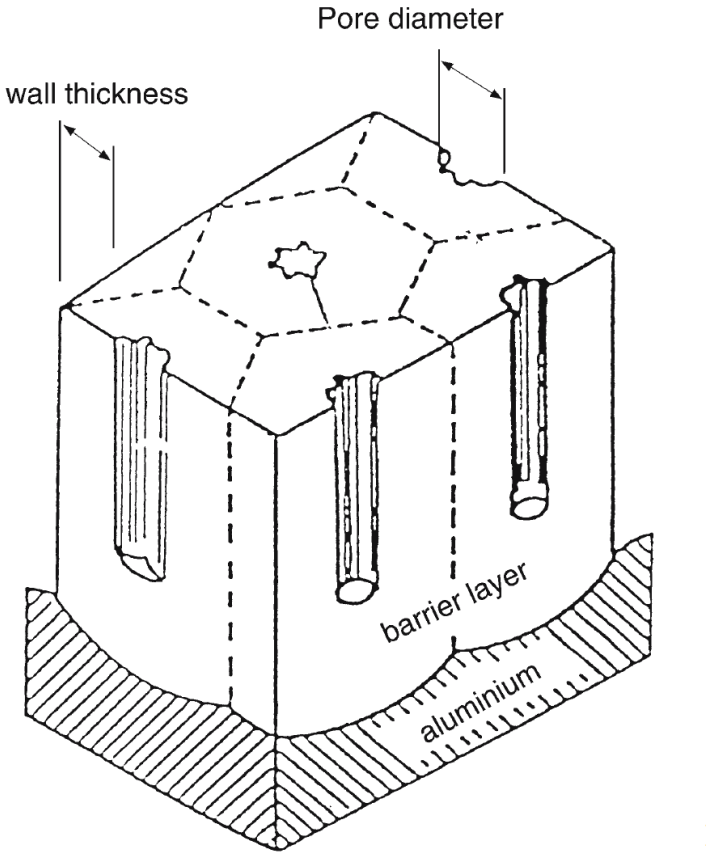

Figure 4.2 Schematic illustration of anodic layer formed on aluminium alloys during anodic oxidation (KHR Model)

The modern micro-arc oxidation process is based on a conventional anodising process. It may therefore be performed on any of the so-called “valve metals”; metals whose oxides exhibit rectifying behaviour. These include aluminium, magnesium and titanium.

Metals such as iron do not develop a stable, continuous and adherent oxide film under the conditions used, and cannot therefore be effectively anodised (McNeill & Gruss, 1966)

4.3.1 Coating Formation

Van et al (1977) concluded that the applied potentials could be sufficiently high to exceed the dielectric breakdown field at flaws in the growing oxide film. Furthermore, from direct measurement of the duration and current for a single spark, they could estimate the power and energy of these discharges. They estimated the energy to be ~3 MJ, but, given conservative estimates of the volume in which this event occurred, the energy density must have been at least 20 MJ per mole of Al_2O_3 formed in the coating. Such an energy density is easily sufficient to account for formation of molten alumina, and other observed details of the process such as the concurrent generation of gaseous oxygen.

Optimisation of the process, however, has since resulted in highly complex systems for which no complete theoretical description is available. In particular, coating growth rate and porosity have been observed to be strongly dependent on electrolyte components, temperature, and characteristics of applied current (Xue et al., 1998). Their influences on the process remains exactly unexplained.

4.3.2 Electrochemical Characteristics of MAO Process

A schematic current-voltage plot for the micro-arcing process across the oxide layer is shown in Figure 4.3.

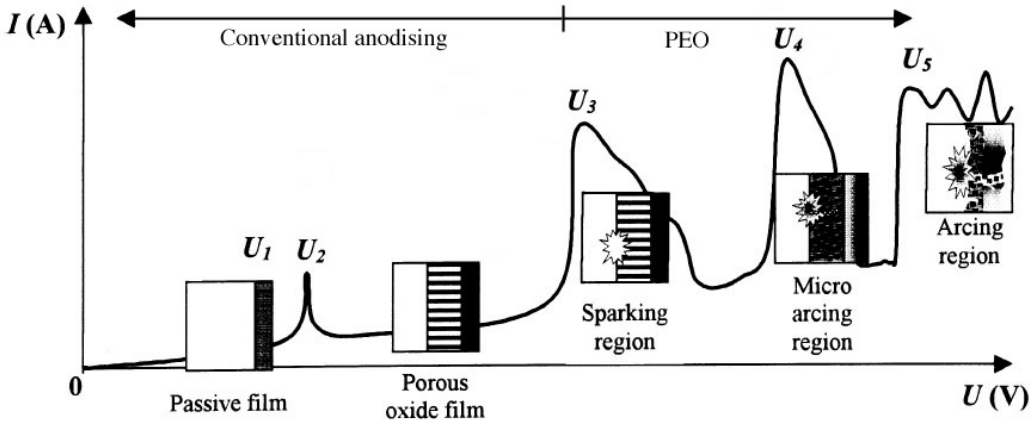

Figure 4.3 Current-voltage plot for the PEO processing regime (Yerokhin et al., 1999).

This generally accepted theory explained by Yerokhin et al (1999). Initially, as relatively low anodic potentials ($<U_1$) are applied to the immersed component, the system conforms to Faraday's laws and the current-voltage characteristics of the electrolytic cell vary according to Ohm's law. This is the region from 0 to U_1. Because the materials are valve metals, they passivate and an insulating barrier oxide film grows slowly at the metal/electrolyte interface. At U_2, which is the corrosion potential of the metal, the passive film begins to re-dissolve. As the potential is increased further (in the region U_2-U_3), re-passivation occurs and a porous oxide film begins to grow. This is the regime utilized by conventional anodising.

However, as the potential across this film is raised beyond the breakdown potential (U_3) for the given thickness of oxide film, dielectric breakdown occurs by impact ionisation at discrete locations, accompanied by visible sparks. These migrate across the surface of the film, facilitating its continued growth. The magnitude of U_3 is 150-300 V for a typical barrier oxide film of magnesium depended on the conductivity of electrolyte bath. At U_4, the mechanism of impact ionisation is supported by the onset of thermal ionisation processes, where electron avalanches occur. It is in this regime (in the region U_4 to U_5), that low-power, and relatively short-lived "micro-discharges" occur within the oxide film, gradually building up the coating thickness. Above U_5, the arc micro-discharges transform into powerful arcs, which may be destructive and inhibit further growth of the film.

In the practical application of the MAO process, however, there is no clear transition between the sparking regime and the micro-arcing regime or indeed the arcing regime. Observations are further complicated by the fact that a concurrent set of discharges can occur in a plasma envelope formed by the gas evolved at the electrode surface.(Yerokhin et al, 1999).

Recently, Rakoch et al. (2006) proposed that an another accepted growth mechanism theory of The Oxide Ceramic Coatings (OCC) on the metallic materials during MAO process. According to this theory, plasma discharges in the anodic halfperiod of current arise after the formation of a continuous dielectric layer. The

dielectric layer, i.e., a vapour-gas represents a continuous organic or oxide coating covered with a vapor-gas phase in pores (VGPP). The VGPP is formed as a result of oxygen evolution,

$$4OH^- \rightarrow O_2 + 2H_2O + 4e \quad (4.1)$$

followed by vaporization due to joule heating. When the MAO process is carried out, electrolyte pH in the pores substantially decreases due to anodic reactions.

$$Me + mH_2O \rightarrow Me^{n+}.\ mH_2O + ne \quad (4.2)$$

$$Me^{n+}.\ mH_2O + nOH^- \rightarrow Me(OH)_n + mH_2O \quad (4.3)$$

The coating grows mainly in microdischarge channels and neighboring areas, because these channels are the sites where the plasma-chemical reactions occur, substitiantly energy is libareted and pressure is incredibely increases. They have stated that the coating grow rate on the surface is the function of energy libarated in the microdischarge channel and the microdischarges density. Resulting of the intense exothermic oxidation of the metal at the discharge channel is ionized. Thermal transformations and solidification of plasma components brought out from the discharge channels react with the electrolyte on the coating areas adjacent to these channels. Furthermore dielectrical strength of the coating and VGP depend on the electrolyte composition. The stages of processes occurring after the breakdown of dielectric coating were illustrated in Figure 4.4.

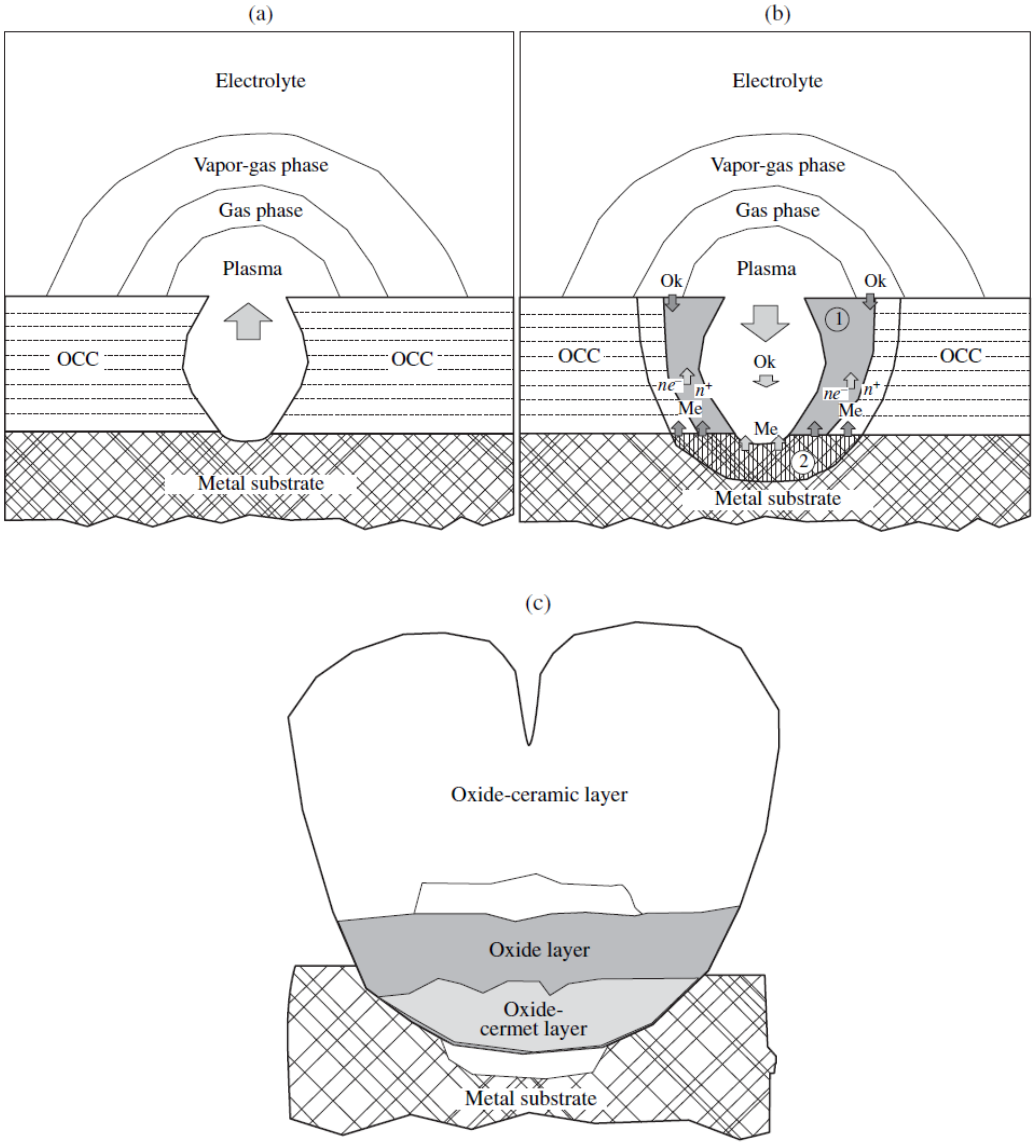

Figure 4.4 Stages of processes occurring after the breakdown of dielectric coating: a) breakdown, (b) high temperature oxidation zone; (c) a local area fragment of the coating formed after breakdown, (1) heat effected zone, (2) fused metal substrate (Rakoch et al., 2006).

4.3.3 Discharge Characteristics

Each discharge is the result of a localised loss of dielectric stability (Van et al 1977). This occurs at flaws in the barrier film. At these flaws, an electron avalanche occurs through the oxide (Bonilla et al., 2002).

Klapkiv (1995) suggested that the duration of a discharge is of the order of 100 μs. In addition to that, Sundararajan & Krishna (2003) proposed that the material within a channel 1-10 μm in diameter is heated up to about 10^4 K.

The time period for heating is estimated to be as little as 1 μs (Yerokhin et al., 1999) and local pressures of up to 1000 MPa (10,000 atm) (Yerokhin et al., 2000) can be inferred. Under these conditions, the material is locally ionised and plasma-chemical reactions occur. The strong electric field draws anionic components into the channel from the electrolyte, while magnesium and other alloying elements are drawn into the channel from the substrate to be oxidised.

According to Sundarajan & Krishna (2003) the initial discharge density is the order of $1x10^4$ μm^{-2}, but this falls exponentially so that once the coating has grown to a thickness of about 10 μm, it is approximately $1x10^3$ μm^{-2}.

More recently, real time imaging of population of visible discharges suggested a spatial density decreasing from an initial density of $3.2x10^6$ m^{-2} to $7.7x10^5$ m^{-2} over 80 minutes (Yerokhin et al., 2003).

4.3.4 Phase Formation During Film Growth

The plasma-chemical reactions which occur during each discharge ultimately result in the formation of metal oxides, phospates, silicates, aluminates and other compounds as they combine anionic components from the electrolyte with the substrate metal and its alloying elements.

According to Wang et al., (2005), the characters of the oxidation process, the anodic coatings can be divided into three types, the passive film, the micro-spark ceramic coating and the spark ceramic coating. The variations in coating growth as function of the oxidation voltage are shown in Figure 4.5. They suggested that the layer grows about 50% into the original magnesium surface and 50% is above the original surface level.

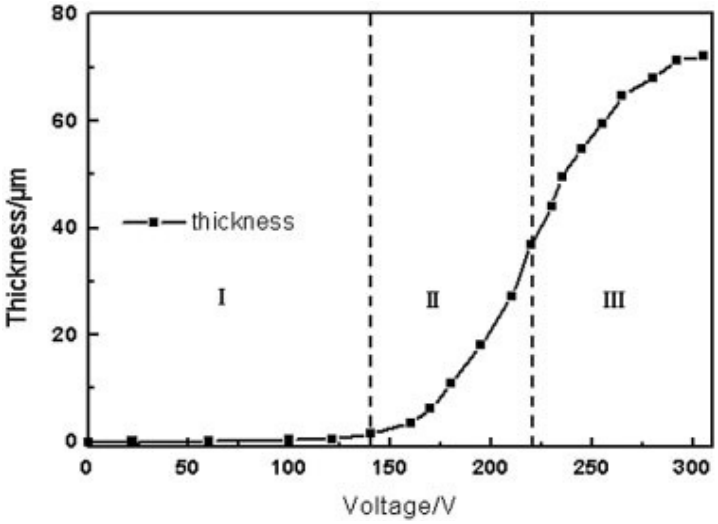

Figure 4.5 Variations in coating thickness with applied voltage (Wang et al., 2005)

In the passive film section (below 140 V), the surface was covered with a passive film which thickness increased tardily with oxidation voltage and finally reached ~1μm. In the micro-spark ceramic coating section (section II), these coatings were gray thick oxide coatings, which thickness increased sharply with impressed voltage and reached about 30 μm, as result of the high-voltage spark treatment. Then, the spark ceramic coating section, with voltage increased from 220 V to 300 V, the thickness of the coating first increased sharply and soon mildly with the thickness of about 75 lm in the end (section III), which was the thickest among the three types (Wang et al., 2005).

When growing a MAO coating on magnesium, the bulk of the coating consists of magnesium oxide (MgO; periclase), although oxides of all the other alloying elements are likely to become incorporated in the coating as well. Hsiao and Tsai (2005) explained that the electrochemical reactions occured on AZ91 magnesium alloys during the MAO process;

$$Mg - 2e^- = Mg^{2+} \quad (4.4)$$

$$Al - 3e^- = Al^{3+} \quad (4.5)$$

$$Mg^{2+} + 2OH^- = Mg(OH)_2 \quad (4.6)$$

$$Al^{3+} + 3OH^- = Al(OH)_3 \quad (4.7)$$

$$Al^{3+} + 2AlO_2^- = MgAl_2O_4 \quad (4.8)$$

$$Mg(OH)_2 = MgO + H_2O \quad (4.9)$$

The composition of MAO coatings is dependent on both the substrate alloy and the electrolyte composition, as well as many other parameters of the treatment regime, such as applied current density and applied voltage profiles. The plasma discharges facilitate rapid mixing and reaction of the compounds present, and a wide range of compounds, phases, and microstructures can be formed. The high temperatures (~10^4 K) and very rapid cooling rates (as high as 10^8 K s^{-1}) to which the coating is subjected can result in non-equilibrium phases. It has been suggested that the material formed during each plasma discharge is rapidly quenched by contact with the electrolyte, with cooling rates of up to 10^8 K s^{-1} (Yerokhin et al., 1999).

4.4 Effect of Process Parameters

The process parameters employed a crucial role in the characteristics of oxide coatings. Zhang et al. (2002) found that the properties of oxide coatings were strongly influenced by process parameters applied. With the increase of solution temperature the film thickness decreases but crystalinity increases. They found that the thickness of MAO coatings depends on treatment time and applied current density. In addition to that, they compared the oxide coating fabricated by MAO process with the anodic coatings formed by HAE and DOW 17 process. It was observed that the MAO coatings were smoother and more uniform.

Much research has highlighted that the significant role which the electrolyte plays in the MAO coating process and in providing the of magnesium and its alloys with the desired coating. Thus, in general, the nature and properties of the coatings formed on magnesium alloys depends on the composition of the electrolyte. The KOH or NaOH serves to promote electrolytic behaviour (by providing sufficient conductivity) and to adjust the electrolyte pH. Silicates enhance the deposition rate, but can result in porosity and lower coating hardness. Phosphates and other additions contribute to coating hardness and to surface smoothness (Liang, Hu and Hao 2007).

The additives such as ammonia or amines dimethylamine, ethylamine, diethanolamine, triethanolamine etc might be use to decrease or to delay spark or plasma discharge in order to obtain crack-less coating microstructure (Guo et al 2004). Hexamethylenetetramine was a useful additive for removing cracks and reducing the size of pores in an oxide coating resulted in an oxide coating with better composition, fewer cracks, lower porosity, smaller pores, and better anti-corrosion ability. (Bai & Chen, 2009) The addition of KF contributes to increase the electrolyte conductivity, and change the spark discharge characteristics which promotes the conversion of the larger spark discharges to fine spark discharges and increases the number of spark discharges (Liang et al., 2005). They found that the introduction of KF into the electrolytic solution results in formation of the microarc oxidation coating of fine grain structure and good homogeneousness. The reason is that the formation of a compact barrier type passive film on the substrate surface in the presence of fluoride ions, which protects the active Mg alloy substrate from severe oxidation and slows down the anodic dissolution in the initial microarc oxidation stage. To modify the interfacial tension, different surfactants can be used as dispersing agent, wetting agent or foaming agent to inhibit the defect development or to improve the coating quality. Guo & An (2006) indicated that surfactants influence strongly the morphology of ceramic coatings and play an essential role to fabricate a ceramic coating with low porosity.

The β-phase in an anodized Mg-Al alloy also plays an important role in the corrosion of the anodized alloy. The corrosion performance of the anodized Mg-Al alloys depends on the same phase constituents that also characterise the corrosion behaviour of the substrate alloys. The corrosion resistance of the MAO coating was closely associated with the corrosion performance of the substrate alloy (Shi et al., 2005). Kotler (1977) showed that the same anodized coating had different corrosion resistance if it was formed on different substrate magnesium alloys such as AZ31B wrought sheet and AZ91B die cast plate. Khaselev and Yahalom have studied the influence of the aluminum content and the amount of the β phase in the magnesium alloy substrate on the anodization process and found that the aluminum content in the alloy is beneficial for passivity of Mg-Al alloys (Khalasev & Yahalom, 1998).

One of the most important phenomenon is “breakdown” of dielectric film on the the surface of valve metals during MAO process. Khalasev et al. (2001) found that the breakdown voltages of Mg-Al alloys increased with an increase in Al content in the alloy composition. They suggested that the growth starts on α-phase and continued on β-phase. Ikonopisov (1977) fully described the fundamantals breakdown phenomenon occured at MAO process. Ikonopisov summarized that the brekdown voltage depend on nature of anodized metal because, the anodized metal has the different band gap of corrosponding their oxide. Moreover, the breakdown voltage depended on electrolyte composition and resistivity. He has developed an equation about the breakdown voltage;

$$V_B = a_B + b_B \log \Omega \qquad (4.10)$$

where a_B and b_B are constants for anodized metal and electrolyte composition respectively and is Ω the electrolyte resistivity. According to Ikonopisov, the breakdown voltage is practically independent of the current density, electrolyte temperature, surface topography, electrolyte stirring rate and the current increasing regime.

An another important process paramater (might be the most important part of process) is power supply modes. At beginning, Direct Current(DC) or Alternative Current (AC) was employed in the MAO process. It is believed that the asymetric AC mode is more effective way to deposit the MAO coatings than DC mode. However, the anodic coatings performed with AC mode are rough and non-uniform. Yerokhin et al (2004) tried to modify the coating morfologies by altering the sparks formation during MAO process. They utilized a pulsed bipolar current to obtain a denser and uniform microstructure with fine-grained on Mg alloys. They achieved that the coating growth rate was up to 10 μm/min. According to Yerokhin et al. (2004), pulsed bipolar current was beneficial to elemination of structural imperfections such as microcracks and pores which decreases corrosion resistance of MAO coatings. Furthermore, they suggested that pulsed bipolar current allows to

recrystalization of quenched molten metal during the formation of ceramic-like structure.

Jin et al. (2006) compared the MAO coating properties on AZ91D magnesium alloy performed with DC mode and Pulsed Bipolar (PB) DC mode. They found that the PB mode gives a higher oxidation rate and the MAO coatings perfomed with PB mode is denser, harder and has lower friction coefficent. This can attributed to pulses which enable the creation of shorter and more energetic micro-discharge events, ensuring a better balance between"oxidazing and fusing/recrystalling aspects of the coating formation. Thus, bipolar system is believed to allow three to five time enhancement of the coating deposition rate combined with substantial improvement in surface layer quality, with less porosity and roughness as well as with different phase composition (Yerokhin et al., 2004).

Liang et al. (2007), stated that the constant current density mode (galvanostatic mode) using for MAO process of magnesium alloys are beneficial to saving time and easy control the oxidation process.

To improve the coating properties, the ultrasonic power technique was employed by Guo et al. (2004). The ultrasound power enhances the growth rate of anodic coatings possibly because of an increase in the rate of mass transfer of reactants and products through the film. It also plays an important role in the formation of coating structure and the distribution of coating composition. They found that the anodic coatings consisted of three layer and ultrasonic power act an important role on coating formation and enhance growth rate. The three layer anodic coatings consisted of an inner dense layer with thickness of 0.5-0.7 μm, a functional layer which has 80-90% of total coating thickness where between dense and rough outer layer and last porous and eventually a rough outer layer. Schematic depiction of the structure of an oxide ceramic coating applied to magnesium- based materials was illustrated in Figure 4.6.

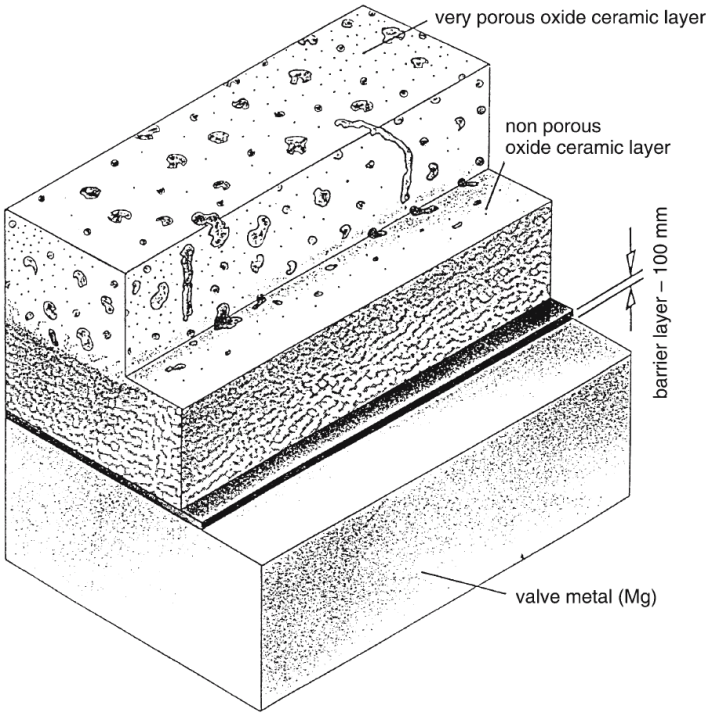

Figure 4.6 Schematic depiction of the structure of an oxide ceramic coating applied to magnesium- based materials.

Lv et al. (2008) investigated the employed current frequency on the morphology of MAO coatings. They found that the current frequency directly affects to coating surface layer quality. Coatings which performed with high frequency, had smaller pore size and much denser than at low frequency due to the longer-time discharges results in high temperature, which make more material molten in the discharge channels was observed with performing low frequency.

Chang & Kim (2008) concluded that the aging treatment has a deleterious influence on the formation and mechanical properties of the coatings on AM60 magnesium alloy because the precipitates cause the decrease of soluble Al playing a role in forming the coatings.

4.5 Corrosion Protection of MAO Coatings

A number of studies on the electrochemical behaviour of magnesium alloys that were MAO coated in silicate (Cai et al., 2006), (Liang, Hu & Hao, 2007), (Duan et

al., 2007) and phosphate electrolytes were published (Arrabal et al., 2008), (Luo et al 2008). Both of the coatings increased the corrosion resistance of Mg alloys excessively. Duan et al. (2007) found that the phosphates were useful to enhance the corrosion resistance of inner barrier layer of MAO films. According to these studies, many factors affect on the corrosion resistance of MAO coatings such as thickness, roughness, porosity, phase composition, electrolyte additives and current density waveform. To sum up, the anti-corrosion properties of MAO films depend on the total amount of porosity, pore size distribution and presence or absence of pore interconnectivity with substrate.

In order to enhance the protective properties of MAO coating on magnesium alloys, there would be of great significance to remedy the surface defects of MAO coating. Thus post sealing treatments play a crucial role for plugging the pores and enhance the protection against corrosion. Also, the sealing agent must be strongly bonded to coating chemically or physically. The theory of sealing firstly proposed by Murphy (1967) suggests that hydroxyl ions penetrate the porous layer and replace the anions of the electrolyte in which the film was formed. The result of this anion exchange is the formation of an inert hydrate oxide skin over the internal pore surfaces and on the pore walls effectively blocking off.

The options for sealing MAO coatings in order to physical barrier with external agents include immersion in phosphate or silicate impregnation treatments, sol-gel, powder-coating and E-coating etc. (Hutchins, Shashkov and Samsonov 2004) and (Hutchins, Shrestha & Sturgeon, 2004). Duan et al. (2006) and Tamar & Mandler (2008) achieved that the significant improvements on the corrosion resistance of magnesium alloys by forming homogenous, crack–free and less porosity containing multilayer composite sol-gel coating. In addition to that, Hsiao et al. (2007) found that the beneficial effect of post-baking-treatment on the corrosion resistance of MAO films by the way of increasing crystalinity depended on baking temperature.

4.6 Applications of MAO

The process has been used commercially in Russia for over a decade, principally for the coating of machine parts subject to high wear rates. It has been used in the textile, aerospace and automotive industries.

The technology spread to Europe and the USA in 1995, although initially the process found only limited use in niche markets, including wear-resistant aluminium kitchen-ware, and lightweight magnesium cases and frames for consumer electronics. It is now becoming more widely accepted in the textile industry and petrochemical industries, again for the coating of machinery subject to high wear.

The useful properties of MAO coatings are slowly being recognised and their use may become widespread in automotive and aerospace applications.

For automotive applications, it is also important that the coating should provide a good base for subsequent application of paint. MAO coatings are very suitable for this, which has led to further interest in the possibility of impregnation by a wide range of compounds including sol-gels and polymers such as Teflon. This can also be exploited to slightly modify resulting oxides, by doping them to enhance properties such as optical characteristics. The prospect of creating black coatings is particularly attractive. It is directly beneficial in optical instruments, where flakes from peeling paint could be a problem, and where conventional black anodising is becoming prohibitively expensive, due to the environmental cost of chromate disposal. Doped MAO coatings can produce a very absorbent and uniform black, which is more stable under long-term exposure than the organic dyestuffs or metallic pigments used to colour anodised coatings (Shrestha et al., 2003).

MAO coatings have also been used in space applications because of their attractive thermo-optical properties, and because they show good resistance to the ‘cold welding’, which might otherwise be induced in aluminium parts by vibrations upon launch (Shrestha et al., 2003). Some of these application areas are:

– Corrosion (including galvanic corrosion) protection of magnesium
– covers (e.g. cam cover),
– housings (e.g. gearbox),
– cases (e.g. computers, mobile phones, consumer electronics), etc.
– panels,
– doors,
– housings,
– covers etc.
– bearing surfaces (e.g. belt pulleys, engine oil pumps),
– turbine components, etc.

The most important factors regarding the MAO process is high electrical energy consumption which result from the high current density used during MAO process. Such high energy consumption is the main problem restricting its industrial application. It has been found that ~90% of the energy involved transforms to heat, cousing an temperature rise of the electrolyte during MAO (Li & Jiang, 2007).

4.7. Industrial Processes

4.7.1 Magoxid-Coat Process

The Magoxid-Coat process has his origins in Russia and was further developed by AHC-Oberflächentechnik GmbH in Germany. In order to obtain coatings that have little or no inherent colour, that can be easily coloured, and that provide a satisfactory adhesive base for lacquering or subsequent processing, a low-alkali aqueous electrolyte is used. It contains borate or sulphate anions, phosphate and fluoride or chloride ions. The pH value is preferably 8-9 is employed. Especially appropriate for buffering the electrolytes are amines that react weakly in alkaline solutions. These amines, in particular cyclic amines such as pyridine, β-picoline, piperidine and piperazine, are generally dissolving readily in water. Other satisfactory water-soluble amines that can be employed are for example sodium sulphanilate, dimethylamine, ethylamine, diethylamine and hexamethylenetetramine. A direct current is applied

and is either briefly turned off or its polarity is completely reversed to allow the formation of manganese phosphate and magnesium fluoride and optionally magnesium aluminate on the surface. It is preferable to work with a voltage that increases to 400 volts. The current density is in particular 1 – 2 A/dm^2. The present process is patented in the United States (U.S. Patent 4,978,432A), Europe (EP 0333048B1) and Japan (JP5-51679B4). Normally, layers with 15–20 micrometer thickness are produced with a growth rate of 1.5 micrometer per minute. The coating consists of a mixture of MgO, $Mg(OH)_2$, MgF_2 and $MgAl_2O_4$. The colour is normally white to light gray, but can be produced in black by appropriate additions to the electrolyte.

4.7.2 Tagnite Process

The Tagnite Coating System was developed in the 1990's in the USA by Technology Applications Group Inc. as a chromate- free anodic surface treatment, and they claim, that it is providing significantly more corrosion and abrasion resistance than any chromate based coating.

The electrolyte used to form the coating is an alkaline solution clear in colour, containing no chromium (VI) or other heavy metals and operates below room temperature (40° to 60 °F). It mainly consists of an aqueous solution containing hydroxide, fluoride and silicate species which are also incorporated into the layer. The rectifier used to apply Tagnite was specifically designed for the coating. It employs a unique waveform optimized for the coating process. To ensure maximum corrosion resistance and high dielectric strength, the Tagnite coating is applied at voltages exceeding 300 volts DC. The abrasion and corrosion resistance were found to be all improved compared to the Dow and HAE processes even prior to organic finishing. The coating consists mostly of hard magnesium oxide with minor surface deposition of hard fused silicates and has a white colour.

4.7.3 Keronite Process

Keronite technology was conceived in Russia and developed in the UK by Isle Coat Ltd, a subsidiary of CFB plc. Light alloys such as aluminium, titanium and magnesium can all be treated, and the technology offers significant improvements compared with traditional methods such as hard anodizing or coating with nickel-silicon carbide. Keronite also compares favourably with spark-anodizing processes currently being developed around the world. Electrical bipolar (positive and negative) pulsed electrical current of a specific wave form in a proprietary electrolyte is used. Energy consumption of 0.01 – 0.03 KWh/µm.dm^2 of the process depends on the controllable coating rate which ranges from 1 to 5 µ/min and temperature between 20 and 50 °C. The electrolyte is a non hazardous, low concentrated alkaline solution (98% demineralized water, chrome and ammonia free), which can easily be disposed. The layer thickness can range from 10 to 80 µm.

CHAPTER FIVE
EXPERIMENTAL STUDIES

5.1 Purpose

The objective of this thesis was to produce of protective ceramic-like micro-arc oxidation coatings on AZ91D, AZ31B, AM60B, AM50B magnesium alloys and investigation of their electrochemical behaviours. With this aim firstly, the electrolyte to produce MAO coatings on AZ91D, AZ31B, AM60B and AM50B magnesium alloy substrate were prepared. A dual pH-conductivity meter was used in order to determine the electrolyte characteristics such as pH values and conductivity which affects coating structure. Prior to MAO coating process, magnesium alloy substrates were ground using various SiC paper and then cleaned with ultrasonic cleaner in 1:1 ethanol-water medium. Magnesium alloy substrates were subjected to various stages of pre-treatment before coating process. The MAO coatings which thickness of 10 µm (K10) and 25 µm (K25) have been formed using KERONITE G2 MAO system with a 25kW pulsed bipolar DC power supply in a bath with heat exchanger and circulation pump in order to investigate the effect of coating thickness on the corrosion resistance of MAO coatings. The MAO coatings of different thickness were grown by varying the processing time.

To obtain a crack free structure, different sealing post-treatment processes were applied on MAO coated AM50B and AM60B Mg alloy. Scanning Electron Microscope (SEM) equipped with Energy Dispersive X-ray Spectrometer (EDS) was used to determine the surface morphology and elemental composition of produced MAO coatings. The crystallographic phase analysis and identification of MAO coatings was carried out by X-ray diffraction (XRD). High resolution surface profilometer was used for mapping of the 3-Dimensional surface features and roughness. Electrochemical tests conducted using potentiodynamic polarization technique in 3.5% NaCl solution at room temperature in order to evaluate the efficiency of MAO coatings on the corrosion resistance of magnesium alloys.

5.2 Materials

5.2.1 Substrates

In order to prepare MAO coatings, AZ91D, AZ31B, AM60B and AM50B magnesium alloys in the form of plates provided by TUBITAK Marmara Research Center Materials Institute TURKEY, were used as substrates. Nominal compositions of the alloys used in this study are given in Table 5.1.

Table 5.1 Nominal composition of key alloying elements in Mg alloys.

Material	Composition, wt %			
	Mg	Al	Zn	Mn
AZ91D	Bal.	9	0.74	0.17
AZ31B	Bal.	2.85	1.05	0.23
AM60B	Bal.	5.9	0.05	0.27
AM50B	Bal.	5	0.01	0.28

5.2.2 Chemicals

The chemicals which were used for production of electrolyte, sample preparation, corrosive solution, cleaning, etchant, pre and post-treatment solution were listed in Table 5.2.

Table 5.2 All chemicals used in this study

Purpose	**Chemical Name**	**Formula**	**Purity**	**Supplier**
Electrolyte	Potassium Phosphate Tribasic	K_3PO_4	99.9%	Sigma
	Potassium Hydroxide	KOH	99.9%	Sigma
	Sodium Aluminate	$NaAlO_2$	99.5%	Riedel-de Haan
	Sodium Metasilicate	$Na_2SiO_3.5H_2O$	SiO_2 44-47%	Sigma

Corrosion Testing Solution	Sodium Chloride	NaCl	99.5%	Sigma Inc
Etchant	Hydroflouric Acid	HF	40%	Merck
Pre-treatment	Sodium Hydroxide	NaOH	99.9%	Sigma
	Nitric Acid	HNO_3	65%	Merck
	Ammonium Hydrogen Diflouride	NH_3HF_2	99.9%	Sigma
Post-treatment	Sodium Silicate	Na_2SiO_3	99.9%	Sigma
	Potassium dihydrogen phosphate	KH_2PO_4	99.9%	Sigma
	Methyltriethoxysilane	$C_7H_{18}O_3Si$	99%	Merck
	Ethanol	C_2H_5O	99.9%	Merck
	Hydrochloric Acid	HCl	37%	Merck
Sample Preparation	Diamond Paste	DP- HP Fine	3 micron	Struers
	Methanol	CH_3OH	99.9%	Merck -
	Lubricant	DP Blue		Struers

5.3 Preprocessing

5.3.1 Substrate Preparation

Rectangular AZ91D, AZ31B, AM50B and AM60B Mg alloy plates were supplied in high pressure die-cast plates of nominal dimension 140mm x 80mm x 3mm. To determine the phase structure and corrosion behaviour of uncoated magnesium alloys, firstly, specimens were cut off the supplied plates into 24x24 mm size. Subsequently, the metallographic test samples were cold moulded into non-conducting epoxy resin which carried out to provide contact between only top-flat exposed surfaces of the specimen with the etchant solution. All these samples were ground up to 2400 grit SiC papers and then polished with 3 µm diamond paste to obtain a mirror like surface. Afterwards they were ultrasonically cleaned with 1/1 high purity methanol-DI water to remove all residues before pre-treatment process. Etching was performed by submerging the metallographic AZ91D, AZ31B, AM50B and AM60B samples into mixture of 90 ml DI water and 10 ml 40% HF etchant solution for 3 seconds, following etched specimen surfaces were rinsed with DI water and air dried was performed for microstructure observation

5.3.2 Pre-treatment

As mentioned previous chapter, one of the most important part of coating magnesium alloys is pre-treatment process. By the pre-treatment of magnesium alloys, prior to MAO process, uniform coating can be obtained. With this purpose, Mg plates were pre-treated using various chemicals at various stages in order to clean, etch and activate the Mg surface. The pre-treatment procedures included three stages; as illustrated in Figure 5.1.

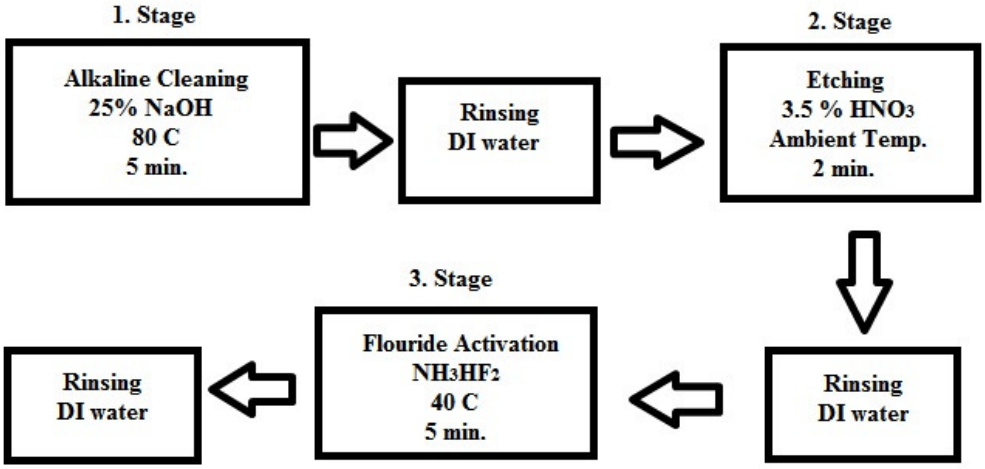

Figure 5.1 Pre-treatment stages

The etching step serves to remove surface layers of the magnesium alloys which assists in the initial anodization process. Flouride activation forms a passivating MgF_2 barrier layer which inhibits to extremely dissolution of the substrate during initial anodization process.

5.3.3 Electrolyte Preparation

The exact composition of the electrolyte can be tailored to the substrate alloy involved and the desired properties of the coating. In order to obtain uniform crack-free and continues MAO coatings in the exact stoichiometries and homogenous electrolyte must be prepared. As mentioned above, many alkaline solution including

silicates, phosphates, aluminates, borates, tungstates species and mixture of these can be used as an electrolyte. Therefore, phosphate – aluminate based solution prepared to use as an electrolyte in this research to fabricate corrosion resistant MAO coating on magnesium alloys according to literature overview. These relatively benign electrolytes present significant environmental and economical benefits.

After preparation of homogenous electrolyte, pH and conductivity values of the electrolyte were measured using dual working Mettler Toledo Sevenmulti pH and conductivity meter. The conductivity of DI water that used in electrolyte preparation is 1 μS/cm. The pH, conductivity and constituents of electrolyte that used in MAO process are given in Table 5.3

Table 5.3 pH, conductivity and constituents of electrolyte that used in MAO process

Constituents		pH (at 25°C)	Conductivity(mS/cm)
Chemical	Amount (g/l)	12.5	25.3
K_3PO_4	10		
$NaAlO_2$	5		
KOH	2		

5.4 Preparation of MAO coating

The equipment used for MAO is similar to that used for conventional anodising, but more complex, primarily due to the need for higher potentials and controlled pulses of current. In essence, however, it consists of an array of capacitor banks, which can be charged by a 50 Hz three phase supply. Their capacitance may be controlled to produce pulses of positive and negative charge to a pair of electrodes at frequency of 50 Hz. More complex equipment can provide control of the pulse frequency.

Magnesium substrates were electrically connected via an insulated aluminium or brass sample holder to the copper bus bar, and immersed in the bath of electrolyte.

KERONITE G2 MAO system with a 25kW pulsed bipolar DC power supply, heat exchanger and circulating pump was used for coating Mg alloys. In the MAO treatment Mg alloy specimen was primarily used as the anode while the stainless steel was primarily used as the cathode. Conformal electrodes can be used to enhance coating uniformity. The schematic of MAO process given in Figure 5.2. The electrolytic cell used for the MAO process was drawn in Figure 5.3.

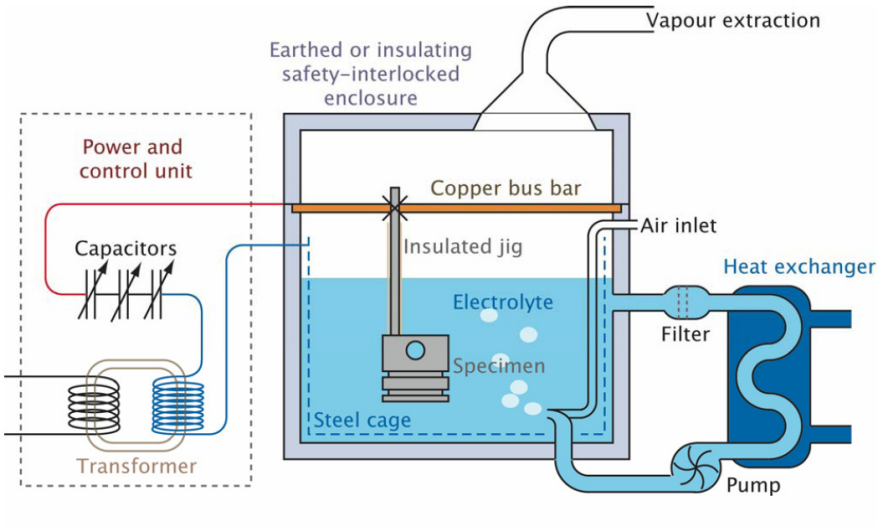

Figure 5.2 Schematic of MAO Equipment, as described above

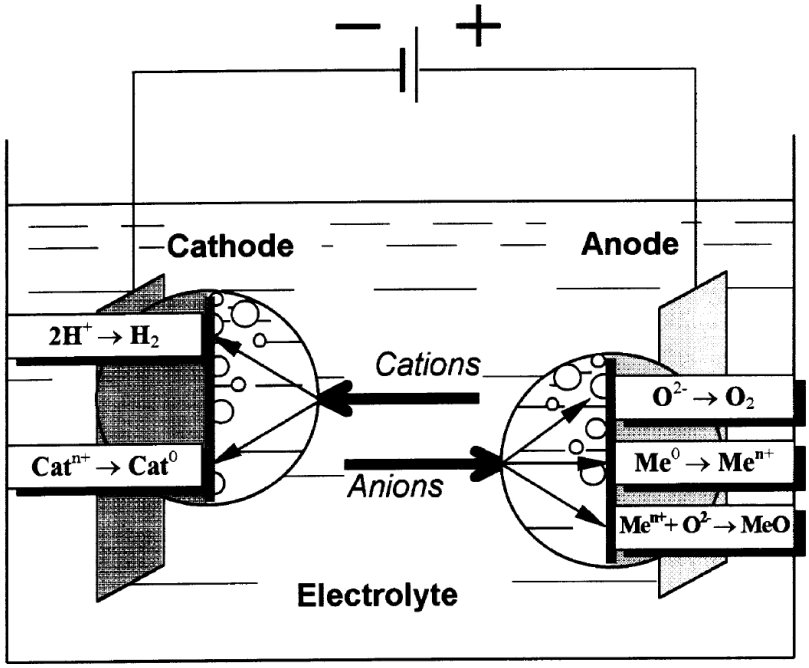

Figure 5.3 Schematic view of electrolytic cell (Yerokhin et al., 1999)

The electrolyte temperature was kept below 30ºC, if it is allowed to heat up beyond 30ºC, the coating process can be faster but the electrolyte is depleted of active ingredients much more rapidly. In our process, the electrolyte is circulated through a heat exchanger, cooled by re-circulated water, and is returned to the tank together with air, via a whistle pump, which also serves to ultrasonically agitate the electrolyte. Agitating helps to provide sufficient dissolved oxygen in the system.

Treatment times were selected to give the desired coating thicknesses, based on an expected average growth rate of 0.6- 0.7 μm/min. Therefore the electrical parameters of MAO treatment such as current density and process time were adjusted in order to keep the thickness of MAO coatings on each Mg alloys at the same value of nearly 12±2 μm(K10). In addition to that, the thickness of 24±2μm (K25) MAO coatings formed on AM50B and AM60B magnesium alloys in order to investigate the coating thickness effect on corrosion resistance of magnesium alloys.

The MAO equipment was used in autocontrol mode, whereby the effective capacitance of the pulsing power supply is set to a fixed value. This maintains a constant current output. The capacitance was adjusted to give an initial current density of 20 A /dm^2, after an initial ramp-up over 30 seconds (1. stage). During first stage, the discharging would begin, and a root-mean-square(RMS) voltage of approximately 200 V would be achieved in the positive cycles(V+), with approximately 30 V in the negative cycles (V-). Since the coating thickness grows at a constant current, these voltages increase during the process (2. and 3. Stage) . Typical profiles of the voltage amplitudes of positive and negative pulses as a function of processing duration are shown in Figure 5.4.

MAO process parameters were listed in Table 5.4. After the MAO treatment, the samples were taken out from electrolyte, rinsed using DI water and dried in the air. These samples then ready for post-treatment, corrosion testing and analysis.

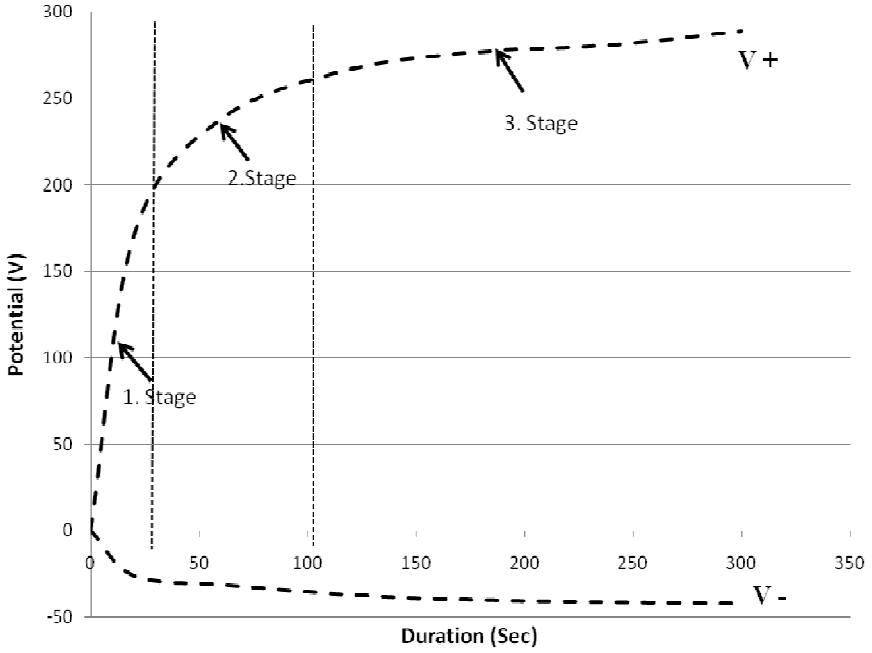

Figure 5.4 Variation of voltage amplitude of anodic (V+) and cathodic (V-) pulses of AZ 31B magnesium alloy that used during the MAO treatment

Table 5.4 MAO treatment parameters

Substrate	Electrical parameters			Treatment time (min.)		Coating thickness (µm)		Electrolyte Temperature (°C)
	Frequency (Hz)	Power supply	Current density (A/dm^2)	K10	K25	K10	K25	
AZ91D	50	25kW Pulsed bipolar DC	20	7	-	12±1	-	14-18
AZ31B					-		-	
AM50B					15		24±2	
AM60B					15		24±2	

5.5 Post-Treatment Processing

In order to enhance the protective properties of MAO coating on magnesium alloys, there would be of great significance to remedy the surface defects of MAO coating. Thus post sealing treatments play a crucial role for plugging the pores and enhance the protection against corrosion.

Following to MAO process, MAO coated AM50B and AM60B Mg alloys were immersed into alkaline phosphate (AP), alkaline silicate (AS) and silan based sol-gel post treatment solutions. Alkaline phosphate and alkaline silicate solutions consist of 12% potassium dihydrogen phosphate (KH_2PO_4) and 5 % sodium silicate (water-glass; Na_2SiO_3) in distilled water respectively. The sealing process was performed in AP and AS solutions at 60 ^oC and 95 °C respectively. MAO coated specimens were dipped into AP solution for 5 minutes and AS solution for 15 minutes then pulled up. Afterwards post treatment applied coatings were rinsed with deionised water to remove excess of solution then dried.

The sol–gel process involves the formation of a colloidal suspension of appropriate compounds (sol) and its gelation through hydrolysis followed by polycondensation until a solid network (gel) is formed. In this study, Methtriethoxlysilane (MTES) was used as sol-gel precursor which is one of the organic silicates with organosiloxane structure. Silan based sol-gel solution was prepared dissolving 14 ml MTES in 1.2 ml high purity ethanol. This solution was hydrolysed adding 2.5 ml distilled water acidulated with 0.35 ml HCl. This mixture was stirred for one hour and subsequently aged at 60 ^oC for three hours then cooled inside the oven in order to form a polymerized network structure. Afterwards MAO coated specimens were dipped vertically into the sol for 1 minute and pulled up with a rate of 5 cm/min. This procedure was repeated for three times in order to increase the thickness of the sol-gel coatings. It is believed that procedure is the one of the best way that provides optimal composite coatings by sealing the cracks and reducing porosity on the outer layer of MAO coating. Subsequent to pore sealing process, specimens were rinsed with distilled water for 3 minutes and dried at

ambient temperature for 1 day. All post treatment specimens were stored in a desiccator to prevent any contamination or gathering moisture.

5.6 Material Characterization

5.6.1 Scanning Electron Microscopy (SEM)/Energy Dispersive Spectroscopy (EDS)

The surface morphology and elemental composition of MAO coatings were examined by a Scanning Electron Microscope (JEOL-JSM 6060 SEM) with an Energy Dispersive X-ray spectroscopy (IXRF System EDS) system attachment. The SEM is equipped with a LaB_6 gun and is capable of operating as a conventional high vacuum SEM. The SEM is fully equipped with a range of secondary electron (SE) and back-scattered electron (BSE) detectors. The maximum resolution of 100nm in BS mode and 1µm in mapping mode and maximum useful magnification is 30000 X. Accelerating voltage of 20 kV was used for the SEM imaging and SEM/EDX analyses. Weight percentage distributions and X-ray mapping of elements were determined by EDS. EDS analyses including light elements are done semi-quantitatively. Corrections for atomic number, absorption and fluorescence (ZAF) are achieved through a virtual standard calibration routine. Before SEM/EDS analyses, all MAO coatings formed on magnesium alloys were sputtered with gold films to make conductive surface on ceramic like MAO coatings.

5.6.2 Optical Microscopy Analyses

A Nikon ECLIPSE ME600D digital video camera system was used to observe microstructure of the substrate magnesium alloys. The optical image analyse was carried out using LUCIA digital imaging software.

5.6.3 X-Ray Diffractions (XRD)

The phase analyses of MAO coatings were determined using Rigaku D/Max-2200/PC Model X-ray diffractometer (XRD) with a Cu K_α radiation as excitation

source and the scans were performed between 2θ values of 0^o and 90^o at a step of 1^o. Measurements were performed by applying 40 kV voltages and 36 mA current. The phase compositions of MAO coatings were determined by using Xpowder software.

5.6.4 Three Dimensional (3D) Surface Roughness Analyses

The surface imperfections such as cavities, cracks, pores affect on the surface roughness which is the most important parameter influenced on corrosion resistance of MAO coatings. 3D surface profile and corresponding average surface roughness (R_a) of MAO coatings was measured by Ambios XP-2 Model Stylus-Type Profilometer.

Surface roughness is determined with the gentle surface applied load (0.05 mg) scan through the use of a stylus with 1µm tip radius. Measurements were carried out with linear-scan stage. Step Detection, Auto level, and Auto measure options were used to assist in right and efficient data collection and analysis. 3D Rendering of MAO coating was using TrueMap software. Each roughness value is given an average of three test values. The accuracy of the roughness tests is 0.01 µm.

5.7 Electrochemical Corrosion Testing

The electrochemical tests of K10, post-treated K10, K25 MAO coatings and bare Mg alloys were performed using potentiodynamic polarization module of Gamry Reference 600 Potentiostat in naturally aerated 3.5% wt. NaCl solution at ambient temperature (298 K). The schematic representation of potentiostat was drawn in Figure 5.5. Mg and its alloys are very susceptible to corrosion especially in chloride containing environments and thus using NaCl solution in electrochemical tests allowed us a better investigation of the electrochemical properties of MAO coatings. Standard three-electrode electrochemical cell setup with a saturated calomel electrode (SCE) as reference electrode (RE), a graphite bar as counter electrode (CE) and test specimen with 3 cm^2 surface area as working electrode (WE) was used in electrochemical polarization tests. The ratio of the volume of NaCl solution/sample area was 300 ml/cm^2. Prior to starting of the polarization tests, the Open Circuit

Potential (OCP) of test specimens was allowed to stabilize for 30 minutes. After the OCP reached a stationary value, the potential was shifted from –100 mV below OCP in the noble direction at a scan rate of 0.25 mV/s. Once a current density of 1 mA/cm^2 was reached in the external circuit between the working and auxiliary electrodes, the potential scan was stopped.

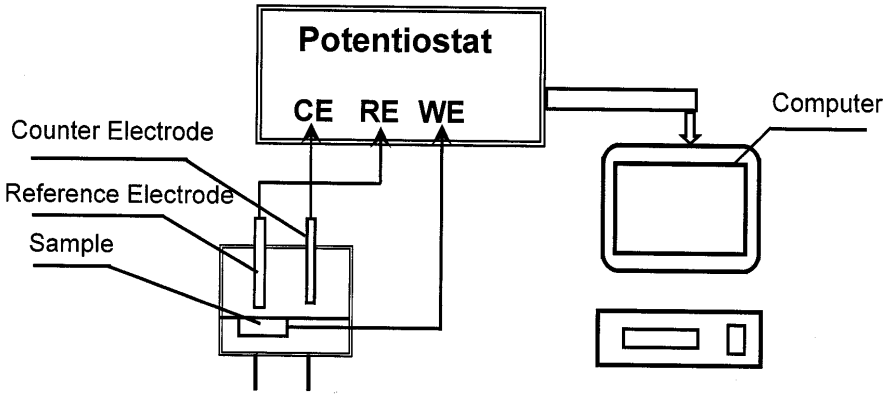

Figure 5.5 Schematic diagram of three electrode cell setup connected with potentiostat-PC

All of the electrochemical tests were performed in a PVC cell as shown in Figure 5.6.

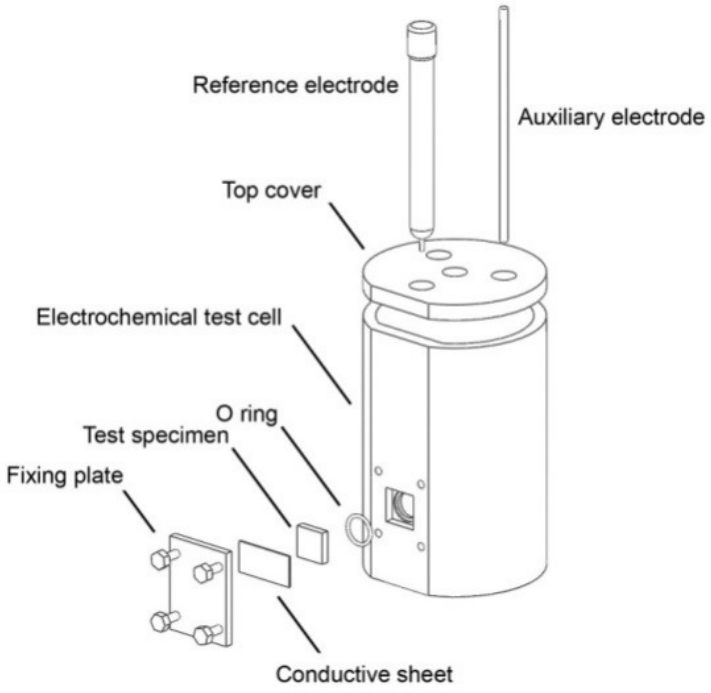

Figure 5.6 Electrochemical cell used for potentiodynamic polarization experiments of MAO coatings

Following the potentiodynamic polarization testing, the corrosion current densities, anodic and cathodic tafel constants were determined by approximately linear tafel extrapolation of polarization curves. The polarization resistance of specimens was calculated for comparison. The results were analysed using the Echem Analyst software provided by Gamry Instruments.

The corrosion current density (I_{corr}) and corrosion potential (E_{corr}, also referred as the open circuit potential OCP) are determined by extrapolation of linear parts of the polarization curves, as illustrated in Figure 5.7. The regions of linearity (with slopes β_a and β_c) are referred to as Tafel regions. The intersection point between the extrapolated regions gives the values of I_{corr} and E_{corr}. Based on approximate linear polarization resistance at E_{corr}, the polarization resistance (R_p) values were determined using the Stern-Geary Equation (Eq. 5.1).

$$Rp = \beta_a \beta_c / 2.302\, I_{corr} (\beta_a + \beta_c) \qquad (5.1)$$

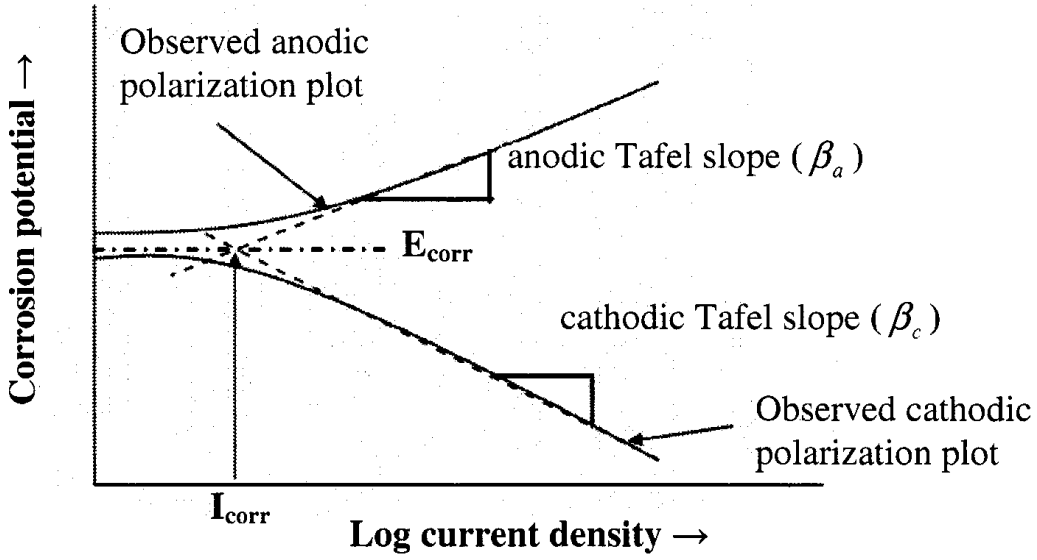

Figure 5.7 Determination of corrosion current density by extrapolation of linear parts of the polarization curve.

Acording to Faraday's Law, the corrosion current density is related to the corrosion rate (CR) by the relationship from the Equation 5.2.

$$CR = a\ Icorr / n.F \qquad (5.2)$$

where F is the Faraday's constant (96500 coulombs/ equivalent), a is the atomic weight and n is the number of electrons exchanged. From the equations 5.1 and 5.2, it can be clearly seen that there is an inverse proportional between the Rp and CR.

In many practical situations, this number needs to be transformed into a penetration rate to make a practical corrosion prediction, to enable comparison with mass loss derived from potentiodynamic test results.

$$\text{Corr Rate} = K.I_{corr}.EW \qquad (5.3)$$

where EW is equivalent weight of alloy (g/equivalent), K is a constant with a value of 0.0895 that defines the unit for the corrosion rate (mg/cm^{-2}/year).

The equivalent weight is more complex in the case of alloys because it must account for all of the elements that are being oxidized and contributing to corrosion. If corrosion does not occur selectively then all metallic components have to be considered at their concentrations in the alloy. If only certain elements participate, then only those elements need be considered. The equivalent weight for the alloy is given by:

$$EW = \sum (n.f) / A \qquad (5.4)$$

N is valance of alloying element (equivalent/mole), f is the mass fraction of alloying element and A is atomic mass of element(gram/mole). Elements that have a mass fraction of less than 0.01 (less than 1% by weight) can be ignored in the calculation. Valence assignments for elements having more than one valence state can be tricky. One approach to making the estimate of the proper valence is to

measure the corrosion potential of the alloy in the environment and measure the pH. Placing that coordinate on the potential-pH diagram for the element would allow an estimate to be made of the most stable valence under those conditions. Oxidation reactions of the main elements are present in the chemical composition of Mg alloys in the aqueous solutions;

$$Mg \rightarrow Mg^{+2} + 2\,e^{-} \quad (5.5)$$

$$Al \rightarrow Al^{+3} + 3e^{-} \quad (5.6)$$

$$Zn \rightarrow Zn^{+2} + 2\,e^{-} \quad (5.7)$$

Calculated EW values according to nominal compositions of magnesium alloys were given in Table 5.4

Table 5.4 Equivalent Weight(EW) of Magnesium alloy that used in this study

Magnesium Alloy	**Equivalent Weight (EW) (g/equivalent)**
AZ91D	12.00
AZ31B	12.3
AM60B	12.1
AM50B	12.07

CHAPTER SIX
RESULTS AND DISCUSSION

The results of this research can be categorized into two parts; (a) characterization of AZ91D, AZ31B, AM60B and AM50B magnesium alloy substrates, and MAO coatings and (b) electrochemical tests.

6.1 Substrate Characterization

6.1.1 Microstructures of Mg Alloy Substrates

In order to prepare MAO coatings, AZ91D, AZ31B, AM60B and AM50B magnesium alloys in the form of plates provided by TUBITAK Marmara Research Center Materials Institute TURKEY, were used as substrates.

Magnesium is subject to dissolution by most acids. There are a few exceptions, such as chromic acid and hydrofluoric acid. Very slow dissolution of magnesium in chromic acid is due to its becoming passive in this acid. An insoluble surface film of MgF_2 is formed which protects against further attack, is the reason why magnesium is resistant to hydrofluoric acid. Nonetheless, β phase in magnesium alloys is sensitive to hydrofluoric acid attack which reacts with HF. Therefore etching was performed by submerging the metallographic AZ91D, AZ31B, AM50B and AM60B samples into mixture of 90 ml DI water and 10 ml 40% HF etchant solution for 3 seconds in order to investigate the microstructure of magnesium alloys.

Figure 6.1(a-d) shows the microstructures of AZ and AM series magnesium alloy substrates. It is found that the microstructures of magnesium alloys consist of two phases. The α Mg matrix is an a Mg-Al solid solution with the same crystal structure as pure magnesium. The β- intermetallics ($Mg_{17}Al_{12}$) which have grown from the primary dendrites, are homogeneously dispersed along boundaries of α grains in the fine veined particles. The β precipitates, which are easily distinguished by the black

colour. The β precipitates sometimes present as Mg_4Al_3. The finer α Mg and thicker β dendrites were observed on the surface layer of AZ series magnesium alloys depended on a higher content of β phase. Al is known to have a beneficial effect on the passivity of Mg alloys (Khaselev & Yahalom, 1998) With the increasing Al content in the solid-solution, the β phase increases (Lunder et al., 1989). In AZ series, zinc is added as alloying element which decreases the grain size of bulk alloy (Becerra & Pekguleryuz, 2009) hindering the movement of the recrystallized grain boundary and thus enhances the corrosion resistance improving the stability of compact passive film formed on the surface (Yin et al., 2008). The presence of Zn (1% at wt) in the ternary intermetallics of Mg-Al-Zn system transforms β phase ($Mg_{17}Al_{12}$) to $Mg_{17}(Al,Zn)_{12}$ (Bowles et al 2007) which leads to increase the volume fraction of β phase (Czerwinski, 2008) so that increasing volume fraction results in homogenous distribution of β phase particles in the bulk alloy.

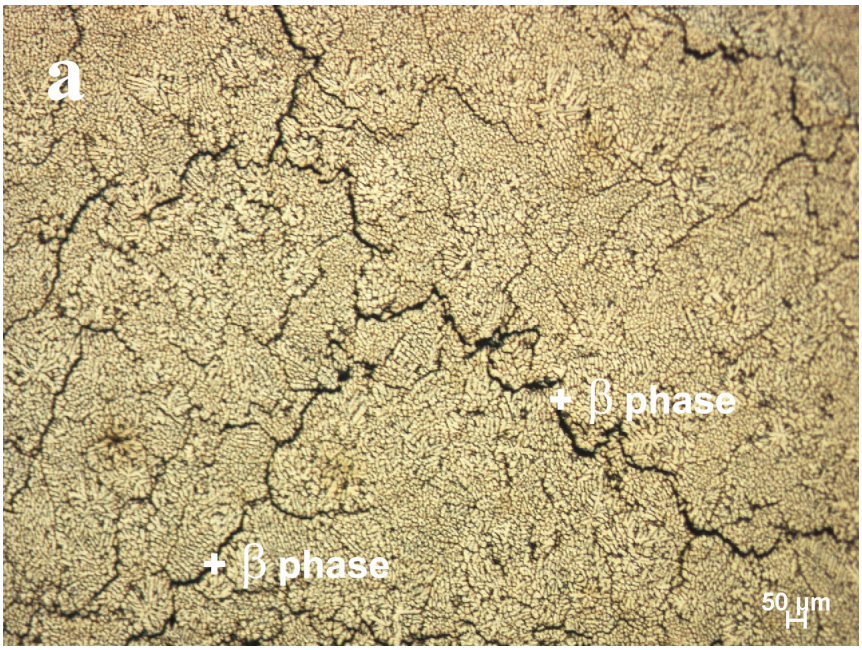

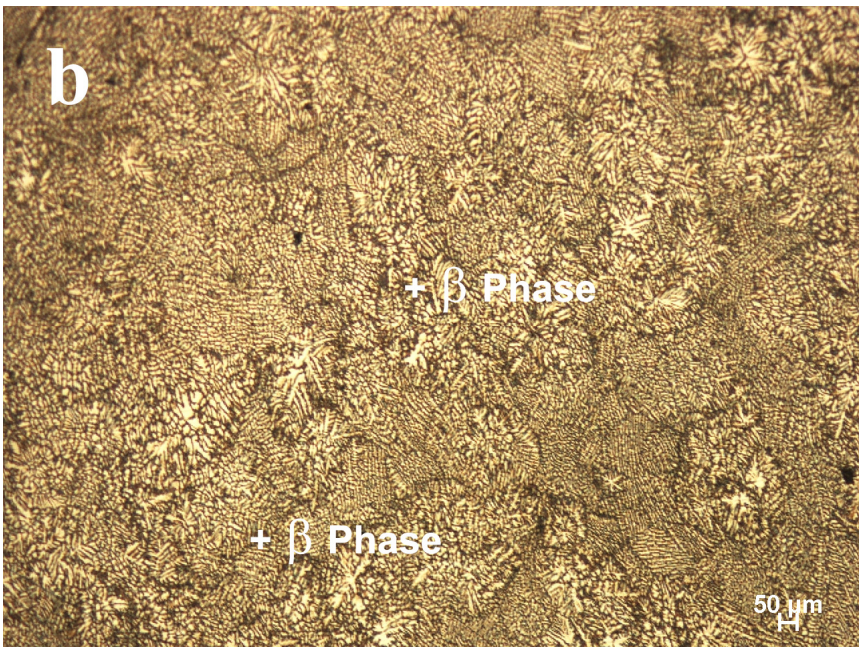
b
+ β Phase
+ β Phase
50 µm

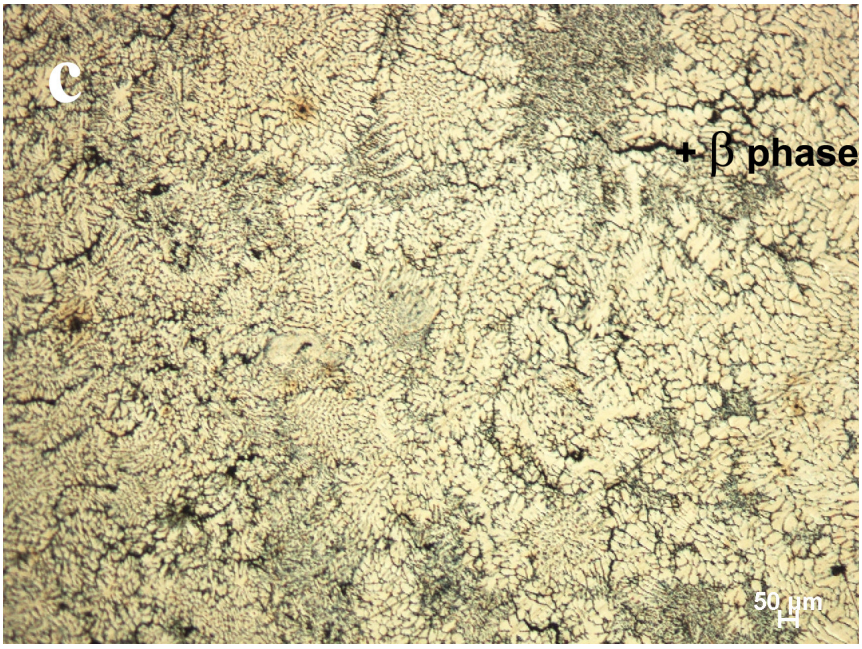
c
+ β phase
50 µm

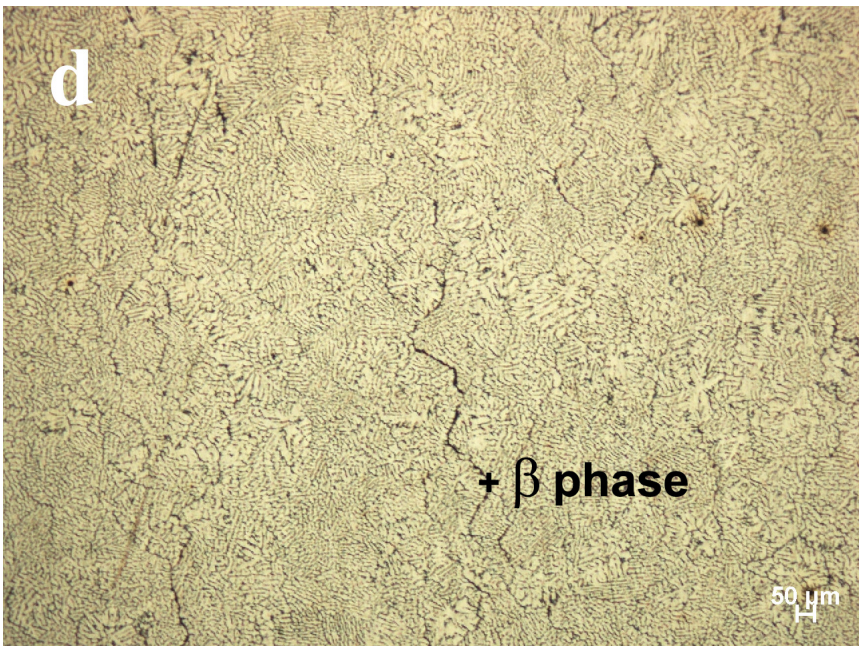

Figure 6.1 The microstructure images of Mg alloy substrates taken from the surface after etched with HF solution a) AZ91D, b) AZ31B, c) AM60B, d) AM50B

6.1.2 XRD Analyses of Mg Alloy Substrates

XRD analysis results of magnesium alloy substrates that used in this study are shown in Figure 6.2. It is clear that hexagonal-Mg phase is apparent in all magnesium alloys. Differences in intensities of peak values are due to different amounts of alloying elements forming solid solution with magnesium matrix.

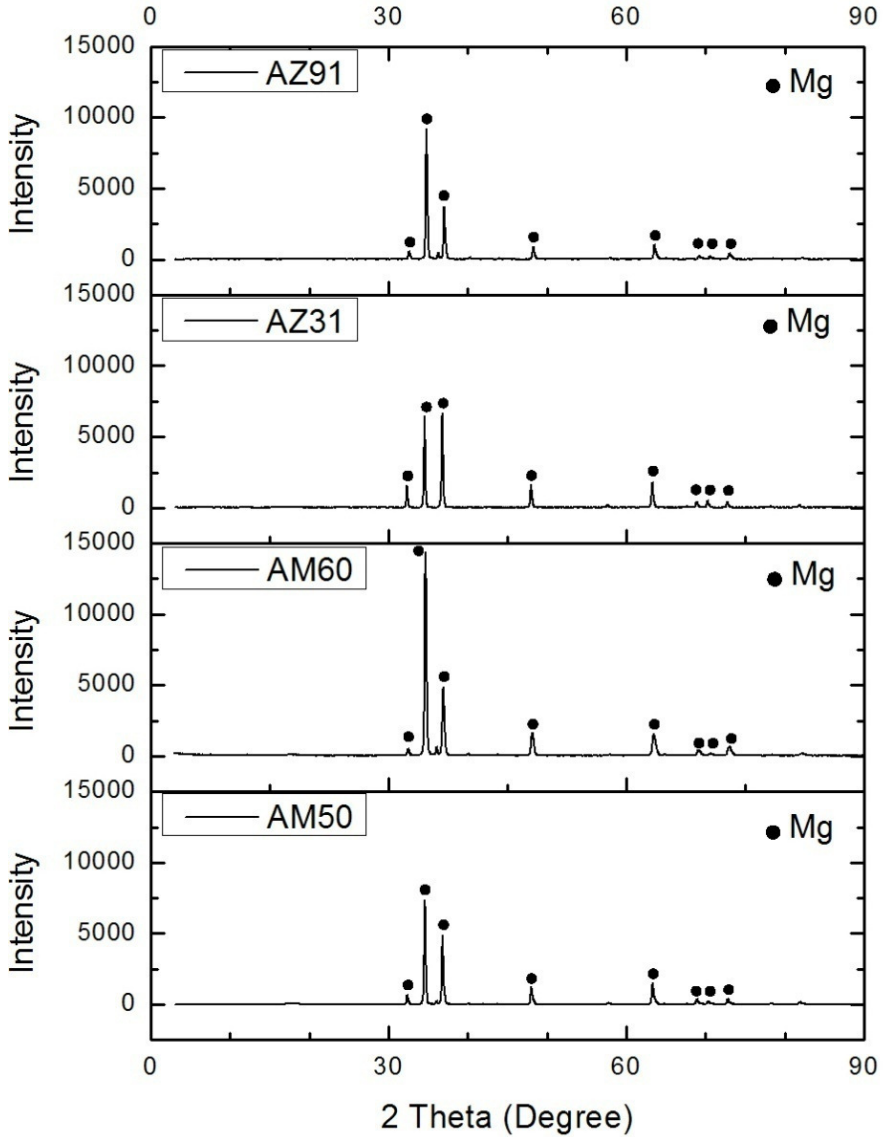

Figure 6.2 XRD spectrums of uncoated Mg alloy substrates

6.2 Characterization of MAO Coatings

6.2.1 Surface Morphology and Structure of MAO Coatings

The SEM images of K10 MAO coating surfaces taken with secondary electrons (SE) fabricated on different magnesium alloy substrates by micro-arc oxidation method using with DC power supply applied with a 50 Hz modulation and both

positive and negative potential pulses at a constant applied current density in solutions containing phosphate, aluminate and hydroxide, are shown in Figure 6.3.

As the current density was kept constant at 20 A/dm^2 during the MAO treatment, the voltage increased promptly to breakdown potential 160 V (Figure 5.3; 1.stage) in a few seconds. Bright fine sparks could be found moving quickly at the anode surface companied with shrill sounds. The voltage continued to rise but with a relative lower speed.

To begin with, the insulated passivating film was formed on the surface of the substrate. When the supply voltage reached the breakthrough value, many dispersing discharge channels developed. The plasma in the discharge channels achieved high temperature and high pressure instantaneously, which made magnesium and other components melt and react. Then, these oxides got deposited on the electrode surface because of sudden cooling by the electrolyte.

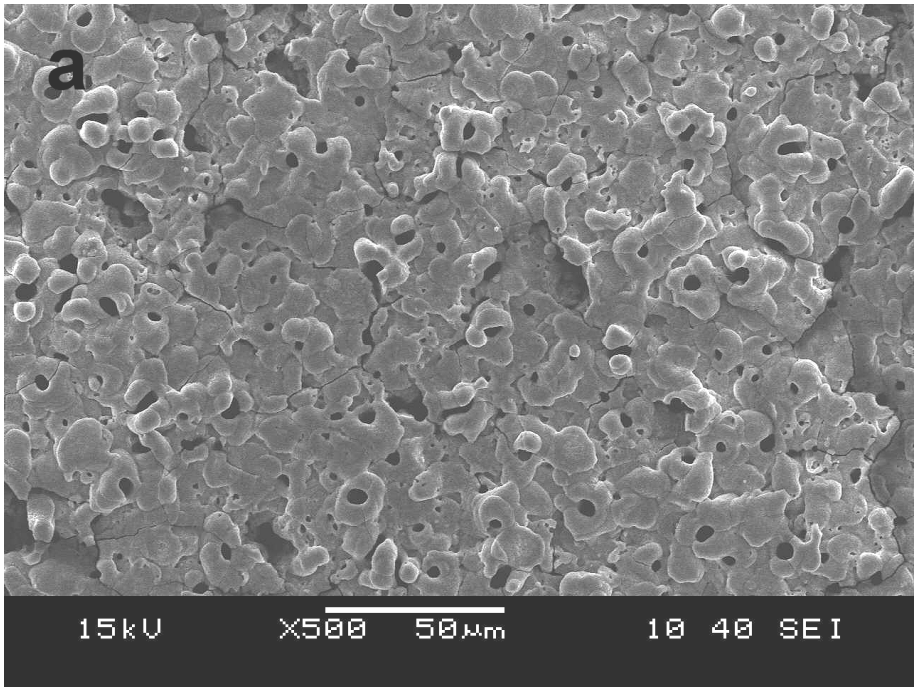

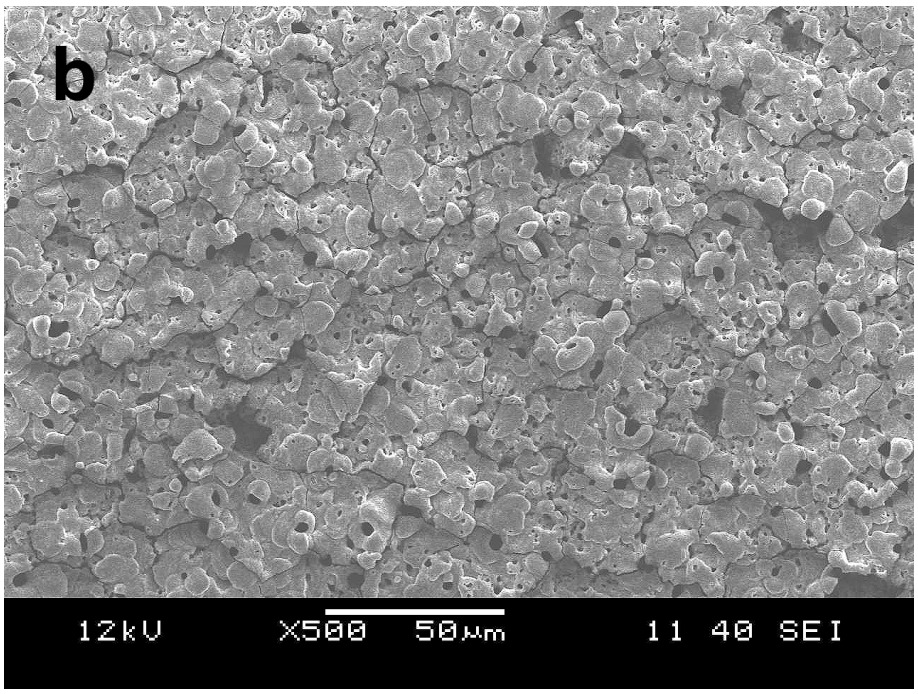
b
12kV X500 50µm 11 40 SEI

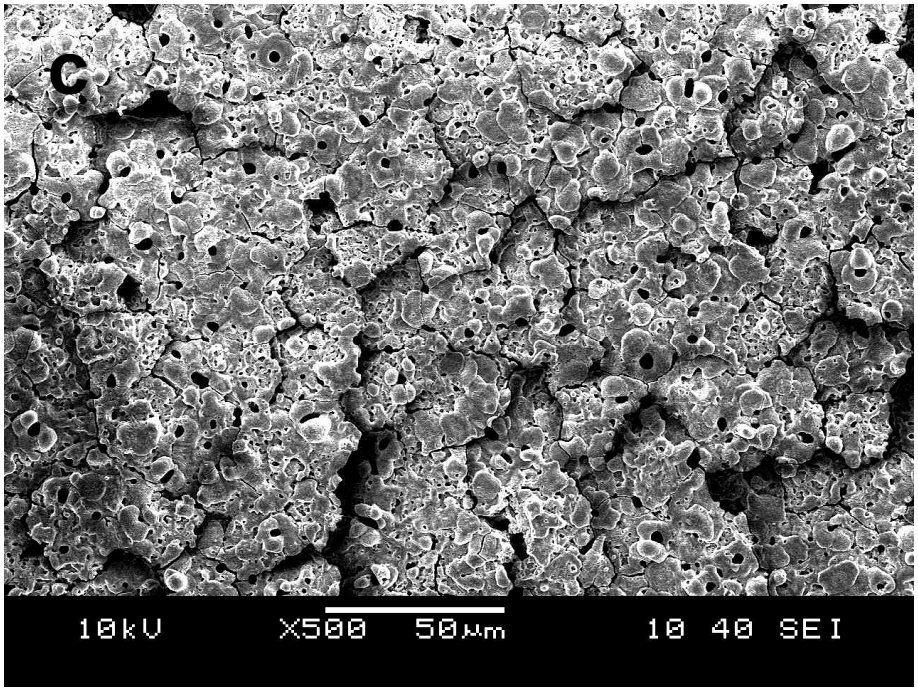
c
10kV X500 50µm 10 40 SEI

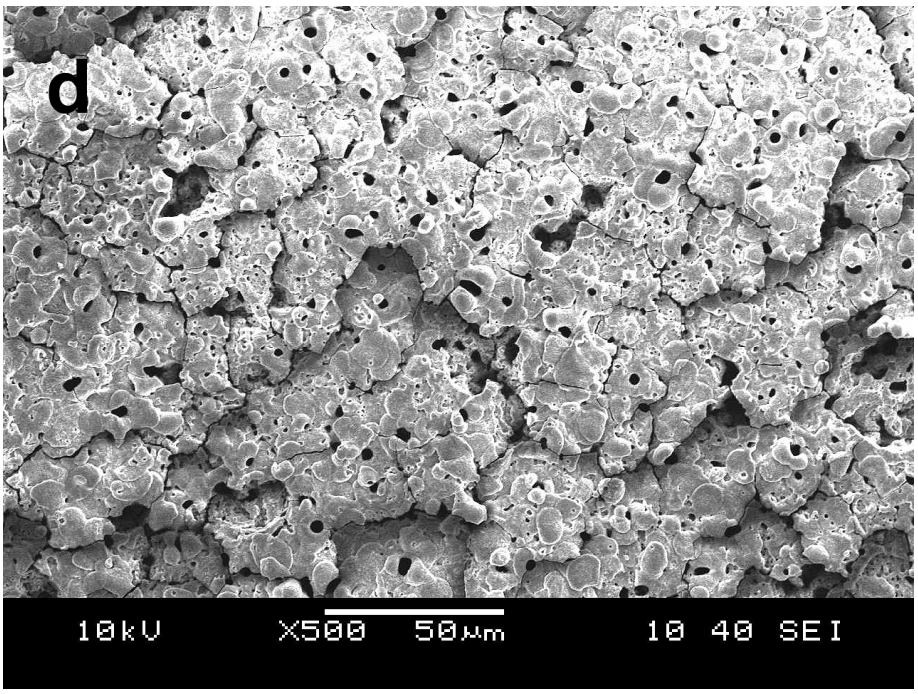

Figure 6.3 SEM images of K 10 MAO coating surface on (a) AZ91D, (b) AZ31B, (c) AM60B and (d) AM50B Mg alloys.

The structural flaws were observed on the coating surface result from the great heat stress during the quick curdling of melting oxide. A few circular micro-pores with different sizes are apparent as black contrast holes on the surface. In micro-discharging period these micro-pores similar to the volcanic eruption spout, which are the results of the generation of sparks and the simultaneous evolution of oxygen gas from the oxidation of water or the electrolyte anion dissolved in the water. If the molten oxides cannot fill in the discharge channel, there will leave many micropores on the coating surface, the diameter of micropore is mainly dependent on the size of the discharge channel (Cai et al., 2006). The non-uniform growing layer of the coating and heavy oxygen bubbles out in the coating growth process may be responsible for the porosity of the ceramic coating.

Pilling & Bedworth (1923) first correlated the porosity of a metal oxide with the specific density. The Pilling-Bedworth ratio (R), is defined as the ratio of the volume of the metal oxide, which is produced by the reaction of metal and oxygen, to the consumed metal volume, as described in equation 6.1.

$$R_{PB} = V_{oxide} / V_{metal} = M_{oxide}\, d / amD \qquad (6.1)$$

where M and D are the molecular weight and density of the metal oxide whose composition is $(Metal)_a(oxygen)_b$; m, and d are the atomic weight and density of the metal. Pilling and Bedworth realized that, when R is less than 1, a metal oxide tends to be porous and non-protective because it cannot cover the whole metal surface. The lower Pilling–Bedworth ratio (PBR) of magnesium is also the main reason for high porosity of MAO films on magnesium alloys (Duan et al., 2007).

The SEM results are showed that the micro-pores on the K10 MAO coatings are not so similar with another one, all coatings were irregularly porous but MAO coatings on AM series alloys have more continuous large cavities and inhomogeneous surface structure. On the other hand the K10 MAO coatings formed on AZ series alloys has fewer pores and had a smoother and more continuous surface. It might be attributed to the different phases of the substrate. As mentioned above, there are α and β phases in magnesium alloys according to its different aluminium content. During the MAO process, α phase has higher reactivity and tends to release more Mg^{2+} to take part in the coating formation reactions under effect of high electric field and high Joule heat (Ambat et al., 2000). Thus, higher concentration of Mg^{2+} around α-phase provides more active sites for plasma sparking. Meanwhile, β-phase is relatively more stable, which need stronger energy for sparking than α-phase. In the early treatment period, it need very low breakdown energy since the insulated coating is quite thin, so the influence of different phases is not distinct. As the coating grows, more breakdown energy is needed and more discharges take place at the α-phase site.

As shown in Figure 4.5, the thickness of coating increases with treatment time. It is believed that the thicker coating is beneficial to the corrosion and wear resistance. Nevertheless, the increasing treatment time causes to form a long lasting arc which generates a coating with a loose rough morphology. It is observed that the discharges became larger gradually with the increasing treatment time. The SEM images of K25

MAO coatings taken with secondary electrons (SE) fabricated on different magnesium alloy substrates were given in Figure 6.4(a-c).

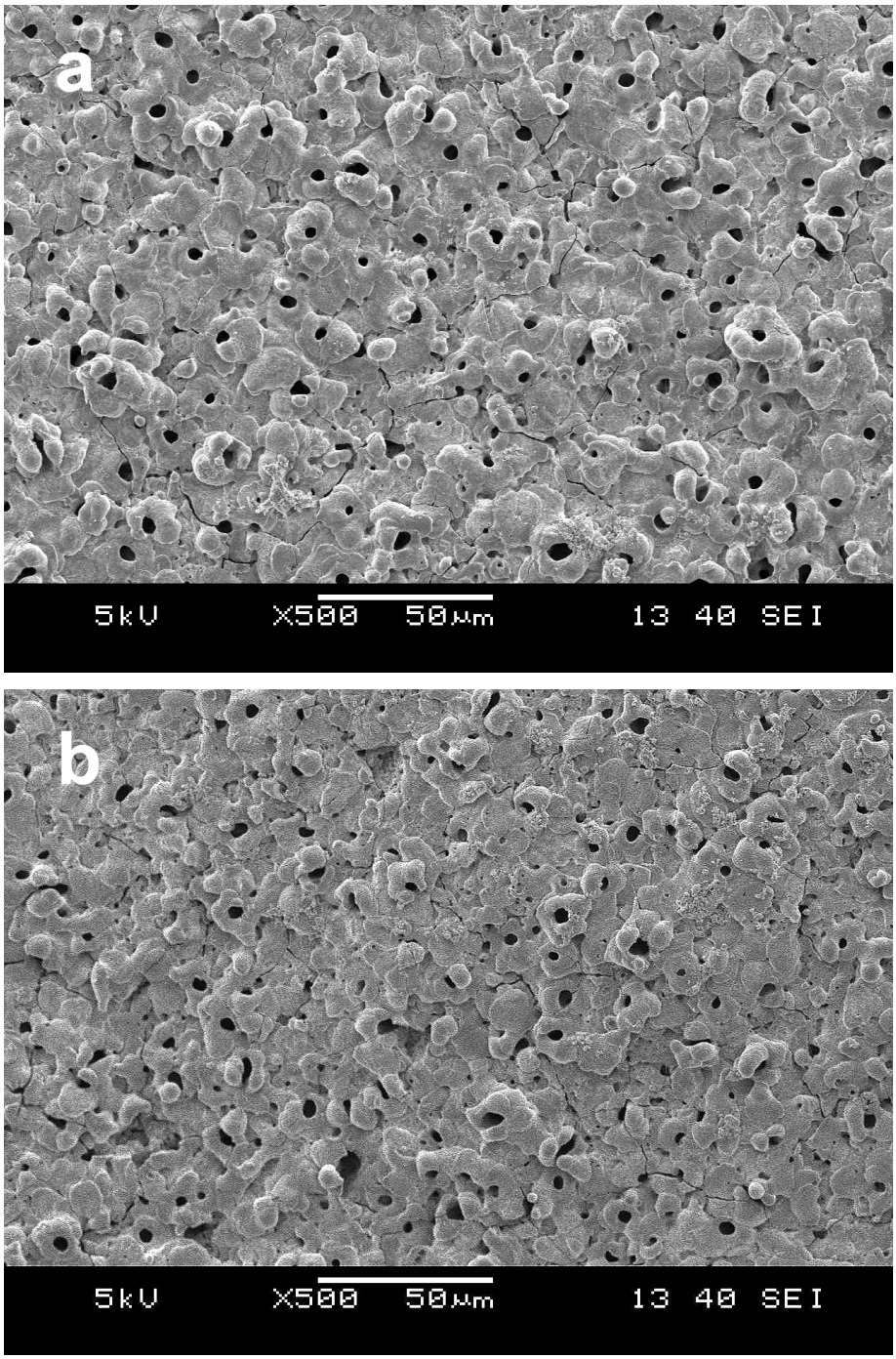

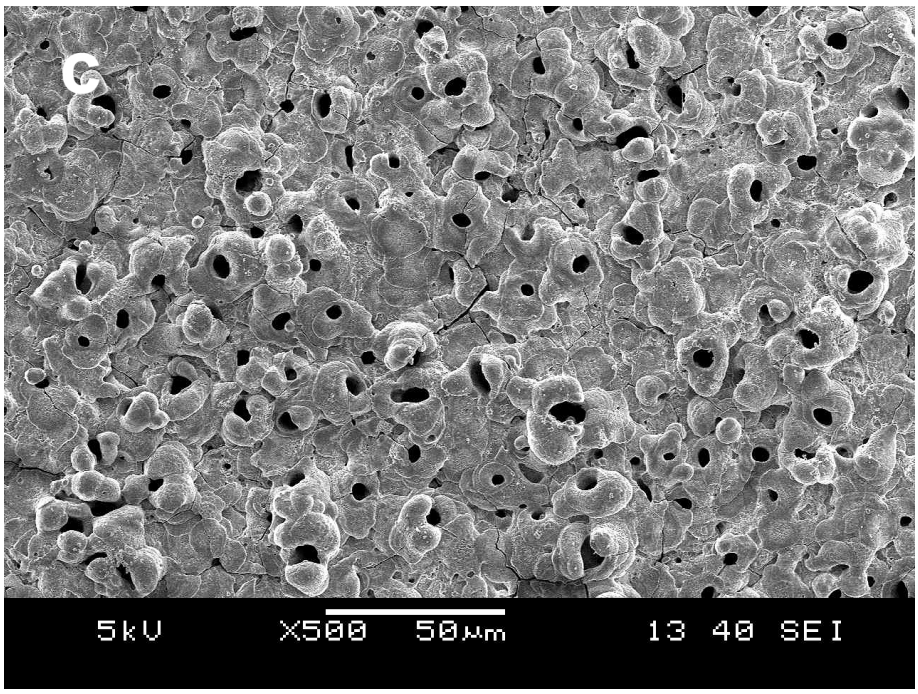

Figure 6.4 The SEM images of K 25 MAO coating surface taken on (a) AZ91D, (b) AM60B and (c) AM50B Mg alloys.

It is clear that treatment time is highly effective to the morphology of MAO coatings. In the initial spark stage, the insulating coating is thin and weak breakdown energy is required. Thus, the small size pores of high density spread uniformly in the whole coating layer. As the treatment goes on, the density of the discharge crates drops off and the surface roughness rises, which reflects the increasing of the energy and violence of individual discharge.

Elemental compositions of the K10 and K25 MAO coatings determined by EDS are listed in Table 6.1. Mg, O, Al, P, K and Na elements are detected in the EDS spectrum of coatings. Al contents of MAO coatings are greater than Mg substrates and the presence of P, K and Na elements in the composition of the MAO coating indicates that elements in the electrolyte are incorporated in the coating. This can be attributed to the elemental co-deposition from the electrolyte. Also high percentage of O content in the composition indicates the formation of Al oxides besides Mg oxides. The concentrations of O maintain the similar contents in all coatings, independent of the formation conditions. However, the measured concentrations of O

in coatings are lower than the real concentrations, as the precision limit of the EDS analysis facility is poor for some light elements.

Table 6.1 Elemental composition of K 10 and K25 MAO coatings

Substrate	Coating Thichness	Composition, wt. %					
		Mg	Al	O	P	K	Na
AZ91D	K10	46.80	20.58	25.47	5.33	0.39	1.43
	K25	46.33	21.72	25.21	4.23	0.44	1.35
AZ31B	K10	48.72	17.32	26.07	5.84	0.48	1.54
AM60B	K10	46.81	19.74	24.73	6.75	0.40	1.53
	K25	48.29	20	27.74	2.52	0.22	1.18
AM50B	K10	48.00	18.47	25.35	6.17	0.48	1.51
	K25	49.85	19.21	24.16	5.23	0.36	1.31

6.2.2 Cross-Sectional Structure of MAO Coatings

The structure of a MAO coating can be described as the one that consists of a compact barrier layer on the surface of the metal followed by a porous interconnected layer over the compact layer. While the porous layer is formed as a result of plasma interaction with the metal and electrolyte, the barrier layer is formed as a result of the applied potential over the metal. Hence, the electrochemical breakdown of this film depends on the chemistry of the alloy where pores on the surface generally grow in size and decrease in number with the treatment time (Khaselev, Weiss & Yahalom, 2001).

Cross-sectional SEM images of the K10 MAO coatings are shown in Figure 6.5(a-d). It is clearly seen that the MAO coatings are composed of two layers, a porous outer layer (90 % of total thickness) and a dense inner layer (< 1 μm). Also it

is observed that the presence of extensive networks of fine-scale micro-cracks and pipe-like defects from the surface layer to substrate.

MAO coatings on AZ91D and AZ31B alloys have uniform cross-section structure with few amounts of blind micro-pores while AM series alloys have large interconnected micro-pores.

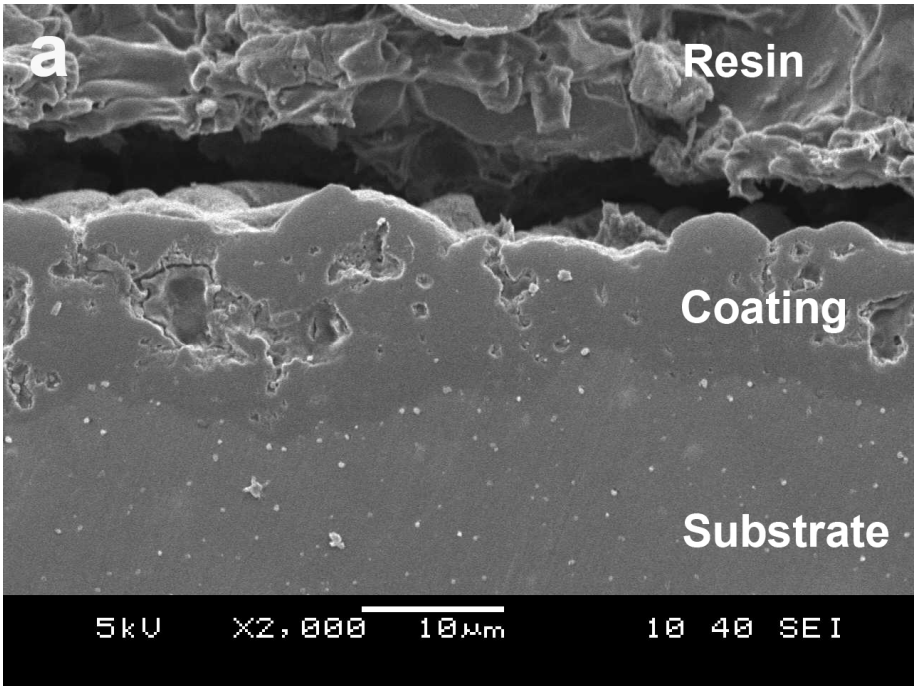

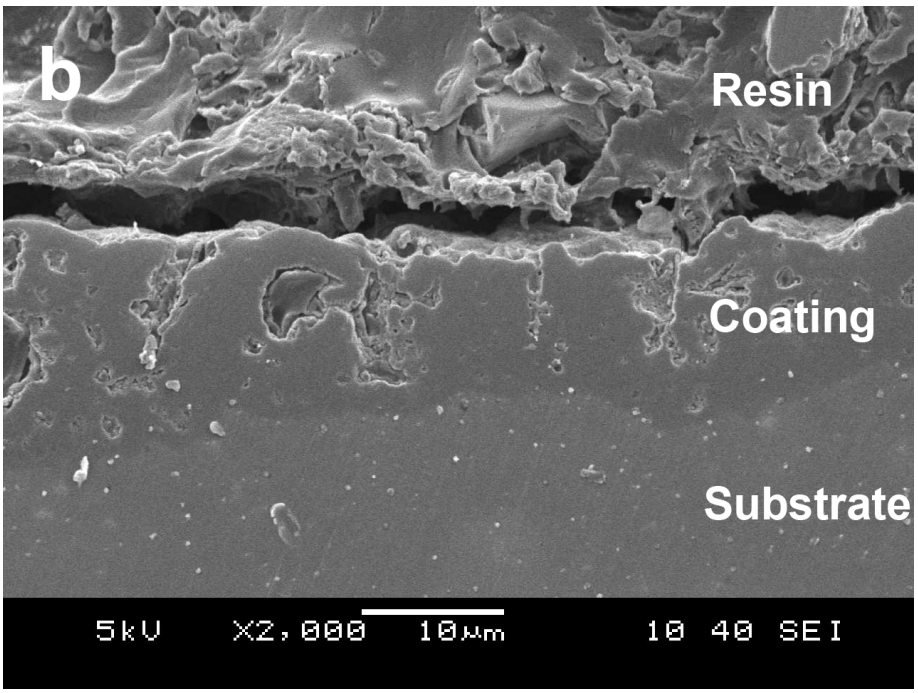
b
Resin
Coating
Substrate
5kV X2,000 10µm 10 40 SEI

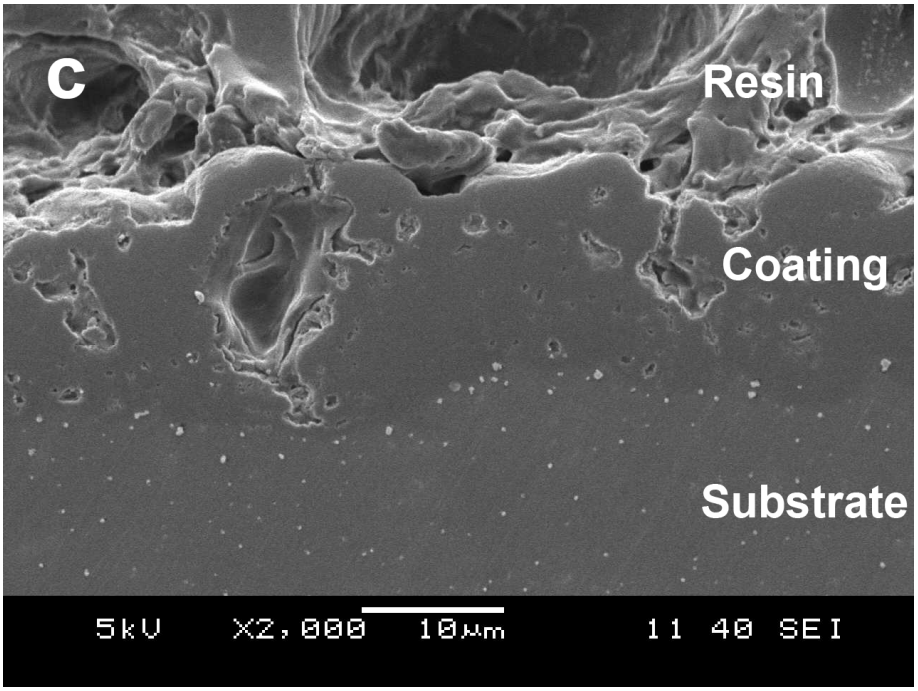
c
Resin
Coating
Substrate
5kV X2,000 10µm 11 40 SEI

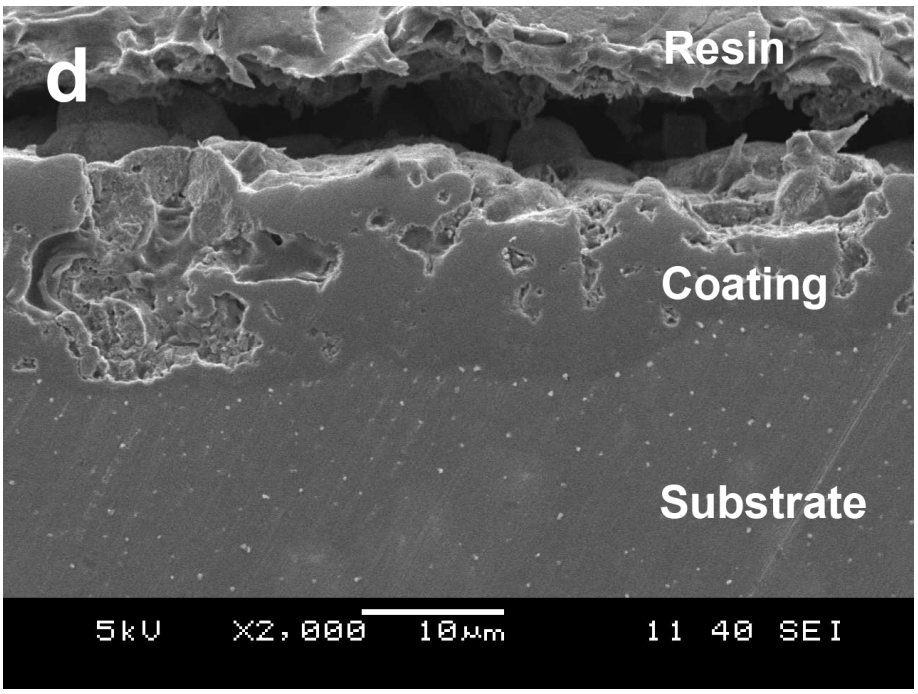

Figure 6.5 Cross-sectional SEM images of K10 MAO coating formed on (a) AZ91D, (b) AZ31B, (c) AM60B and (d) AM50B Mg alloys

Elemental mapping analyses carried out in the cross section of K10 MAO coatings is shown in Figure 6.6(a-c).

a

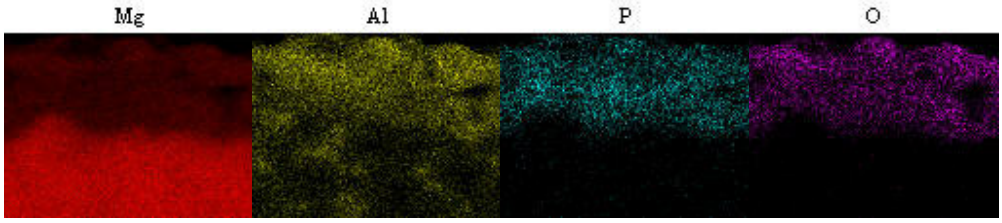

b

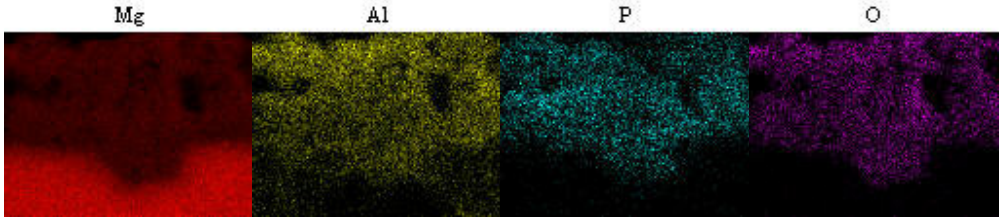

c

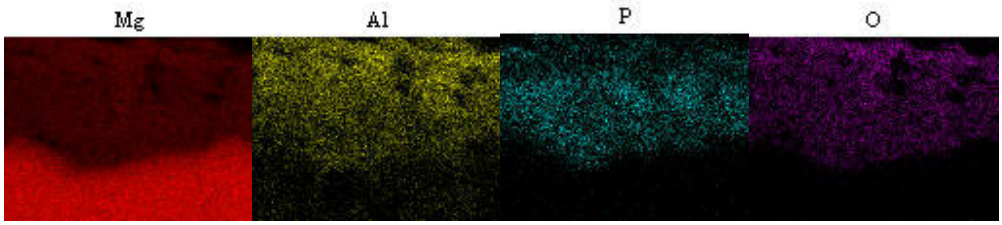

Figure 6.6 Elemental mapping results of K10 MAO coatings formed on a) AZ91D, b) AM60B and c) AM50B Mg alloys

Homogenous distribution of elements through the MAO coatings was observed for all magnesium alloy substrates. Phosphorus which appeared in concentrated near the top of substrates. This can be related to further incorporation of phosphate based electrolyte additives in the initial stages of MAO process as compared to the final stage. In case of AZ91D Mg alloy, elemental distribution of Al in discrete substrate regions beneath the interfacial boundary is related to the presence of $Mg_{17}Al_{12}$ (β phase) intermetallic component. This intermetallic phase is formed due to excessive Al content of AZ91D as compared to other Mg alloys.

Cross-sectional SEM images of K25 MAO coating formed on AZ91D, AM60B and AM50B magnesium alloys were given in Figure 6.6(a-c). All the K25 MAO coatings were observed to have a wavy jagged interface with the substrate, which is most likely as a result of the dissolution of the substrate in the early stage of treatment. The difference of the cross-section can also be attributed to the discharge characteristics during the MAO process. In the initial stages, weak micro-discharges distribute uniformly on the substrate surface moving quickly and uniform layer is formed. Then, with the increase of electric field intensity, the micro-discharges become stronger and move more slowly, which results in the non uniform coating. However, further oxidation process leads to even more intense discharge which makes the existent coatings broken.

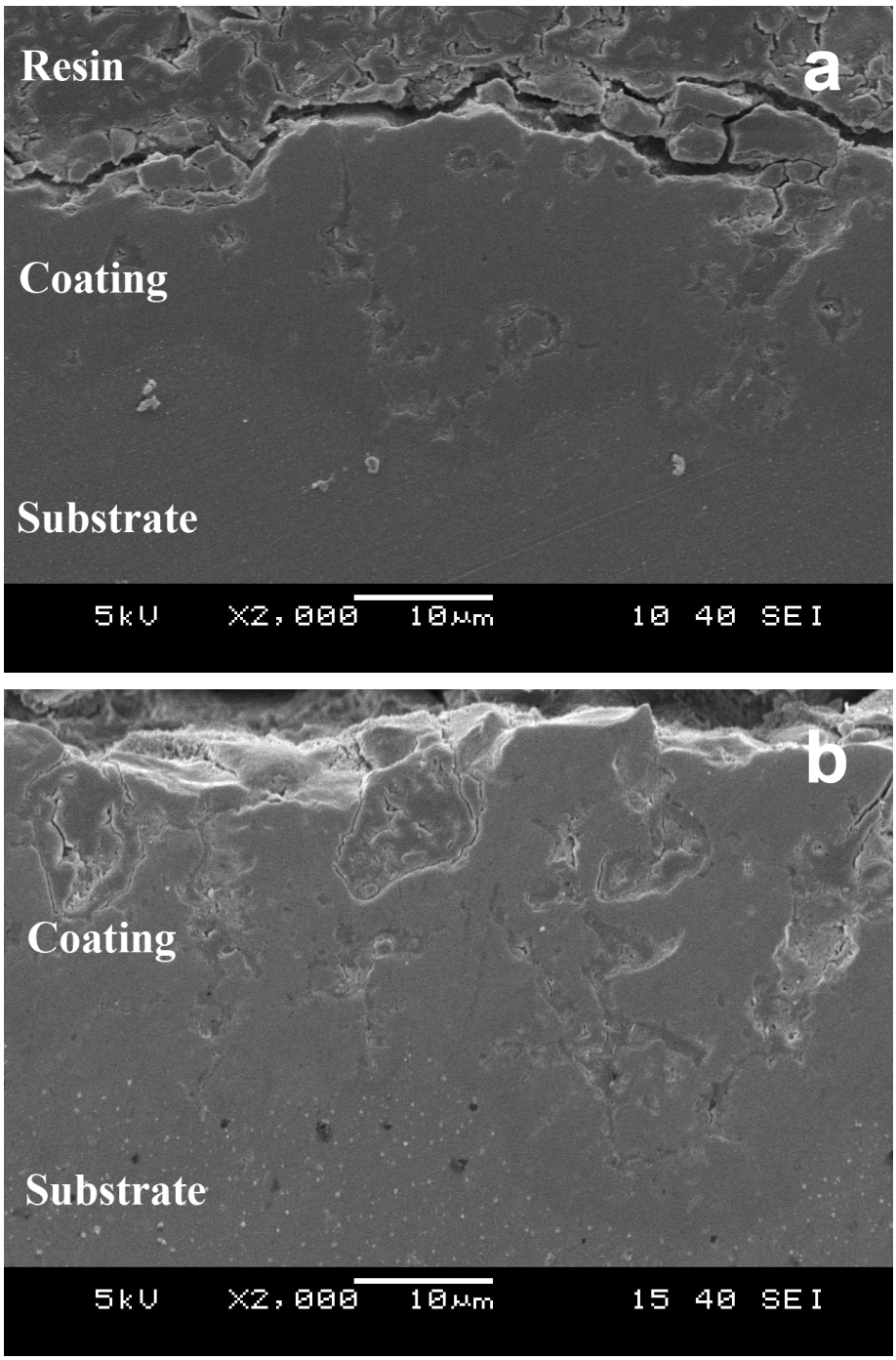
Resin
a
Coating
Substrate
5kV X2,000 10µm 10 40 SEI
b
Coating
Substrate
5kV X2,000 10µm 15 40 SEI

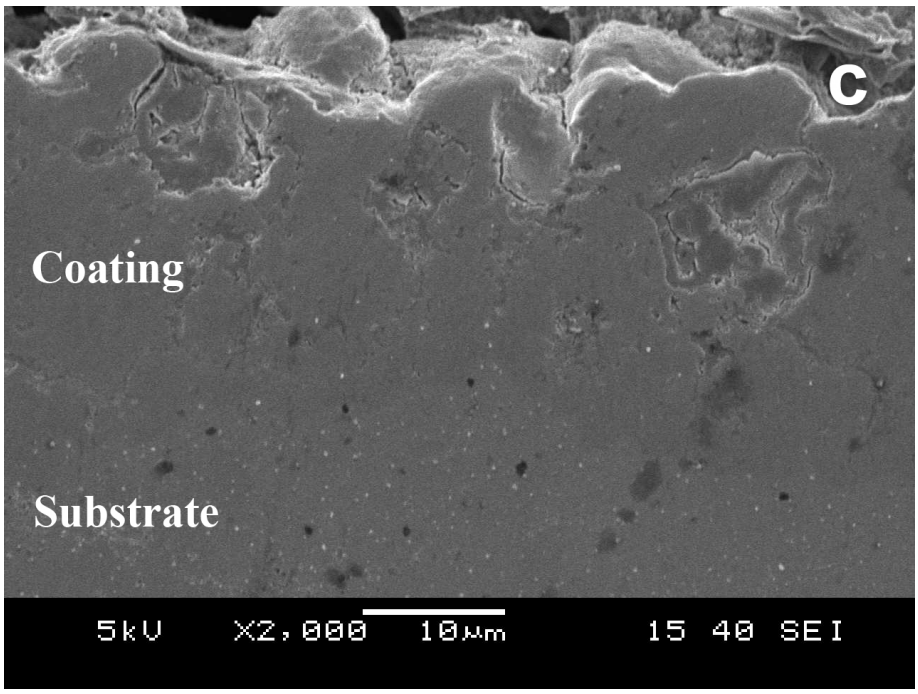

Figure 6.6 Cross-sectional SEM images of K25 MAO coating formed on (a) AZ91D, (b) AM60B and (c) AM50B Mg alloys

The coatings obtained at relatively short-term (K10) were more compact and the coatings produced at higher treatment duration had a higher degree of micro-cracks. The development of such defects in the MAO coatings is attributed to the thermal stresses during the evolution of coating as a result of melting and solidification of hard ceramic compounds such as magnesium oxide, spinel, etc. The higher energy input and the resultant higher thickness of coatings in the longer operations were responsible for such formation.

There was no significant difference in thickness for the coatings was observed except for the coating on AZ series alloys being a little bit thinner but not significant depended on the β phase content. There are not fracture sites in the interface of all MAO coating and substrate which is indicating that the good adhesion between the coating and substrate.

6.2.3 XRD Analyses of MAO coatings

XRD analysis results of K10 and K25 MAO coatings are shown in Figure 6.7 and 6.8 respectively. It is clearly seen that the MAO coatings are composed of MgO as main phase and other phases such as $AlPO_4$, $MgAlPO_5$ and $MgAl_2O_4$. Periclas (MgO) formed via substrate metal oxidation during MAO treatment while $AlPO_4$ and $MgAlPO_5$ phases resulted from the contribution of alkaline electrolyte components to the coating structure. Nevertheless spinel phase $MgAl_2O_4$ could be formed in the presence of both MgO and Al_2O_3 phases in coating structure. Khaselev et al. (2001) pinpointed that the spinel phase enhance the corrosion resistance of the coatings on magnesium alloys.

In case of crystalinity of MAO coatings, the peaks of oxidized compound phases of the K10 coatings are weak and coatings may be contain an amorphous compounds, as indicated by peak intensity. The amorphous compounds are believed to form during rapid localised quenching, which occurs around each individual discharge during the formation process. When the coating is oxidized for 15 min (K25), the peaks of the compound phases grow higher. This predicates that intense discharges in the later oxide process provide higher energy and temperature which is favourable to form crystal phases. With thickening of the oxide coating, the discharge process gets deeper into the coating and it becomes more difficult for the electrolyte to penetrate into interior, thus leading to the decrease of the cooling rate. At the same time, homogeneous discharges gradually change into local drastic discharges, which result in the higher temperature at local regions inside the oxide coating. Owing to the decrease of the cooling rate and the higher temperature, melted materials can be relatively easy transformed into the crystal phase, so the content of crystalline MgO increases. The melting point of MgO and $MgA1_2O_4$ were 2800 and 2135 ^oC respectively. This shows that the temperature of micro-arc discharge channels is very high, the thickness of the coating increased, as more and more MgO, $MgA1_2O_4$, and other compounds were formed in the coating. It is believed that Al and P in the electrolyte and Mg from the substrate participate in the oxidation process. Therefore, the compositions of the ceramic coatings can be adjusted by

changing solution components and concentration to prepare ceramic coatings consisting of the required elements. The presence of $MgAlPO_5$ and $AlPO_4$ in coating suggests that the PO_4^- anions in the electrolyte penetrate into discharge channels and react with the metal substrate during the microarc oxidation process. It is estimated that the instantaneous temperature in the micro-spark zone can reach several thousand degrees, thus the oxide products synthesized by plasma chemical interactions possess a stable chemical thermodynamic property.

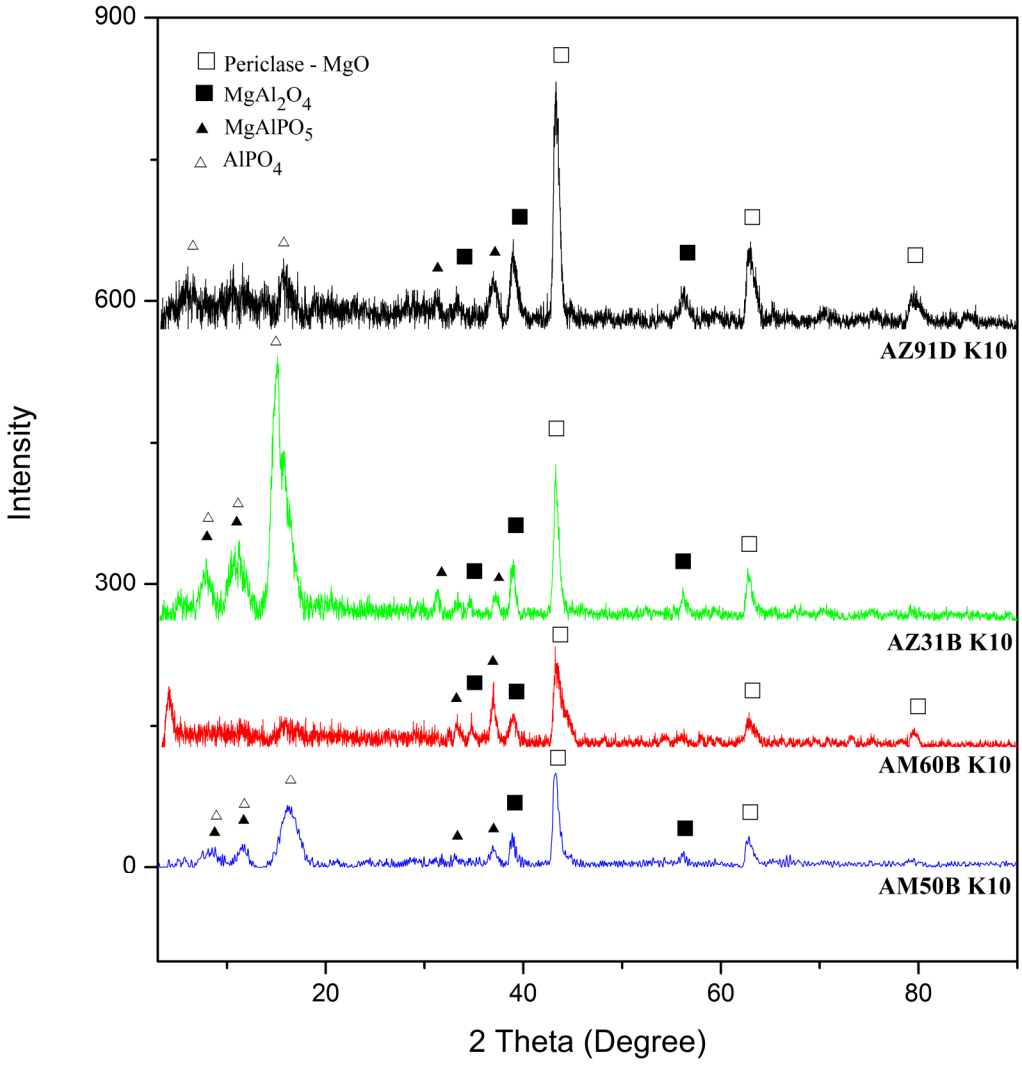

Figure 6.7 XRD analysis results of K10 MAO coatings

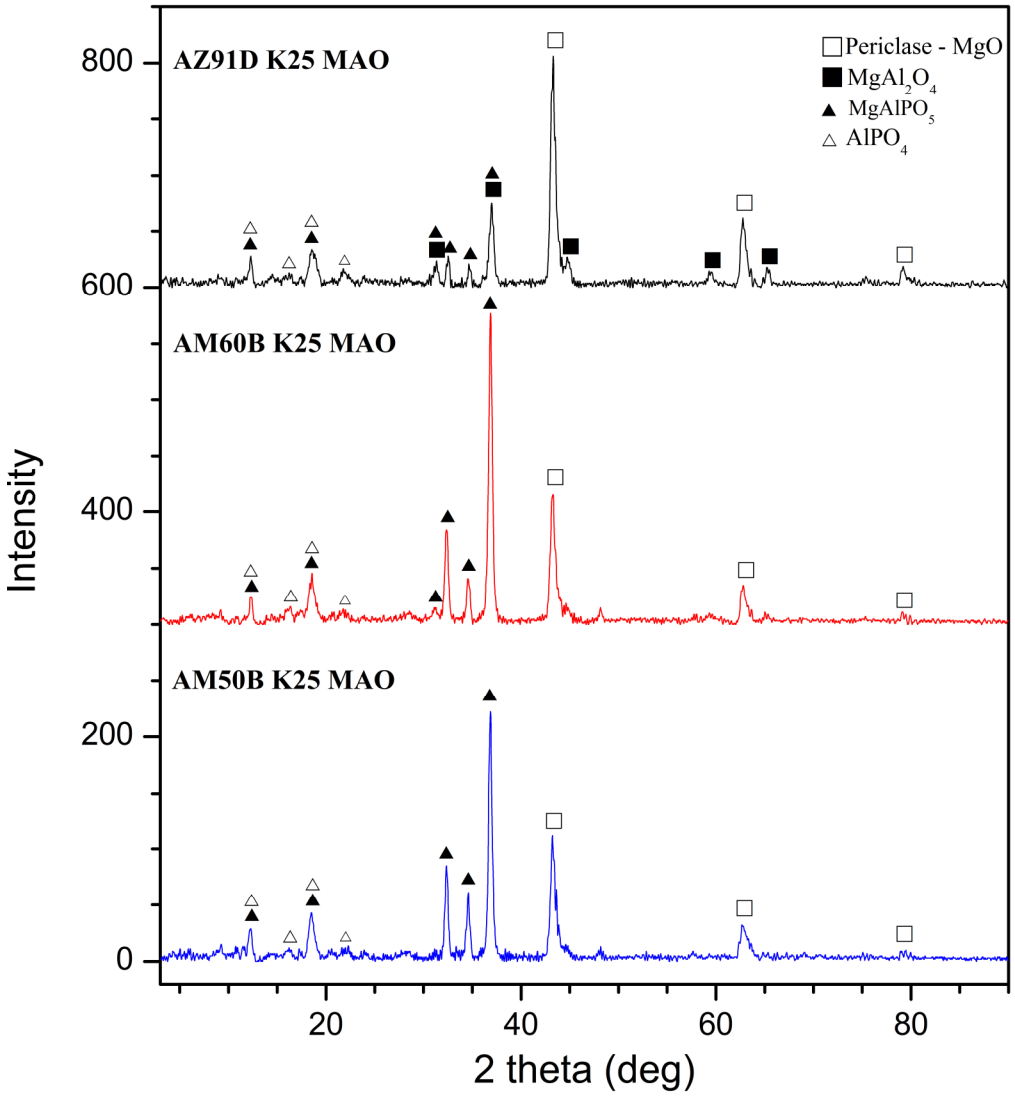

Figure 6.8 XRD analysis results of K25 MAO coatings

It is observed that X-ray patterns of K10 and K25 MAO coatings do not involve any corresponding hexagonal Mg phase diffracted from Mg alloy substrate. The absence of peaks of Mg means that X-ray penetration occurred only the MAO coatings. It might be assumed to presence of barrier layer at the interface of substrate-coating.

6.2.4 Surface Profile (3D) and Roughness Measurements of MAO Coatings

3-Dimensional surface profiles and surface roughness of K10 and K25 MAO coated magnesium alloys are shown in Figure 6.8(a-d) and Figure 6.9(a-c) respectively. In case of K10 MAO coatings, large cavities and ridges are apparent on the surface of MAO coated AM series alloys. AZ series alloys have smoother surface morphology than AM series alloys. It can be clearly seen that surface roughness of MAO coated AM series alloys is greater than AZ series alloys.

It give rise to thought that MAO coatings have a rough surface structure which can provide good adhesion for top-coats like PTFE, sol-gel, PVD and CVD coatings. It should be note that the increasing surface roughness can deteriorate the corrosion resistance properties.

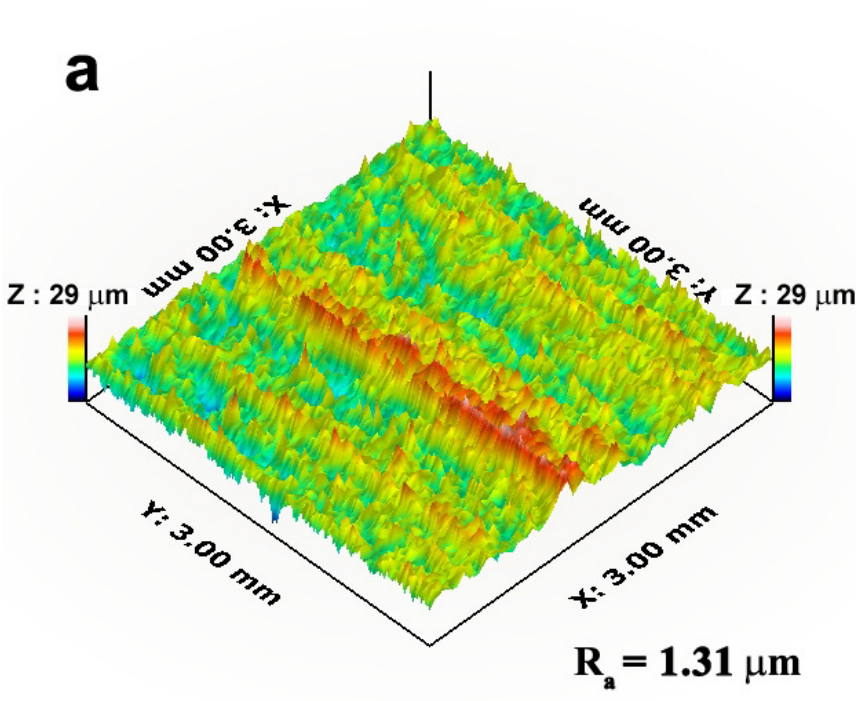

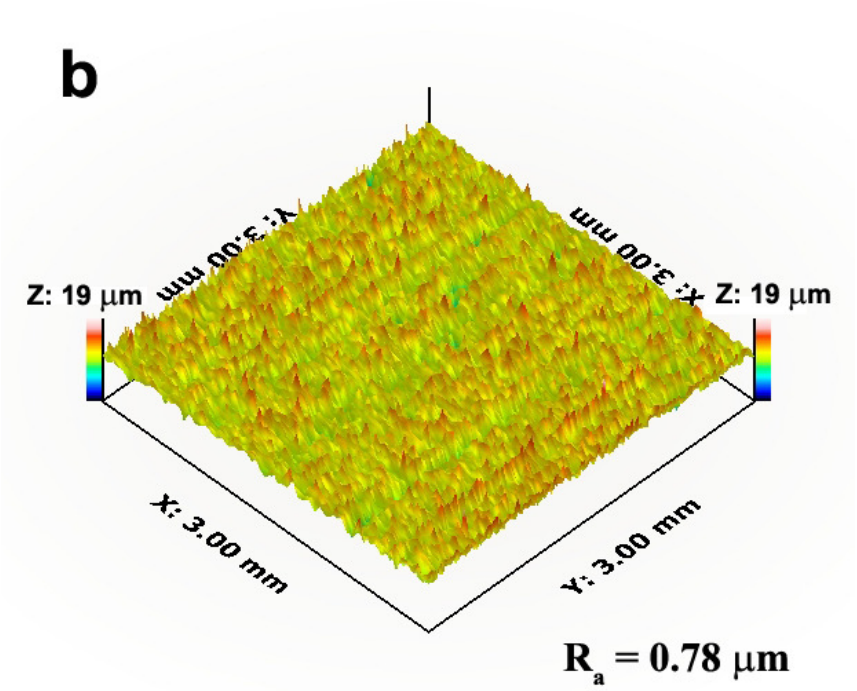
b
Z: 19 μm
Y: 3.00 mm
X: 3.00 mm
X: 3.00 mm
Z: 19 μm
X: 3.00 mm
Y: 3.00 mm
$R_a = 0.78$ μm

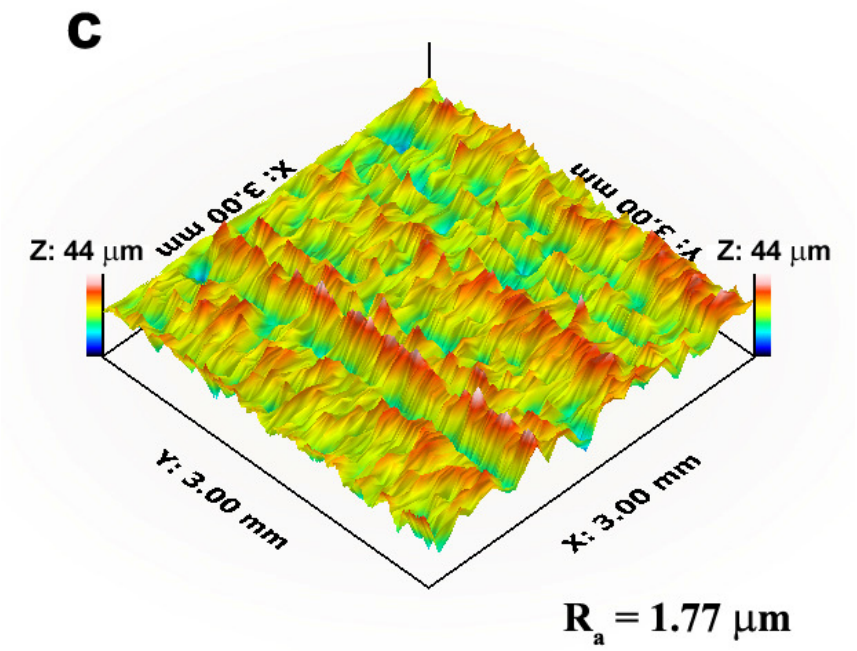
c
Z: 44 μm
X: 3.00 mm
Y: 3.00 mm
Y: 3.00 mm
Z: 44 μm
Y: 3.00 mm
X: 3.00 mm
$R_a = 1.77$ μm

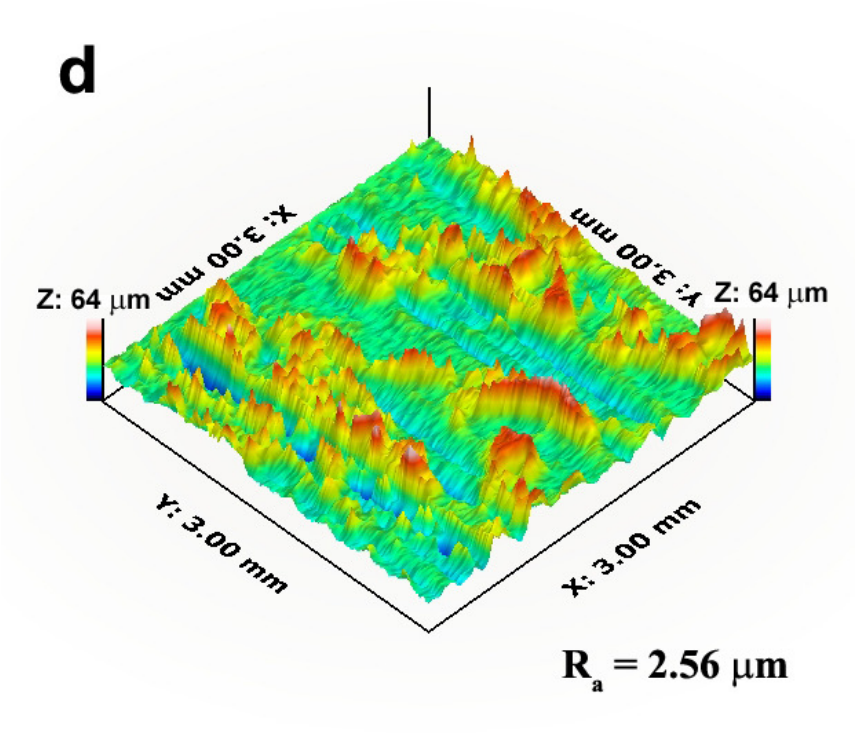

Figure 6.8 3-Dimensional surface profiles and corresponding surface roughness (R_a) of K10 MAO coating on (a) AZ91D, (b) AZ31B, (c) AM60B and (d) AM50B Mg alloys

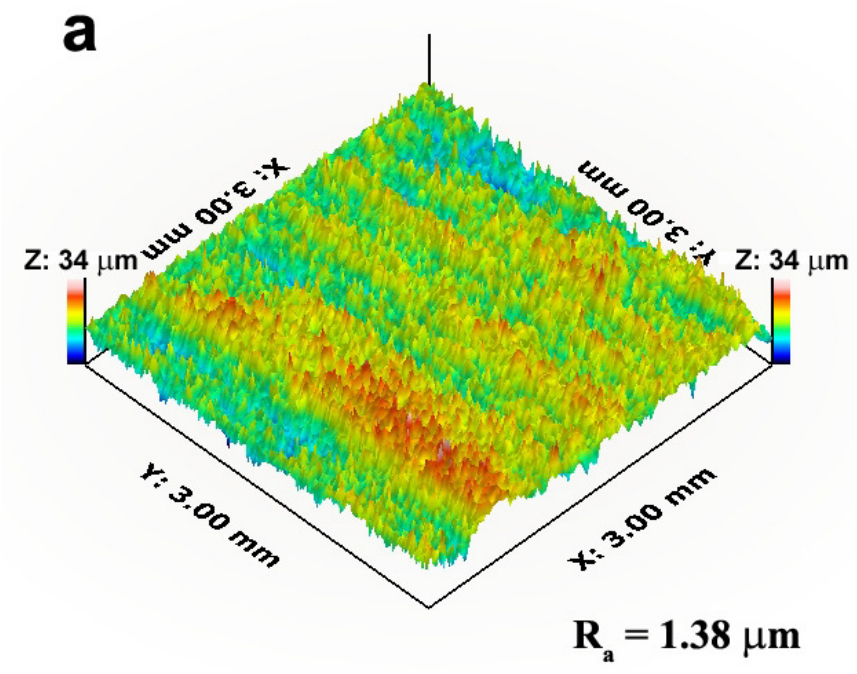

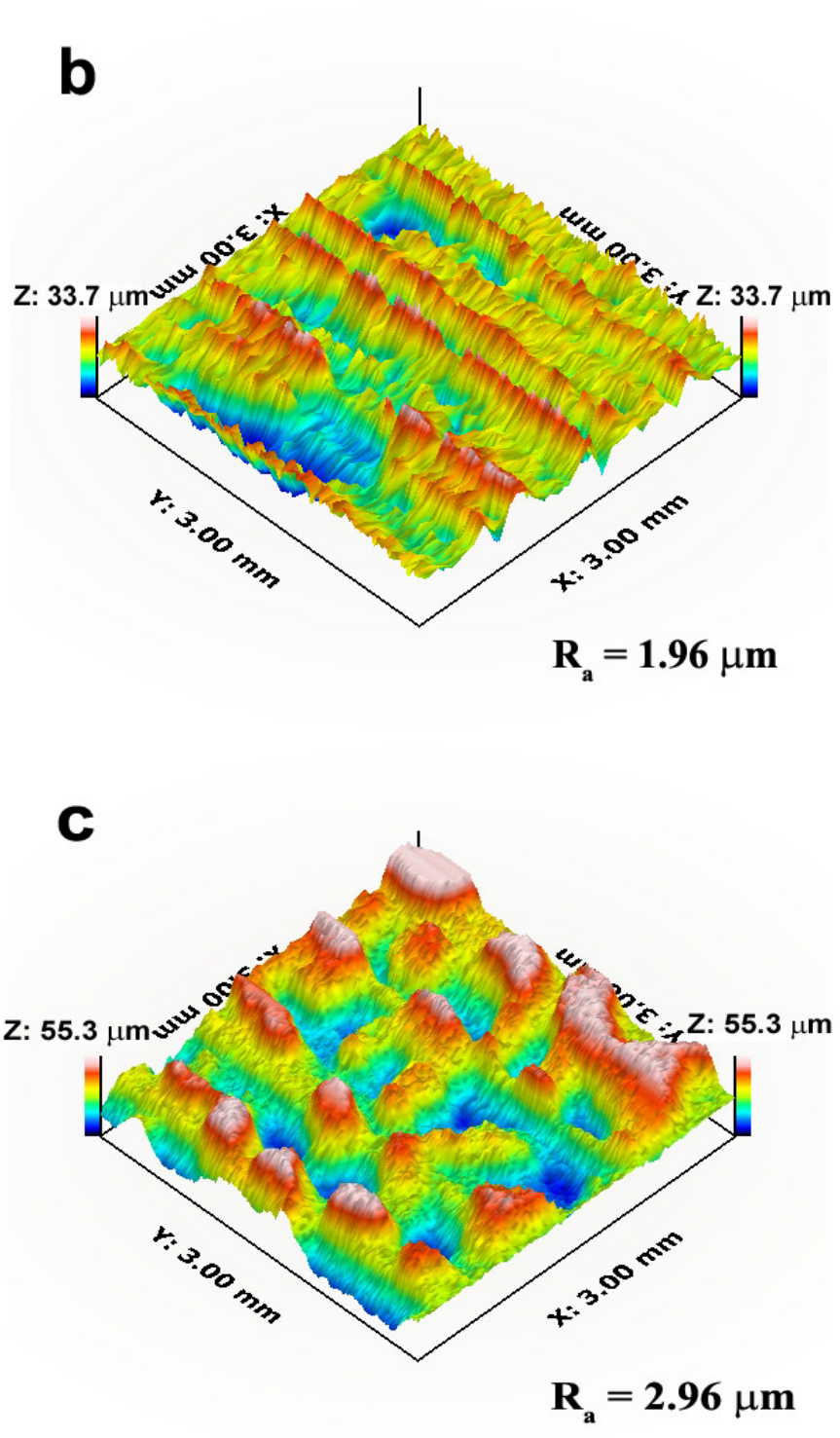

Figure 6.9 3-Dimensional surface profiles and corresponding surface roughness (R_a) of K 25 MAO coating on (a) AZ91D, (b) AM60B and (c) AM50B Mg alloys

The roughness values of the coatings were also found to be higher with increase in coating thickness. The formation of oxide coating as large chunks and the large pore sizes are responsible for the increased surface roughness. It can be seen that the thickness and surface roughness of the MAO coatings increase the treatment duration increased. The 3-Dimensional surface profile analyses of the MAO coatings are indicated that the uniformity of the coatings reduces and the diameters of the micropores and the amount of the molten oxides also increases with increasing treatment time. The surface roughness results are in accord with that of SEM analyses.

6.3 Characterization of Sealed MAO Coatings

6.3.1 Surface Morphology of Sealed MAO Coatings

SEM images of a typical surface of unsealed and sealed K10 MAO coatings on AM60B and AM50B magnesium alloys taken with secondary electrons (SE) are shown in Figure 6.10(a-d) and Figure 6.11(a-d) respectively. As mentioned above K10 MAO coatings formed on AM series alloys (Fig. 6.3; c-d) has a porous, discontinues, inhomogeneous appearance with an irregular pore size. Many micro pores and some micro cracks were seen as black contrast holes on the surfaces.

K10 MAO coatings formed on AM50B and AM60B Mg alloy surfaces are sealed by different post-treatments in order to obtain fully efficiency from the coatings.

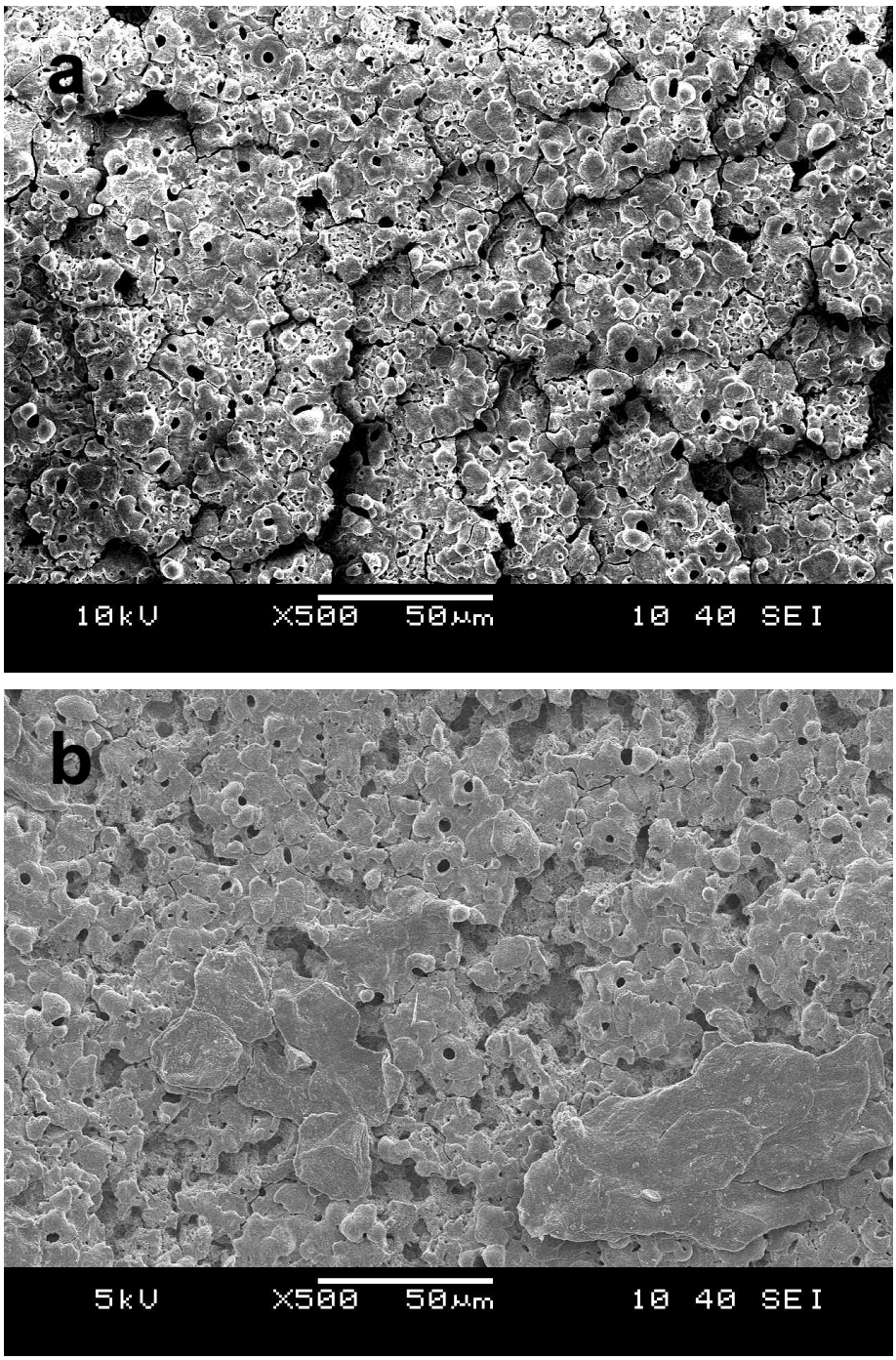
a
10kV X500 50µm 10 40 SEI
b
5kV X500 50µm 10 40 SEI

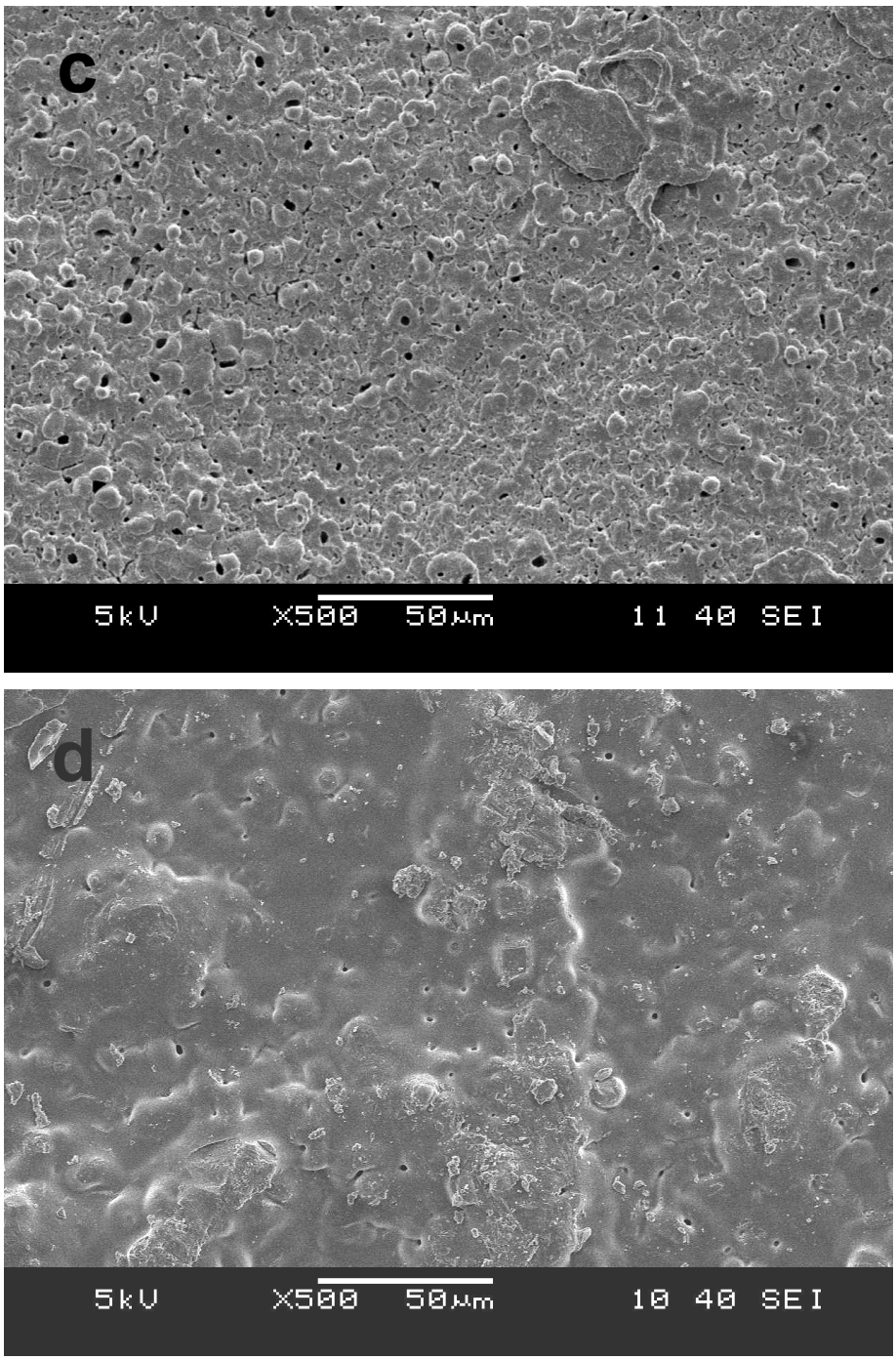

Figure 6.10 SEM images of MAO coating surface on AM60B (a) K10 MAO coating, (b) Alkaline Phosphate, (c), Alkaline Silicate and (d) Sol-gel post treatment.

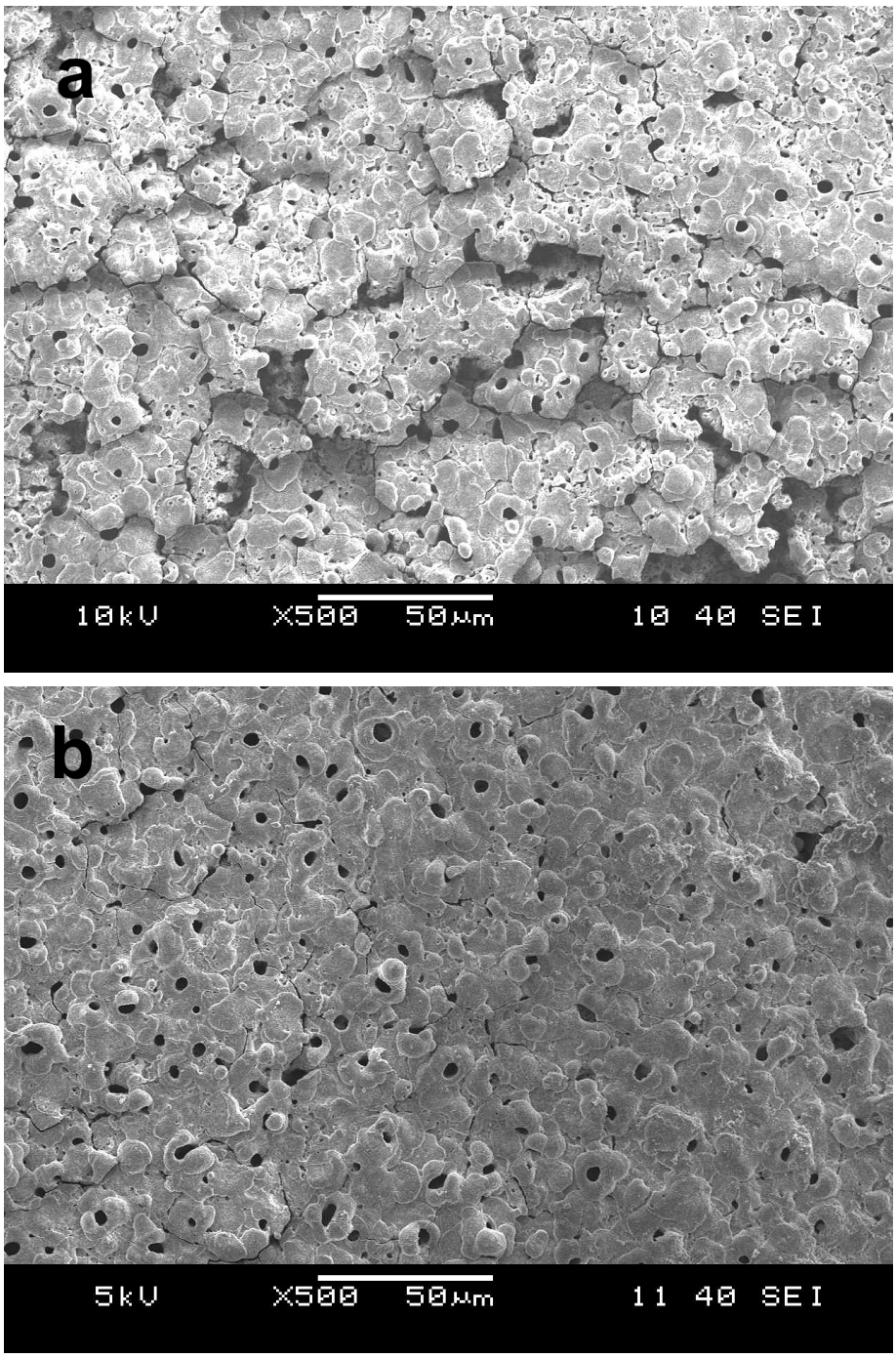
a
10kV X500 50µm 10 40 SEI
b
5kV X500 50µm 11 40 SEI

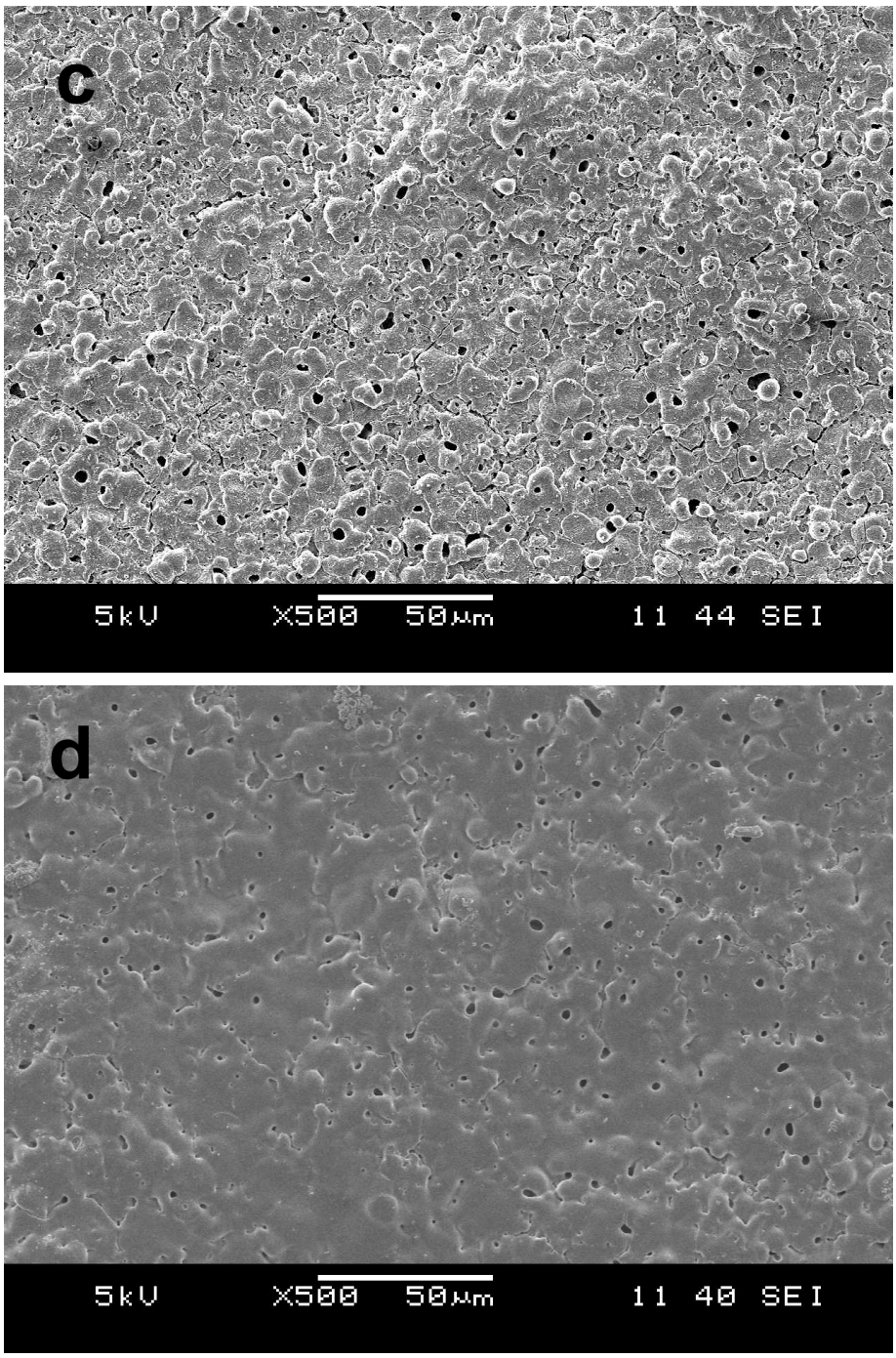

Figure 6.11 SEM images of MAO coating surface on AM50B (a) K10 MAO coating, (b) Alkaline Phosphate, (c), Alkaline Silicate and (d) Sol-gel post treatment.

In general, hydrothermal sealing processes consists of a dual mechanism with preliminary hydration of the porous and barrier layers causing a volume increase on the oxide layer. As a consequence, after a short time the circulation of solution

through the pores is impeded, and only the outermost surface layer of the coating continues to be hydrated until the upper portions of the pore channels are plugged (Patermeakis et al., 1992). Two kinds of sealing models have been proposed with respect to coating thickness by Patermaeakis et al. (1992) and Barker et al. (1994) as illustrated in Figure 6.12. According to these models, at the beginning of the sealing process, the sealing solution quickly penetrates into the pores of the oxide film along the pore wall and adsorbed to the pore walls and other internal surfaces. The result of this is the formation of a skin of inert hydrated oxide upon the pore walls; this will effectively initiate the pore diameter decrease. Also during the initiation time, solution diffuses down the pore length to the barrier layer where hydration occurs. This process effectively reduces the pore length by filling in the pore from its base. As the sealing reaction proceeds, the concentration of sealing reactants at the film solution interface decreases gradually and the reaction products increase, leading to reduction of the rate of the sealing reaction, then the reaction stops. For oxide film, the sealing reaction takes place throughout the surface and pore wall. The products gradually seal the pores from the pore wall to the center of the pore. For thick oxide film, the sealing reaction mostly occurs at the outer layer of film, but the inner layer remains unfilled.

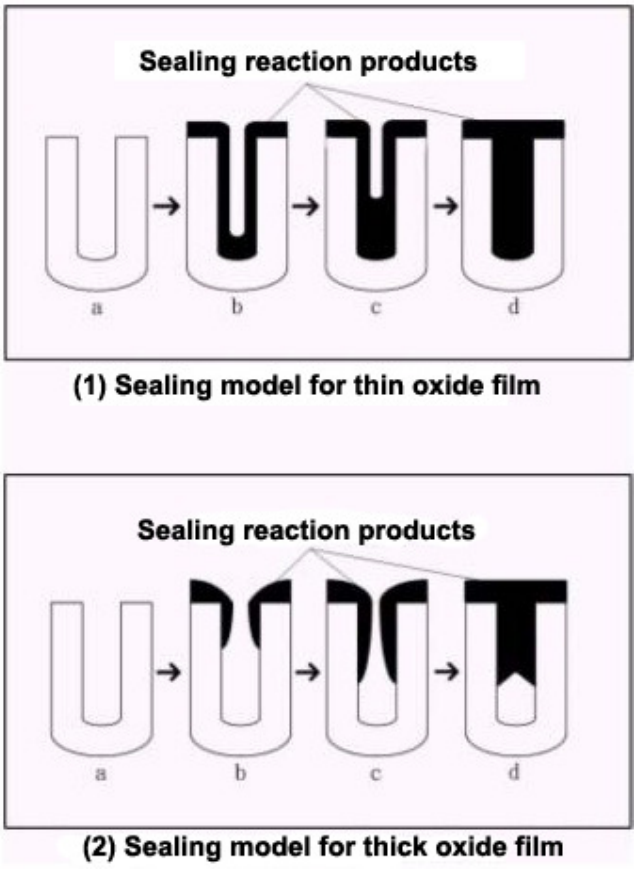

Figure 6.12 The sealing model for thin and thick oxide films (Barker et al., 1994).

With implementing of phosphate based alkaline (AP) post treatments, slightly crack-less, stabilize and more uniform microstructure was observed for each MAO coated AM series alloys (Fig. 6.10;b, Fig. 6.11;b). It is seen that the phosphate containing solution leaks between the microcracks and fills up gradually. The importance of the anions present upon the oxide surface prior to hydration. The phosphate anions considerably retard the subsequent hydration process which is difficult to replacement by hydroxyl ions as independent of sealant involved in sealing process of coatings produced by anodic oxidation methods (Diggle et al., 1968)

The decreasing in pore diameter of silicate (water glass) based alkaline (AS) post-treated MAO coating was observed. It is well-known that increasing temperature

improves the ionic transport of substance and so ion-exchange rate and the chemical adsorbtion reactions of silicate anions in the pore walls accelerate. This proceeding gradually slows down with a decrease in free energy.

The appearance of AS post-treatment applied MAO coatings (Fig. 6.10;c and Fig. 6.11;c) is more homogeneous than AP post treated specimen for each magnesium alloy due to the their application temperature and duration.

Figure 6.10(d) and Figure 6.11 (d) shows a surface structure of the sol-gel post-treatment applied K10 MAO coatings on AM60B and AM50B magnesium alloys. It can be clearly seen that the sol–gel layer covers most macropores and microcracks in the MAO coatings and few tiny micropores are visible on the surface layer. At the beginning this process initially formed gel type substance which was responsible for pore blockage of the oxide throughout the film, as the slow continual crystallization on the pore mount and so overlies or diminishes most pore and microcrack. According to thickness measurements, using eddy-current thickness gauge taken from 10 different points, the thickness of the sol–gel layer reaches up to about 3.8 μm.

According to measurement of multipoint SEM image analyses taken from MAO coated AM50B surface, the average pore size of K10 MAO, AP post-treated, AS post-treated and sol-gel treated MAO coatings was determined as 3.2 ±0.8, 3,9 ±1, 2.8 ±0.6, 2.5 ±0.6, 2.2 ±0.3 μm respectively. For MAO coated AM60B, these values were measured as 3.4 ±0.6, 4.3 ±0.6, 2.7 ±0.6, 2.2 ±0.6, 1.9 ±0.2 μm. respectively.

Under the experimental conditions, the average layer thickness of AP post-treated, AS post-treated and sol-gel treated K10 MAO coatings is 13.2±0.8 14.5.0±0.6 and 15.2±0.6μm and the growth rates are 4.0, 2.8 and 54 $nm.s^{-1}$ respectively.

Elemental compositions of the sealed K10 MAO coatings determined by EDS are listed in Table 6.2. The oxygen percentage content is higher for both alkaline post-

treated specimens due to hydration of the anodic layer during the sealing process. Elemental distribution of MAO-Sol-gel dual layer is consisting of Si, Mg, O and Al.

Table 6.2 Elemental composition of post treatment applied MAO Coatings

% Elemental Compositon	AM50B				AM60B			
	K10 MAO	Phospate PT	Silicate PT	Sol-gel PT	K10 MAO	Phospate PT	Silicate PT	Sol-gel PT
Mg	48	40.67	43.99	25.45	46.81	41.86	42.82	29.86
Al	18.47	19.45	19.3	12.95	19.74	21.42	19.7	13.93
O	25.35	30.54	27.87	21.24	24.73	27.57	26.3	20.39
P	6.17	6.6	5.55	1.64	6.75	7.59	5.95	1.87
K	0.48	0.9	-	0.17	0.4	0.77	0.71	-
Na	1.51	1.9	1.5	0.3	1.53	1.22	1.24	0.42
Si	-	-	1.7	38.22	-	-	1.6	33.5

6.3.2 XRD Analyses of Sealed MAO Coatings

Crystallographic phase analyses of unsealed and post treatment applied MAO coatings were singly given in Figure 6.13 and Figure 6.14. The patterns were analyzed with Xpowder software based on JCPDS database.

XRD patterns of the sol-gel applied MAO coatings show the existence of an additional phase, namely silicon oxide. All post sealing treatments slightly affected on the intensity of the MgO phase of the MAO coatings. Surprisingly, with the applying sol-gel sealing treatment on the MAO coating significant increasing on the intensity of MgO phase was observed notwithstanding decreased elemental composition ratio of Mg and O analyses taken from surface of coating via EDS.

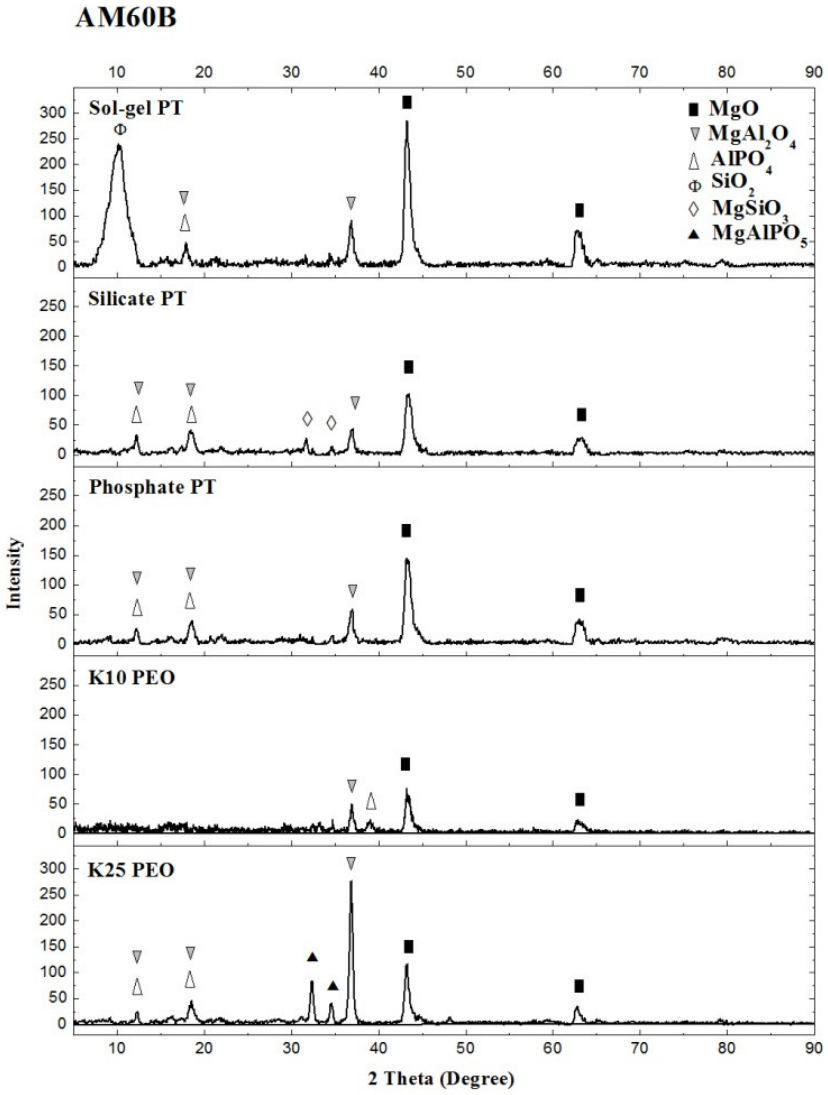

Figure 6.13 XRD analysis results of unsealed and sealed MAO coatings and uncoated AM60B Mg alloy.

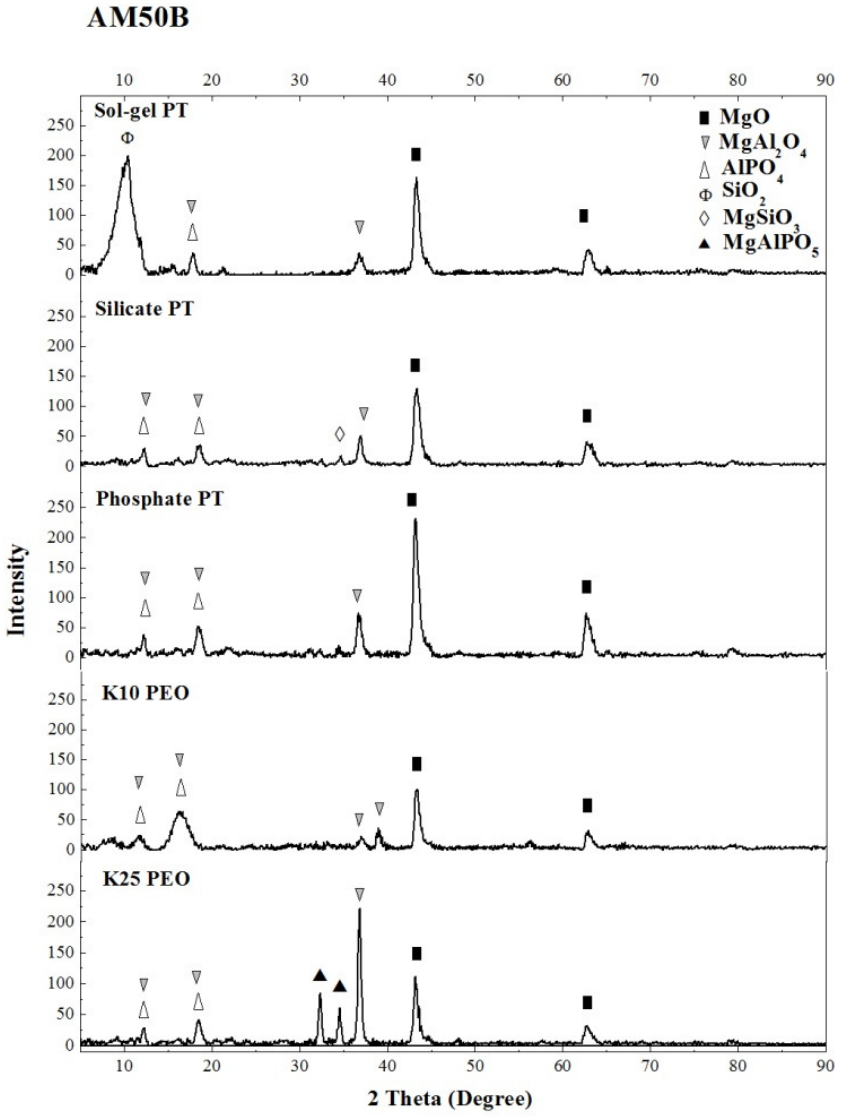

Figure 6.14 XRD analysis results of unsealed and sealed MAO coatings and uncoated AM50B Mg alloy.

6.3.3 Surface Profile (3D) and Roughness Measurements of Sealed MAO Coatings

3-Dimensional surface profiles and surface roughness of post-treatment applied MAO coatings on AM60B and AM50B Mg alloy are shown in Figure 6.15 and Figure 6.16 respectively. These tests were carried out after post-treatments to quickly assess the effectiveness of the sealing operation. According to the microstructural and topographical observations, large cavities and ridges are apparent on the surface

of K10 MAO coatings on AM50B and AM60B Mg alloys. As mentioned before that with the increasing of MAO coating thickness depends on process duration, increases surface roughness of MAO coatings formed on each Mg alloys. On the other side the surface roughness of K10 MAO coatings reduces with applied post treatments. The best surface morphology obtained from MAO-sol-gel dual layer.

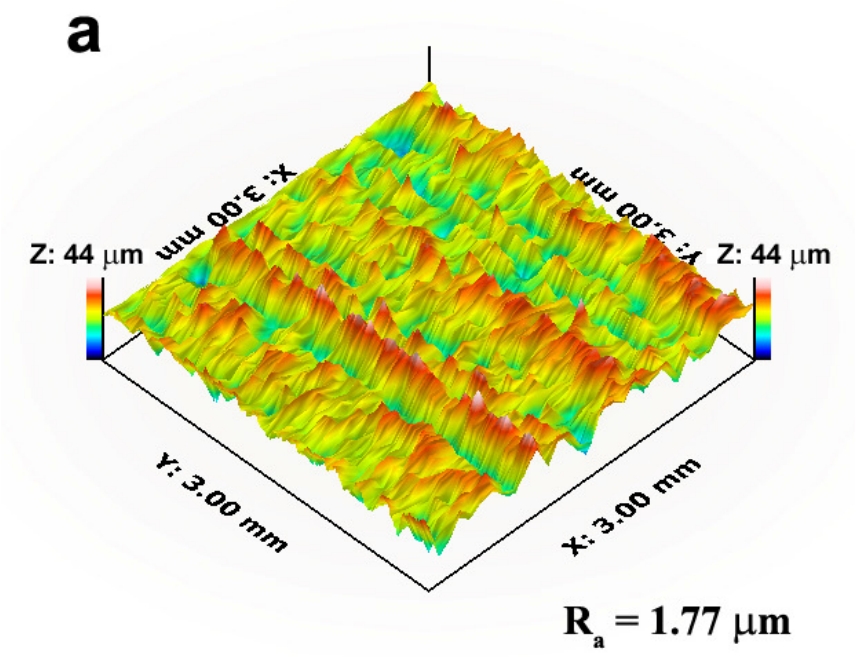

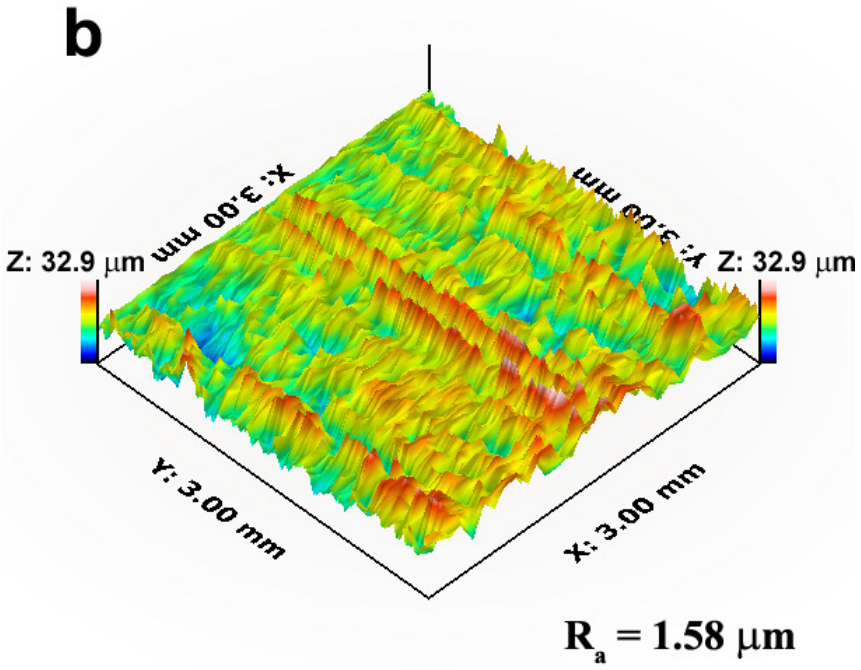

$R_a = 1.58\ \mu m$

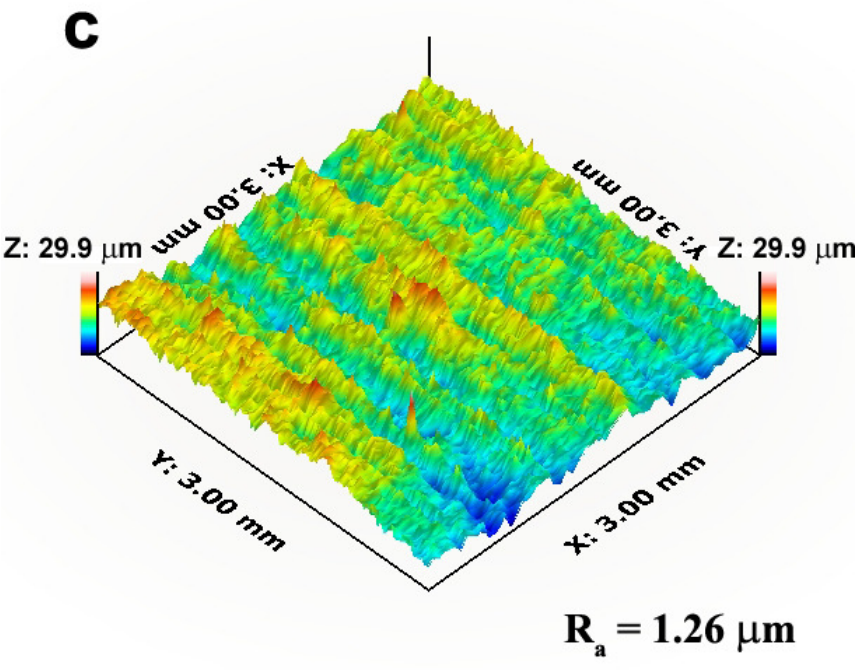

$R_a = 1.26\ \mu m$

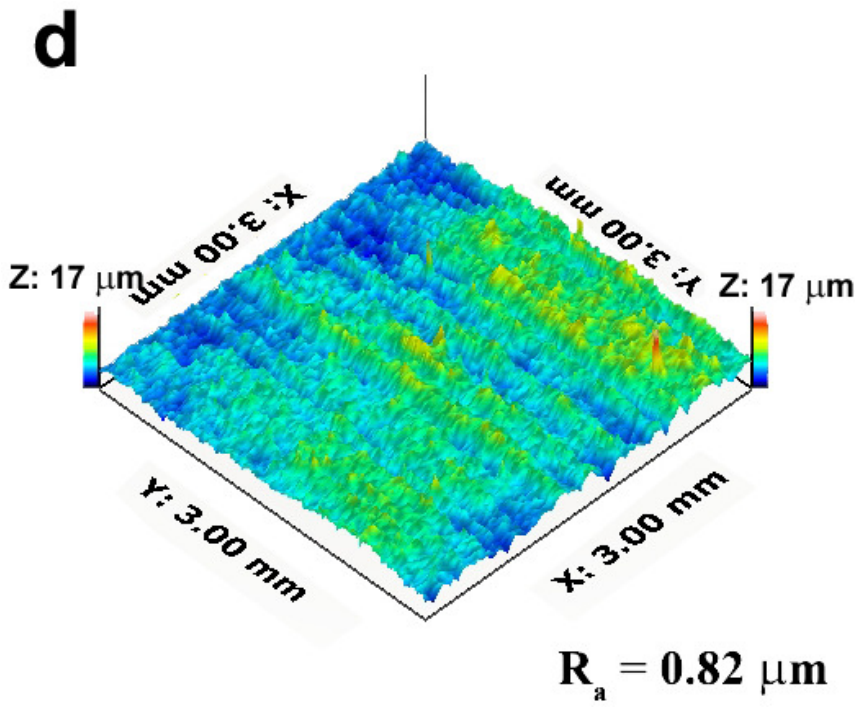

Figure 6.15 3-Dimensional surface profiles and corresponding surface roughness (Ra) of the coatings on AM60B Mg alloys (a) Untreated K10 MAO coating, (b) Phosphate based, (c) Silicate based and (d) Sol-gel post treatment.

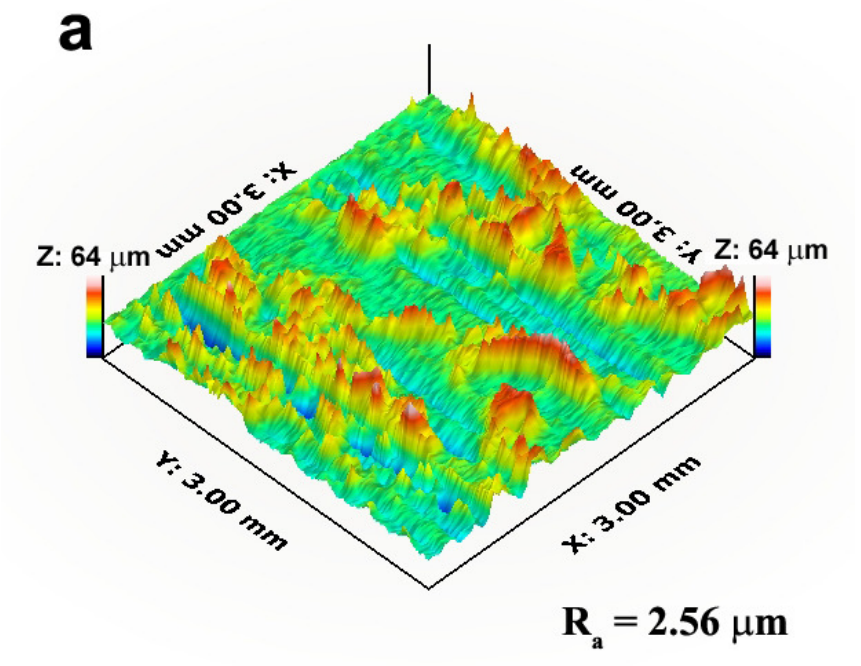

b

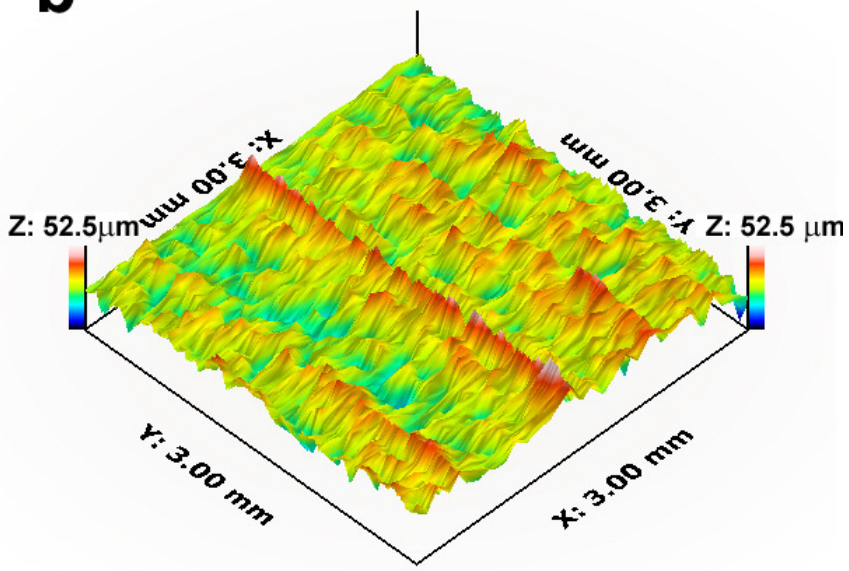

$R_a = 1.64\ \mu m$

c

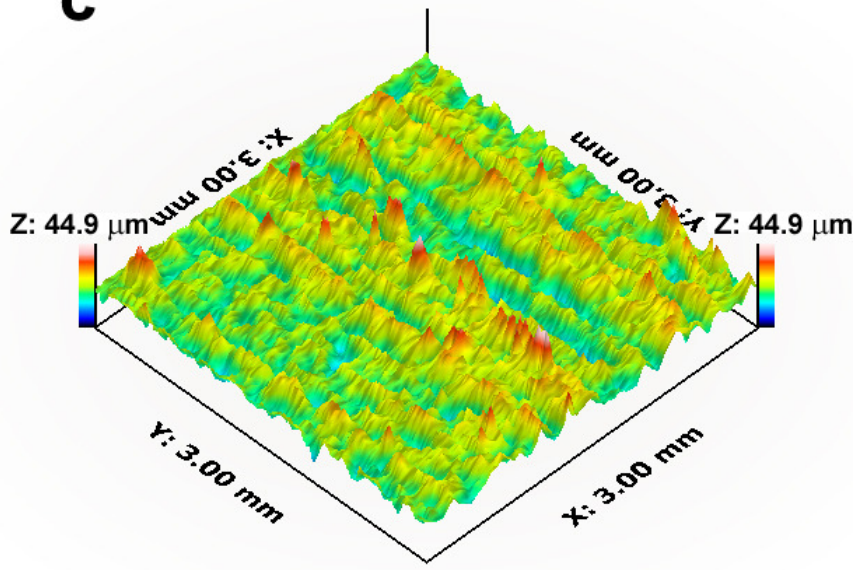

$R_a = 1.52\ \mu m$

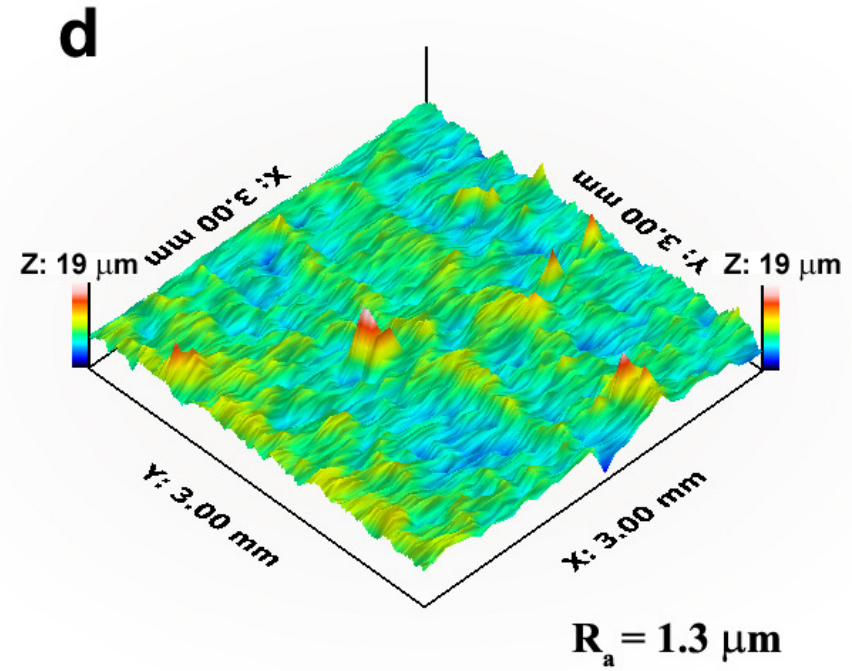

Figure 6.16 3-Dimensional surface profiles and corresponding surface roughness (Ra) of the coatings on AM50B Mg alloys (a) Untreated K10 MAO coating, (b) Phosphate based, (c) Silicate based and (d) Sol-gel post treatment.

6.4. Electrochemical Corrosion Behaviour of MAO Coated Mg Alloys

6.4.1 Potentiodynamic Polarization Behaviour of MAO Coatings

The rapid corrosion rate of magnesium in the electrolytic environment is one of the greatest limitations for its use in many applications. Unprotected magnesium exposed to a typical atmosphere will develop a gray oxide film of magnesium hydroxide $Mg(OH)_2$ which slows corrosion. These films of $Mg(OH)_2$ are slightly soluble in water, however severe corrosion occurs in aqueous environments where chloride ions are present at levels on the order of 150 mmol/L, as $Mg(OH)_2$ reacts with Cl^- to form highly soluble magnesium chloride and hydrogen gas. Pitting of magnesium is observed for Cl^- concentrations exceeding 30 mmol/L (Staiger et al., 2006).

It is observed that magnesium is an electrochemical active substrate, when a bare specimen is initially immersed in 3.5% NaCl solution, hydrogen evolution is seen to occur immediately and the surface is covered with bubbles. The hydrogen bubbles nucleate and periodically release from the surface. Once pitting initiates, a white precipitate, likely $Mg(OH)_2$ is seen to form around the pits and to fall into solution, and the alloy surface becomes porous and gray in colour. It is well known that increasing aluminium content leads to an increased amount of β phase. AZ31B, AM50B and AM60B contains β phase and AZ91D alloys contain more β phases. The fastest corrosion occurred on the AM series alloys with intermediate aluminium content. The impurities (copper, nickel and iron) contents are almost the same in all the alloys, so the difference in corrosion resistance cannot be due to the impurities. The low corrosion resistance of uncoated AZ31B, AM60B and AM50B magnesium alloys can be attributed to the microgalvanic effect between α phase and the β phase. The β phase is an effective cathode which accelerates the corrosion of the adjacent α phase. The maximum galvanic current occurs at a certain ratio of anodic area over cathodic area in the case of galvanic corrosion. It is important to mention that the different surface potential might be affect on the coating difference between the phases.

The β phase acts two roles, as a barrier and as a galvanic cathode (Zhou et al 2008). If the β phase is present in the a matrix as intergranular precipitates with a small volume fraction, then the β phase mainly serves as a galvanic cathode, and accelerates the corrosion of the α matrix. If the β fraction is high (Al content higher than 8% wt), then the β phase may mainly act as an anodic barrier to prevent the overall corrosion of the Mg alloy (Lunder et al., 1989).

The potentiodynamic polarization curves of uncoated, K10 and K25 MAO coated magnesium alloys that used in this study were exhibited in Figure 6.17. The potentiodynamic polarization curves indicated that as the potential increased from the corrosion potential in the noble direction rapid anodic dissolution on the surface of uncoated magnesium metal took place.

In the anodic branch of potentiodynamic polarization curve of uncoated AZ31B, AM60B and AM50B, slightly pseudo-passive behavior was observed due to coverage of the working electrode surface with the corrosion products formed in the stabilization period. Although there is no passivity zone for uncoated AZ91D Mg alloys in the anodic branch of potentiodynamic polarization curve it is exhibited better corrosion resistance than the other bare Mg alloys due to a high level of Al in the solid solution. Even so, the inflection point of uncoated magnesium alloys was maximum 20 mV higher than the corrosion potential which revealed that the uncoated magnesium alloys is over sensitive to localized corrosion.

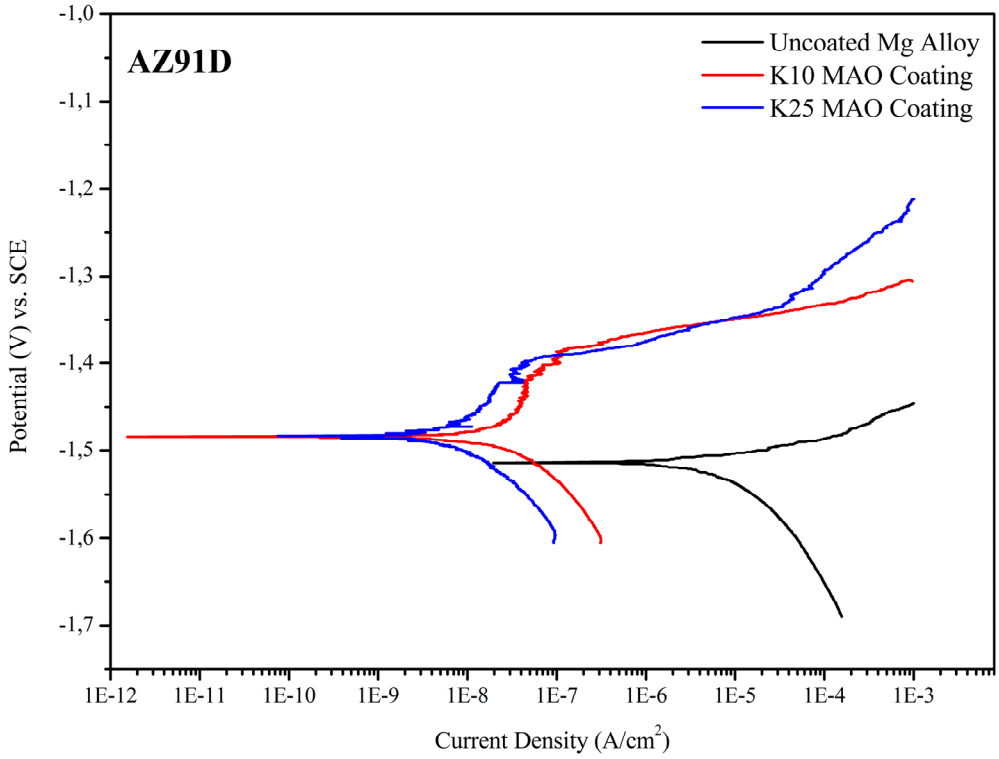

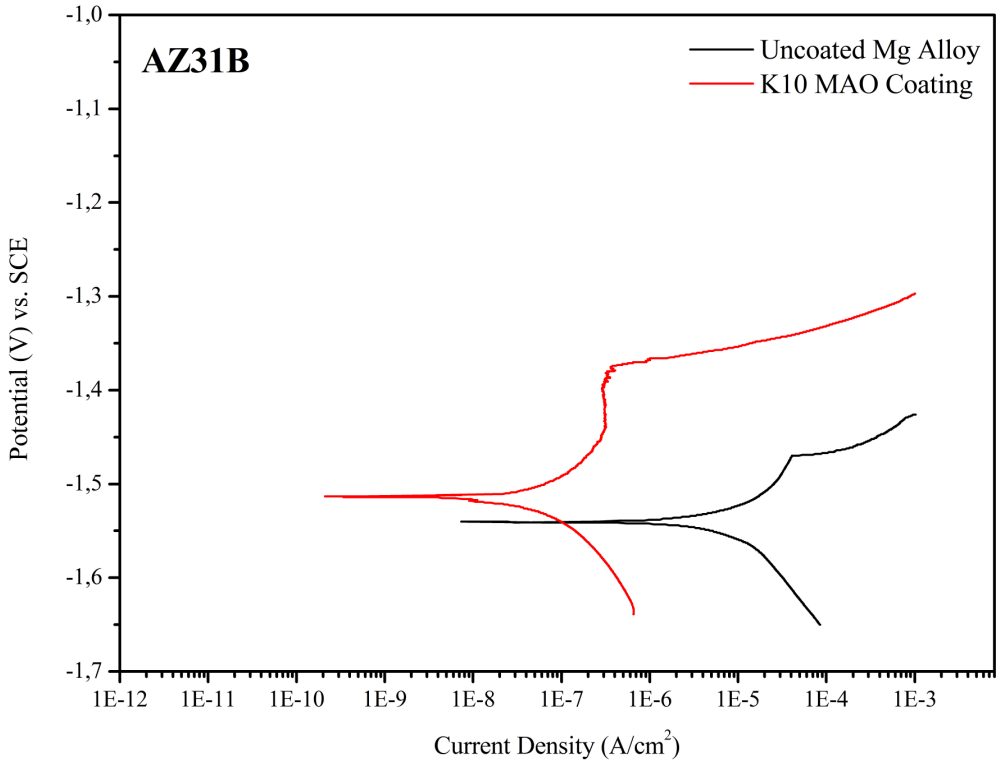
AZ31B
Uncoated Mg Alloy
K10 MAO Coating
Potential (V) vs. SCE
-1,0
-1,1
-1,2
-1,3
-1,4
-1,5
-1,6
-1,7
1E-12
1E-11
1E-10
1E-9
1E-8
1E-7
1E-6
1E-5
1E-4
1E-3
Current Density (A/cm2)

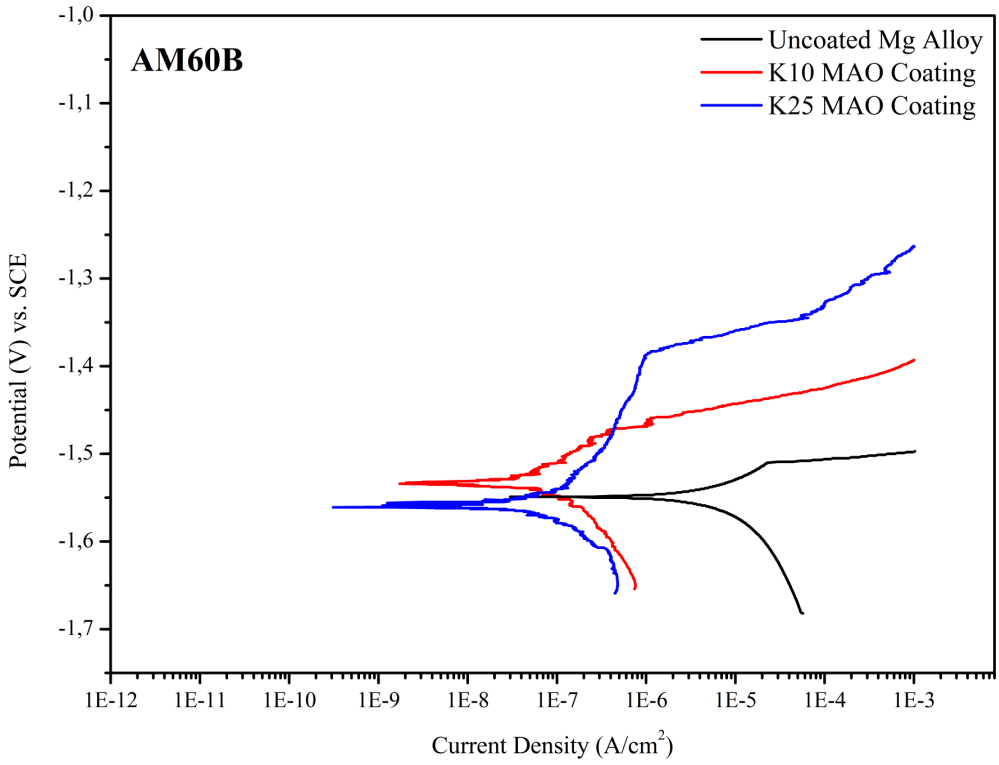
AM60B
Uncoated Mg Alloy
K10 MAO Coating
K25 MAO Coating
Potential (V) vs. SCE
-1,0
-1,1
-1,2
-1,3
-1,4
-1,5
-1,6
-1,7
1E-12
1E-11
1E-10
1E-9
1E-8
1E-7
1E-6
1E-5
1E-4
1E-3
Current Density (A/cm2)

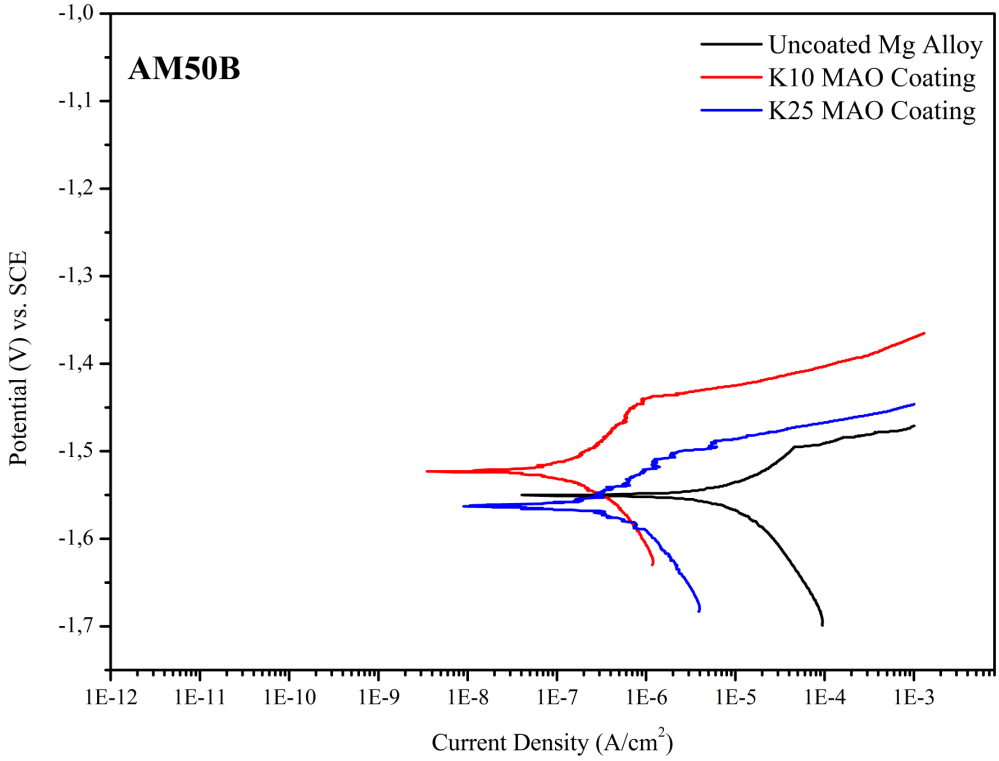

Figure 6.17 Potentiodynamic polarization curves of K10 and K25 MAO coated and uncoated Mg alloys at a scan rate of 0.25mV/s in 3.5wt% NaCl solution at 298 K

In case of MAO coated AZ91D and AZ31B Mg alloys there is a slight passivity region up to -1.40 and -1.37 V and then in this region current density values are nearly constant at 6.10^{-8} and 3. 10^{-7} A/cm^2 respectively. However, this kind of passive region was not seen on MAO coated AM series alloys.

The polarization resistance (R_p) and corrosion rate values of bare and MAO coated Mg alloys were calculated by using the following equations (6.2) and (6.3) respectively

$$R_p = (\beta a.\beta c) / 2.303.I_{corr}(\beta a + \beta c) \quad (6.2)$$

$$\text{Corr Rate} = K.Icorr.EW \quad (6.3)$$

where EW is equivalent weight of alloy (g/equivalent), K is a constant with a value of 0.0895 that defines the unit for the corrosion rate (mg/cm^{-2}/year) (ASTM G-102). The calculated values were listed in Table 6.3.

Table 6.3. Electrochemical parameters of MAO coated and bare Mg alloys

Material		Ecorr (V)	Icorr ($A.cm^{-2}$)	βa (V)	βc (V)	Corrosion rate ($mg.cm^{-2}.y$)	Polarization resistance ($k\Omega.cm^{-2}$)
AZ91D	Uncoated Mg Alloy	-1.512	$5.2x10^{-6}$	0.071	0.144	23.97	3.631
	K10 MAO	-1.491	$17x10^{-9}$	0.299	0.151	0.26	650.512
	K25 MAO	-1493	$6x10^{-9}$	0.162	0.136	0.02	4350.476
AZ31B	Uncoated Mg Alloy	-1.543	$6.9x10^{-6}$	0.103	0.161	34.41	2.714
	K10 MAO	-1.518	$22x10^{-9}$	0.315	0.168	0.33	590.089
AM60B	Uncoated Mg Alloy	-1.551	$7.2x10^{-6}$	0.0965	0.135	35.70	2.634
	K10 MAO	-1.537	$35x10^{-9}$	0.178	0.153	0.43	480.359
	K25 MAO	-1.562	$27x10^{-9}$	0.164	0.141	0.35	548.855
AM50B	Uncoated Mg Alloy	-1.554	$7.1x10^{-6}$	0.0958	0.179	35.40	2.665
	K10 MAO	-1.523	$78x10^{-9}$	0.127	0.192	0.56	329.615
	K25 MAO	-1.572	$104x10^{-9}$	83.8	98.1	0.72	222.316

Generally, the corrosion potentials correspond to the chemical thermodynamic tendency to corrosion of coated samples, which is mainly related to the chemical composition of the oxide coatings. Thermodynamically, spinel ($MgAl_2O_4$) is more stable than MgO in corrosive environment (Liang et al., 2007). The corrosion potential of coated magnesium alloys remained almost the similar value (± 20 mV), which might be indicated that the dense layer formed on the substrate-coating interface is very thin.

i_{corr} is an important parameter to evaluate the corrosion protective properties of the coatings. The lower the i_{corr}, the better corrosion resistance the material performs. The corrosion current density of the samples with MAO coatings are 120 fold lower than that of the magnesium substrate (see Table 6.3), which indicates that the corrosion resistance of magnesium alloy has been greatly improved by MAO treatment. The main difference in current density between the uncoated and MAO coated alloys could be caused by their effectively exposed electrode areas. The effective exposed area of a coated sample was much smaller than that of its bare counter-part as most of the surface of the coated sample was covered by the MAO coating.

When the surface roughness is considered, as mentioned above, the coating structure is one of the most important factors for the corrosion performance. As can be seen in SEM images (Figure 6.3) AZ series coatings are more uniform and compact which benefits for suppressing the transfer of corrosion medium during the corrosion process and their corrosion rates are lower than MAO coated AM series alloys.

The corrosion behaviour of MAO coating can be simply described as following: when the MAO coatings were immersed in 3.5 wt. % NaCl solution, the corrosive solution would penetrate through the outer porous layer by diffusion quickly, and reached the interface of the porous layer and inner compact barrier layer. As time went on, the corrosive solution penetrated into the barrier layer and reacted with the barrier layer and the substrate, and then the intermedium products were produced and adsorbed on the barrier layer. Due to the transportation of salt was more difficult than that of the water molecules in the compact layer, the reaction maybe occurred as the following equation (6.4) or (6.5):

$$MgO + H_2O = Mg(OH)_2 \quad (6.4)$$

$$Mg + 2H_2O = Mg(OH)_2 + H_2 \quad (6.5)$$

After that, the intermedium products ($Mg(OH)_2$) adsorbed at the interface of the barrier layer and the substrate, but they could not transfer or diffuse into the solution in time, because of the special closed structure of the coating the inner barrier layer exhibits better corrosion resistance than the outer porous layer, that is because the barrier layer is more compact and less defects than the porous layer, the corrosion resistance of the whole MAO coatings would be mostly determined by the barrier layer.

Furthermore the corrosion resistance of MAO films are not only depended on the structure and composition of MAO film, but also strongly lie on the electronic properties of the MAO film (Ahn & Kwon, 2004). When the electrode with MAO film was immersed in electrolyte, space charge layer will be formed at the interface between electrolyte and electrode because of transformation of donor or acceptor, which is resulted from different electrochemical potential of electron carrier in electrolyte and in oxide film on electrode. Thus, investigating the semiconducting properties of magnesium electrode with MAO films was expected to be of crucial importance in understanding the corrosion characteristics of magnesium alloy with MAO films (Duan et al., 2007). Because the donors of an n-type semiconducting electrode are mainly oxygen vacancies ($VO^{2+)}$ and some metal interstitials (M_i^{n+}) with superfluous positive charge at the interface of electrode/electrolyte (Lin et al 2005), this make the electrode tended to react with anions in electrolyte during immersion. In solutions containing Cl^-, oxide films may be destroyed by aggressive ions (Cl^-) by the penetration/dissolution mechanism: Cl^- migrates or diffuses in the oxide, penetrates through and finally destabilizes oxide films, then causes active dissolution of the substrate. Li et al (2006) showed that much negative flat band potential and lower donor concentration make the surface lower reactivity with anions (such as Cl^-) in electrolyte. Hence, the samples with higher donor concentration and anion adsorption would show higher reactivity with some anions (such as Cl^-), which then made the electrode weaker corrosion resistance (Duan et al., 2007).

The pore type is crucially affects on the corrosion resistance of MAO coatings. According to Shi et al. (2005), there are two types of pores: the through-holes (unclosed) and non-through-holes (closed). They can be further schematically illustrated in Figure 6.18 (a) and (b).

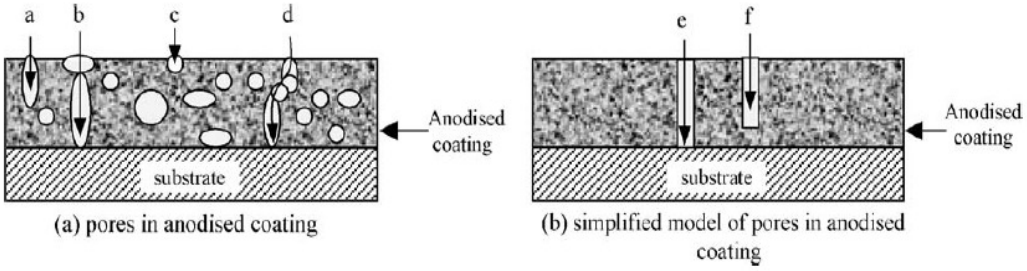

Figure 6.18 Schematic diagrams of (a) the microstructure of an anodised coating on the magnesium alloys and (b) the simplified microstructure of the coating

The non-through-holes could provide corrosion protection because this type of structure can block corrosive media from contacting the substrate. In the deep through-hole structure, the corrosive media could contact with the substrate and lead to corrosion of the substrate alloys. The differences in microstructure among the coatings could be related to the different microstructures of the substrate alloys because the anodising behaviours on α phase and β phase were different. The distribution of the irregular and coarse pores was related to the distribution of the α phase and the β phase.

Regarding the XRD spectrums of MAO coatings, the composition of MAO film are mainly magnesium, aluminium, and oxygen, indicating that the coating is a mixture of MgO and $MgAl_2O_4$. The films on α-Mg are mainly composed of a single MgO phase (Khaselev et al., 2001). In contrast the film on $Mg_{17}Al_{12}$ consists of a mixture of α-Al_2O_3 and $MgAl_2O_4$ because of the higher Al content in β phase (Song et al 2008). Shi et al. (2005) observed that the β phases can effectively restrain the formation of unclosed-holes and greatly decrease the sizes of pores in the coating during the MAO process. As a result, β phase is beneficial to getting rid of the unclosed-holes MAO coating on magnesium substrates. The presence of Zn (1% at wt) in the ternary intermetallics of Mg-Al-Zn system transforms β phase ($Mg_{17}Al_{12}$)

to $Mg_{17}(Al,Zn)_{12}$ (Bowles et al., 2007) which leads to increase the volume fraction of β phase so that increasing volume fraction results in homogenous distribution of β phase particles in the bulk alloy (Czerwinski, 2008). As mentioned above in the initial stages of MAO process, a dielectric barrier film is formed by substrate conversion and it is believed that the properties of growing oxide coating highly depends on the formation mechanism of this barrier layer. The metal dissolution during the initial stage of MAO treatment begins at primary α phase and then continues on β phase due to the cathodic behaviour of β phase (Khaselev et al., 2001). If the β phase distributes on the surface homogenously, the formation rate of barrier film both on these phases becomes nearly similar. Therefore it is said to be that a compact and physically uniform film formation is achieved in Zn containing Mg alloys. In AZ series alloys, the microstructure includes finer α phase particles than AM series alloys. This is the main reason for the better protectiveness of MAO coatings formed on AZ series alloys.

It is found that the K25 MAO coatings on AM series alloys from the longer treatment operations did not provide expected corrosion resistance despite a higher coating thickness. It is foreseen that the thicker coatings give rise to better resistance to localised damage; however, as the defect level in the K25 AM50B coating was quite significant, for a better localised corrosion resistance the coating needs to be not only thicker, but should be free from defects as well. The best anti-corrosion endurance provided by K25 MAO coatings produced on AZ91D magnesium alloy.

6.4.2 Potentiodynamic Polarization Behaviour of Sealed MAO Coatings

Potentiodynamic polarization curves of sealed, unsealed MAO coatings and uncoated AM60B and AM50B Mg alloys at a scan rate of 0.25mV/s in 3.5wt% NaCl solution at ambient temperature were given in Figure 6.19.

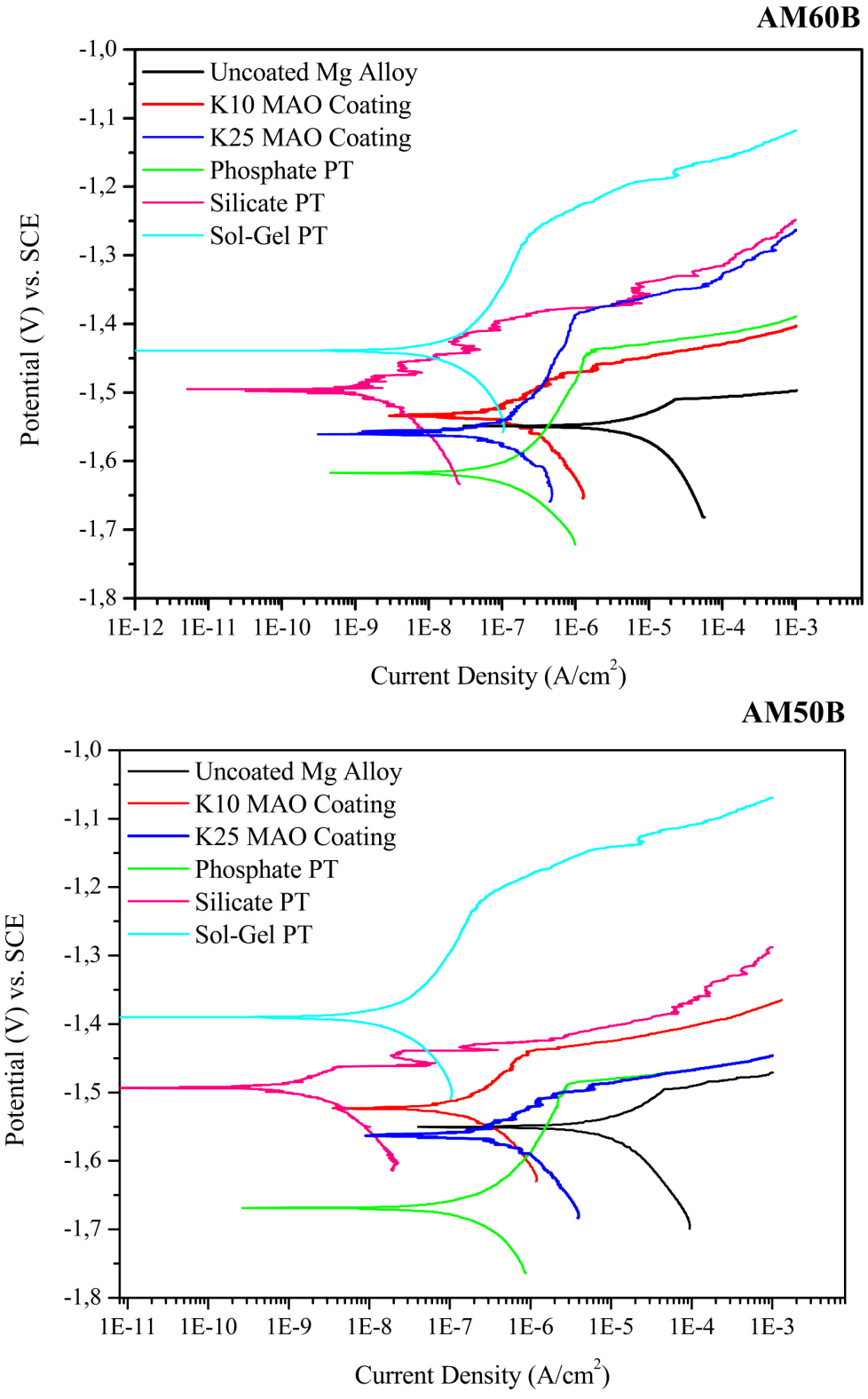

Figure 6.19 Potentiodynamic polarization curves of sealed, unsealed MAO coatings and uncoated AM60B and AM50B Mg alloys

The polarization resistance (Rp) and corrosion rate of unsealed and post-treated K10 MAO coatings on AM60B and AM50B magnesium alloys were calculated by using Stern-Geary equation and were listed in Table 6.4.

Table 6.4 Electrochemical parameters of sealed, unsealed MAO coating and uncoated Mg alloys

Material		E_{corr} (V)	E_{break} (V)	i_{corr} (A/cm^2)	βa (V)	βc (V)	Corrosion rate (mg/cm^{-2}. year)	Polarization resistance ($k\Omega.cm^2$)
AM60B	K10 MAO	-1.517	-1.430	$35x10^{-9}$	0.178	0.153	0.43	480.359
	Phosphate PT	-1.624	-1.490	$31x10^{-9}$	0.278	0.162	0.62	581.951
	Silicate PT	-1.450	-1.405	$1.2x10^{-9}$	0.109	0.080	0.009	7645.315
	Sol-gel PT	-1.392	-1.145	$6.8x10^{-9}$	0.288	0.120	0.097	4275.296
AM50B	K10 MAO	-1.543	-1.450	$78x10^{-9}$	0.127	0.192	0.56	329.615
	Phosphate PT	-1.672	-1.432	$52x10^{-9}$	0.218	0.192	1.24	512.385
	Silicate PT	-1.491	-1.358	$8.9x10^{-10}$	0.073	0.059	0.08	7373.982
	Sol-gel PT	-1.438	-1.196	$9.1x10^{-9}$	0.354	0.237	0.87	3776.100

Results are indicated that further corrosion protection of K10 MAO coated AM60B and AM50B magnesium alloy is achieved by three studied post-treatments in the 3.5% NaCl medium. The current density and corrosion rate of all sealed MAO coatings lower than unsealed MAO coatings. Combined short duration MAO coating (K10) and post-treatment applications are effective way in order to increase anti-corrosion ability of MAO coating in comparison with thicker coatings (K25). Alkaline silicate based post-treated and sol-gel applied specimens showed effective sealing.

Current density and polarization resistance values indicated that the alkaline silicate post treatment provides excellent corrosion protection by physically diminishing or sealing micropores in the MAO coating and acting as a effective barrier. Si compounds may fill the pores; hydrated oxide grows inside and over the pores of the porous layer. Consequently, the access of Cl^- ions to the barrier layer is prevented or slowed down

The phosphate based post-treated and sol-gel applied coatings show a passive behaviour between E_{corr} and E_{break}. However slightly improvement in corrosion resistance is seen between unsealed and phosphate based post-treatment applied MAO coating. The open circuit potential is positively shifted up to 1.390 V with sol-gel layer in a 3.5-wt.% NaCl solution. It is clearly seen that the post treatment applied MAO coatings, have less structural imperfection so it provides a significant corrosion resistance for the magnesium alloy.

On the other hand, silicate based post treatment showed that the best corrosion resistance in spite of similar potentiodynamic behavior with unsealed MAO coatings because of their hydration level of the porous layer might be more completed depended on the longer immersion time and higher process temperature.

Even if, the corrosion potential of phosphate based treatment applied coatings lower than unsealed MAO coating on each Mg alloy the corrosion potential of coated samples depends on the thermodynamic tendency of the surface to corrosion that is mainly related to the chemical composition of the oxide coatings (Liang et al 2005). However, the corrosion resistance of a coated sample was determined by the polarization resistance, which is mainly explained with the microstructure and surface morphology of the coating. As shown in Figure 6.10 and Figure 6.11 the decreasing porosity and increasing uniformity of MAO coatings with post–treatments increased the corrosion resistance. The effect of these factors on corrosion kinetics can be explained by diffusion rate of Cl^- ions moving into the coating. When the surface roughness and porosity level increased, the resultant active regions such as cavities in which Cl^- ion attack enhances greatly increase. Accumulation of Cl^- ions

in the cavities increase the acidity and pitting corrosion can occur at a large area. This results in decreasing corrosion resistance. The lower corrosion rate also represents that the structure of the MAO film is more compact; therefore, the post-treatment process is helpful to get better film properties.

CHAPTER SEVEN
CONCLUSIONS

7.1 General Results

In this study, producing of Micro-Arc Oxidation (MAO) coatings on different magnesium alloys and their corrosion properties were investigated for coated specimens. The following conclusions are obtained from the experimental works:

1- Protective ceramic coatings have been successfully fabricated on four different magnesium alloy substrates by microarc oxidation method using with DC power supply applied with a 50 Hz modulation and both positive and negative potential pulses at a constant applied current density in electrolyte containing phosphate, aluminate and hydroxide.

2- The growth process of MAO coatings formed on magnesium alloy is investigated. The results show that the coatings are mainly composed MgO (Periclase), $MgAl_2O_4$ (spinel) phase $MgAlPO_5$ and $AlPO_4$.phases. As the treatment proceeding, the morphology and phase content of the coatings have different characteristics. As the discharge events become more energetic and more violent, the surface roughness and thickness of the coatings increases with treatment time. Meanwhile, different growth conditions on α-Mg and β-Mg phases result in different pore size in the coating surface.

3- SEM images indicate that the coating is composed of two layers, a porous outer layer and a dense inner layer. A few circular pores are present merely in the porous outer layer, but they do not penetrate the dense inner layer.

4- Potentiodynamic polarization curves have consistently shown that a super corrosion resistance of ceramic MAO coating has been achieved comparing with the

uncoated specimen, which indicates that this technique is a quite effective method to protect magnesium alloy from corrosion.

5- The thickness, roughness and porosity/defect levels of the coatings increase with increase in processing duration. The electrochemical performance of the MAO coatings formed on magnesium alloys is mainly determined by the effective thickness of the coating, not the total thickness. Short-term treatments help in improving the productivity of MAO processing. Relatively thin coatings show more uniform and less defective morphologies, so they perform better corrosion resistance during the potentiodynamic polarization tests. The porous layer of the coating is inconsequential with respect to corrosion, while the corrosion resistance depends on the compact layer of the coating which is in direct contact with the alloy.

6- The corrosion protection of the magnesium alloys achieved by the particular MAO treatment does not correlate with the relative corrosion resistances in the untreated condition, but depends significantly on the composition of the magnesium alloy, and overall, the corrosion resistance of the coating was closely associated with the microstructures and phase compositions of MAO coatings have a significant influence on the corrosion resistance of Mg alloys.

7- MAO coatings on AZ series alloys were smoother and denser than AM series alloys. AZ series alloys exhibited better electrochemical properties as compared to AM series alloys due to their microstructure and chemical composition which are crucially effective on the formation and structural properties of coatings. The low corrosion resistance of the MAO coatings on AM series alloys can be ascribed to the high density of through-holes in the coatings due to less β phase content on the surface layers.

8- MAO coated magnesium alloys should be sealed or covered by protective layers, since coating surfaces are normally porous and cannot protect magnesium alloys from corrosion in aggressive environments for a long period of time.

9- Further corrosion protection of AM50B and AM60B magnesium alloy is achieved by applying alkaline post treatment process and composite MAO-Sol-gel layer, which are not only cover entirely porosity and overlie microdefects present on the outer layer of MAO coatings on the magnesium alloy, but also significantly reduce the surface roughness of the MAO coatings. Combined short duration MAO coating and post-treatment applications are effective way in order to increase anti-corrosion ability of MAO coating in comparison with thicker coatings.

10- Alkaline silicate based post-treated and sol-gel applied specimens showed effective sealing. The alkaline silicate post treatment provides excellent corrosion protection by physically diminishing or sealing micropores in the MAO coating and acting as a effective barrier. Corrosion current density of the post treatment applied coatings are decreased up to 120 fold and the open circuit potential is positively shifted up to 1390 mV with sol-gel layer in a 3.5-wt.% NaCl solution. It is clearly seen that the post treatment applied MAO coatings, have less structural imperfection so it provides a significant corrosion resistance for the magnesium alloy.

7.2 Future Plans

Based on this research, the following suggestions are made for future work:

1. Study the coating formation/growth mechanism and corrosion behaviour of another binary magnesium alloy family such as Mg-Rare earth elements (EV or WE series) Mg-Al-Si (AS series) alloys.

2. Verify the present results with other electrochemical test techniques e.g. weight loss measurement and electrochemical impedance spectroscopy (EIS)

3. Investigate the effect of electrolyte additives such as organic compounds, nanoparticles and tungstate, vanadate, molybdate and borate based

electrolytes on the discharge events and electrochemical behavior of MAO coatings.

4. Verify the present observations on the effects of process parameters on the corrosion resistance of the coatings, e.g. the relationship between discharges, breakdown potential, porosity, thickness, current density and its waveform.

5. Try to seal the MAO coatings with different alternative sealants.

6. Investigate the corrosion behavior of the MAO coatings in different aqueous medium e.g sulphuric acid, nitric acid.

7. Study the variation in the electrolyte concentration, pH and temperature.

8. Reduce the roughness of the thick coatings by adjusting the process parameter.

REFERENCES

Ahn S.J., & Kwon H.S. (2004). Effects of solution temperature on electronic properties of passive film formed on Fe in pH 8.5 borate buffer solution. *Electrochimica Acta, 49*, 3347-3351.

Ambat R., Aung N.N., & Zhou W. (2000). Evaluation of microstructural effects on corrosion behaviour of AZ91D magnesium alloy. *Corrosion Science, 42*, (8), 1433-1455.

Anonymous: (1984). Magnesium the winner in computer housing cost study. *Modern Materials, 40* No. 1.

Anonymous. 1957. The HAE Process. *Light Metal Age, 15*, 10-14.

Arrabal R., Matykina E., Viejo F., Skeldon P., & Thompson G.E. (2008). Corrosion resistance of WE43 and AZ91D magnesium alloys with phosphate PEO coatings. *Corrosion Science, 50,* 1744–1752.

ASTM G-102– 89 (2004). Standard practice for calculation of corrosion rates and related information from electrochemical measurements.

Aung N., & Zhou W. (2002). Effect of heat treatment on corrosion and electrochemical behaviour of AZ91D magnesium alloy. *Journal of Applied Electrochemistry*, *32*, 1397-1401.

Avedesian M., & Baker H. (1999). *Magnesium and Magnesium Alloys,* ASM International, Materials Park, Ohio.

Baboian R., Dean S., Hack H., Haynes G., Scully J., & Sprowis D. (1995). Corrosion Tests and Standarts: Application and Interpretation" *ASTM manuel*, Philadelphia, USA.

Bai A., & Chen Z.J. (2009). Effect of electrolyte additives on anti-corrosion ability of micro-arc oxide coatings formed on magnesium alloy AZ91D. *Surface & Coatings Technology 203*, (14), 1956-1963.

Barker J., Eng K. P., Gabe D. R., Ross D. H., & Dowell A. J. (1994). Characteristics of thin anodic oxide films on aluminium. *Transactions of the Institute of Metal Finishing, 72*, 97- 100.

Barton T.F. (1998). *Anodization of magnesium and magnesium based alloys.* US Patent 5792335, USA.

Becerra A., & Pekguleryuz M. (2009). The grain size of magnesium solid-solution alloys with lithium, indium, and/or zinc. *Materials Research Society, 24*, 1722-1729.

Blawert C., Dietzel W., Ghali E., & Song G. (2006). Anodizing Treatments for Magnesium Alloys and Their Effect on Corrosion Resistance in Various Environments. *Advenced Engineering Materials*, *8*, 511-533.

Bonilla F.A., Berkani A., Liu Y., Skeldon P., Thompson G.E., Habazaki H., et al. (2002). Formation of anodic films on magnesium alloys in an alkaline phosphate electrolyte. *Journal of Electrochemical Society*, *149*, B4-B13.

Bowles A.L, Bakke P., & Westengen H. (2007). A New Look at the Mg-Al-Zn Family. In K.U Kainer,(Ed.). *Magnesium; Proceeding of the 7th International Conference on Magnesium Alloys and Their Applications.* Wiley-VCH Gmbh.

Bunshah, R. (2001). *Handbook of Hard Coatings*. William Andrew Publishing, New York, USA.

Byron B. (1997). Global Overview of Automotive Magnesium Requirements and

Supply & Demand. *International Magnesium Association (IMA) Automotive Seminar* in Aalen.

Cahn R.W.; Haasen P., & Kramer E.J. (1996). Materials Science and Technology – A Comprehensive Treatment. *Structure and Properties of Nonferrous Alloys,* 8.

Cai Q., Wang L., Wei B., & Liu Q. (2006). Electrochemical performance of microarc oxidation films formed on AZ91D magnesium alloy in silicate and phosphate electrolytes. *Surface and Coatings Technology, 200*, (12), 3727–3733.

Carlson B. E., & Jones J. W. (1993). The metallurgical aspects of the corrosion behaviour of cast Mg-Al alloys. *Light Metals Processing and Applications*, 833-847.

Chang S.Y., & Kim Y.L (2008). Effect of Aging Treatment on Microstructural and Mechanical Characteristics of PEO Coatings on Mg-Al Alloy. *Journal of Material Science and Technology*, *24*, (1), 37-41.

Chong K., & Shih T. (2003). Conversion coating treatment for magnesium alloys by a permanganate-phosphate solution. *Material Chemistry and Physics, 80*, 191-200.

Cole G. (2006), Non-Automotive Uses for Magnesium. In H.E. Friedrich & B.L. Mordike (Ed.). *Magnesium Technology,* Springer-Verlag, Berlin, Heidelberg.

Czerwinski, F. (2007). Magnesium and its alloys. In *Magnesium Injection Moulding* (1st ed.);(7-21), N.Y; Springer Publishing.

Davis J. (1991). The Potential for Vehicle Weight Reduction Using Magnesium“, *SAE Technical Paper Series*, No. 910551, USA.

Diggle J. W., Downie T. C., & Goulding C. W. (1968). Anodic Oxide Films on

Aluminium. Rutherford College of Technology, England.

Duan H., Du K.Q., & Yan C.W. (2006). Electrochemical corrosion behavior of composite coatings of sealed MAO film on magnesium alloy AZ91D. *Electrochimica Acta 51*, (14), 2898–2908.

Duan H., Yan C., & Wang F. (2007). Effect of electrolyte additives on performance of plasma electrolytic oxidation films formed on magnesium alloy AZ91D. *Electrochimica Acta 52*, (11), 3785–3793.

Eppensteiner F.W., & Jenkins M.R. (1992). *Metal Finishing Guidebook and Directory, 90*, 413.

Evangelides H.A. (1951). A new finish for magnesium alloys. *Metal Finishing, 55*, 56-60.

Evangelides H.A. (1955). *Method of electrolytically coating magnesium.* US Patent 2,723,952, USA.

Fernando W.A. (1989). Review of corrosion and corrosion control of magnesium alloys. *Journal of Materials Engineering*, *11*, 299-313.

Ghali E. (2000). Corrosion and protection of magnesium alloys. *Materials Science Forum*, *350*: 261-272.

Ghali E., Dietzel W., & Kainer K U. (2004). General and localized corrosion of magnesium alloys: a critical review. *Journal of Materials Engineering and Performance, 13*, 7-23.

Gonzalez-Nunez M., Nunez-Lopez C.A. Skeldon P., Thompson G.E. Karimzadeh H., Lyon P. et al. (1995). A non-chromate conversion coating for magnesium alloys. *Corrosion Science, 37*, 1763-1772.

Gradkovsky R.J., &. Bayles S.N. (1974). US Patent 3,956,080.

Gray J.E., & Luan B. (2002). Protective coatings on magnesium and its alloys – a critical review. *Journal of Alloys and Compounds, 336,* 88-113.

Guerci G., Mus C., & Stewart K. (2000). Surface treatments for large automotive magnesium components. *International Congress Magnesium Alloys and their Applications.*

Gunterschultze, A., & Betz H. (1937). *Electrolytkondensatoren*. Berlin: Krayn.

Guo H., & An M. (2006). Effect of surfactants on surface morphology of ceramic coatings fabricated on magnesium alloys by micro-arc oxidation. *Thin Solid Films, 500*, 186 – 189.

Guo X.W., Ding W.J., Lu C., & Zhai C.Q. (2004). Influence of ultrasonic power on the structure and composition of anodizing coatings formed on Mg alloys. *Surface and Coatings Technology,* 183, 359–368.

Hagans P.L. (1984). Surface Modification of magnesium for corrosion protection. 41st World Magnesium Conference Proceedings, International Magnesium Association, Dayton, Ohio, USA, 30-38.

Hagans P.L., & Haas C.M. (1994). Chromate conversion coatings: In ASM Handbook, Surface Engineering, Vol. 5, (405), ASM International.

Han, Y., Hong S.H., & Xu K.W. (2002). Synthesis of nanocrystalline titania films by micro-arc oxidation. *Materials Letters*, *56*, 744-747.

Hawke D., & Olsen A. (1993). Corrosion properties of new magnesium alloys, Magnesium properties and application for automobiles. *SAE technical paper*, SP-

962, 79-84.

Hillis J.E. (1994). Surface Engineering of Magnesium Alloys. In ASM Handbook, Surface Engineering Volume:5, ASM International.

Hoche H., Scheerer H., Probst D., Brozseit E., & Berger C. (2003). Development of a plasma surface treatment for magnesium alloys to ensure sufficient wear and corrosion resistance. *Surface and Coating Technology*, *174*, 1018-1023.

Hsiao H., & Tsai W. (2005). Characterization of anodic films formed on the AZ91D magnesium alloy. *Surface and Coating Technology, 190*, 299-308.

Hsiao H., Chung P., & Tsai W. (2007). Baking treatment effect on materials characteristics and electrochemical behavior of anodic film formed on AZ91D magnesium alloy. *Corrosion Science 49,* 781–793.

Huo H., Li Y., & Wang F. (2004). Corrosion of AZ91D magnesium alloy with a chemical conversation coating and electroless nickel layer. *Corrosion Science, 46,* 1467-1477.

Hutchins S., Shashkov P., Samsonov V., & Shatrov A. (2004). New generation of Keronite process for corrosion protection of magnesium. In K.U. Kainer (ed.). *Magnesium* (553–558). Procedings of the 6th International Conference Magnesium Alloy and Their Applications.

Hutchins S., Shrestha S., Sturgeon A., Shashkov P., & Shatrov A. (2004). The corrosion performance of sealed Keronite coatings on AZ91D magnesium alloy. . In K.U. Kainer (ed.). *Magnesium* (617–622). Procedings of the 6th International Conference Magnesium Alloy and Their Applications.

Ikonopisov S. (1977). Theory of electrical breakdown during formation of barrier anodic films. *Electrochimica Acta 22,* 1077-1082.

Innes W.P. (1974). Electroplating and Electroless plating on Magnesium and Magnesium alloys. *Modern Electroplating*, 602-610.

Ito T., Sato M., & Kojima Y. (2000). Today's Magnesium Technologies and Applications in Japan", *Transactions,* IMA, 33.

Jin F, Chu P. K., Xu G., Zhao J., Tang D., & Tong H. (2006). Structure and mechanical properties of magnesium alloy treated by micro-arc discharge oxidation using direct current and high-frequency bipolar pulsing modes. *Materials Science and Engineering A 435*, 123–126.

Kainer K. U., & Von Buch F. (2003). Magnesium – Alloys and Technology. In K.U. Kainer (Ed.), Wiley, Weinheim.

Khaselev O., & Yahalom J. (1998). The anodic behavior of binary Mg-Al alloys in KOH-aluminate solutions. *Corrosion Science, 40,* (7), 1149-1160.

Khaselev O., Weiss D. & Yahalom J. (2001). Structure and composition of anodic films formed on binary Mg-Al alloys in KOH – aluminate solutions under continous sparking. *Corrosion Science, 43*, 1295-1307.

Klapkiv M.D. (1995). State of an electrolytic plasma in the process of synthesis of oxides based on aluminum. *Material Science 31*, (4), 494-499.

Kotler G. R., Hawke D. L., & Aqua E. N. (1977). 9th SDEC International Die Casting Exposition and Congress 9, G-T77-022.

Kurze P. (2006). Corrosion and Surface Protections. In H.E. Friedrich and B.L. Mordike (ed.). *Magnesium Technology*. Springer-Verlag Berlin Heidelberg.

Lefebvre F., & Nussbaum G., (1991),"Influence of the microstructure on the corrosion resistance of Mg-Al based alloys", CIM Conference Proceedings, 20-30.

Li J.M., & Jiang B.L. (2007). Towards industrialisation of microarc oxidation (MAO) for ceramic conversion surface treatment of magnesium and aluminium alloys. *International Heat Treatment and Surface Engineering, 1*, 118-123.

Li Y., Zhang T., & Wang F.H. (2006). Effect of microcrystallization on corrosion resistance of AZ91D alloy. *Electrochimica Acta, 51, (14),* 2845.

Liang J., Guo B., Tian J., Liu H., Zhou J., & Xu T. (2005). Effect of potassium fluoride in electrolytic solution on the structure and properties of microarc oxidation coatings on magnesium alloy. *Applied Surface Science, 252*, 345–351.

Liang J., Hu L., & Hao J. (2007). Characterization of microarc oxidation coatings formed on AM60B magnesium alloy in silicate and phosphate electrolytes. *Applied Surface Science, 253*, 4490–4496.

Liang J., Hu L., & Hao J. (2007). Improvement of corrosion properties of microarc oxidation coating on magnesium alloy by optimizing current density parameters. *Applied Surface Science, 253*, 6939–6945.

Lin Y.H., Du R.G., Hu R.G., & Lin C.J. (2005). A Correlation Study of Corrosion Resistance and Semiconductor Properties for the Electrochemically Modified Passive Film of Stainless Steel. *Acta Physico-Chimica Sinica, 21, (7),* 740-745.

Lindstom R., Johansson L., & Svensson J.. (2003). The influence of NaCl and CO_2 on the atmospheric corrosion of magnesium alloy AZ91. *Materials and Corrosion, 54*, 587-594.

Lindstom R., Johansson L., Thompson G., Skeldon P., & Svensson J. (2004). Corrosion of magnesium in humid air. *Corrosion Science, 46,* 1141-1158.

Loughanne T. (2005). The effect of grain refinement on the castability of magnesium permanent mould castings. In N.R. Neelaleggham (ed). *Magnesium Technology* (309–314), TMS, Warrendale, PA.

Lunder O., Lein J.E., Aune T.K., & Nisancioglu K. (1989). The Role of $Mg_{17}Al_{12}$ Phase in the Corrosion of Mg Alloy AZ91. *Corrosion, 45*, 741-748.

Lunder O., Nişancıoğlu K., & Hansen R. (1993). Corrosion of die cast magnesium aluminium alloys. *SAE technical paper*, SP 962, 117-126.

Luo H., Cai Q., Wei B., Yu B., Li D., He J., & Liu Z. (2008). Effect of $(NaPO_3)_6$ concentrations on corrosion resistance of plasma electrolytic oxidation coatings formed on AZ91D magnesium alloy. *Journal of Alloys and Compounds, 464,* (2), 537-543.

Luo, A.; Renaud, J.; Nakatsugawa, I., & Plourde, J. (1995). Magnesium Castings for Automotive Applications. *Journal Of Materials, 47,* (7), 28-31.

Lv G.H., Chen H., Gu W.C., Li L, Niu E.W., Zhang X.H., & Yang S.Z. (2008). Effects of current frequency on the structural characteristics and corrosion property of ceramic coatings formed on magnesium alloy by PEO technology. *Journal of Materials Processing Technology, 208,* (1), 9-13.

Ma Y. (2005). An investigation of Electrolytic Plasma Oxidation Process for Corrosion Protection of Pure Mg and Mg Alloy AM50", The thesis of Master Degree in University of Windsor, Canada.

Makar G.L., & Kruger J. (1990). Corrosion studies of rapidly solidified magnesium alloys. *Journal of Electrochemical Society*, *137*, 414-421.

Makar G.L., & Kruger J. (1993). Corrosion of magnesium. *Journal of International Material Review, 38*, 138-153.

Markov G.A. & Markova G.V. (1976). USSR Patent 526,961.

Markov G.A., Slonova A.I., & Terleeva O.P. (1997). Chemical composition, structure and morphology of microplasma coatings. *Protection of Metals, 33,* (3) 257-262.

Masao O. (1986).Plating method for magnesium alloy. Japan Patent 61,276,982.

Mathieu S., Rapin C., Hazan J., & Steinmetz P. (2002). Corrosion behavior of high pressure die-cast and semi-solid cast AZ91D alloys. *Corrosion Science*, *44,* 2737-2756.

Mazia J., (1990), *Metal Finishing,* 88, 466.

McNeill, W., & Gruss L.L. (1966). Anodic spark reaction processes and articles. US Patent 3,293,158.

McNeill, W., & Nordbloom G.F. (1958). Method of making cadmium niobate. US Patent 2,854,390.

Mittal C.K. (1995). Transactions of the Metal Finishers Association. *Metal Finishing, 91,* (4), 227.

Mordike B.L., & Ebert T. (2001). Magnesium Properties — applications — potential. *Material Science and Engineering A 302*, 37-45.

Mori K., Hirahara H., Oishi Y., & Kumagai N. (2000). Polymer Plating of 2-Dioctylamino-1,3,5-triazine-4,6-dithiol to Magnesium Alloys. *Electrochemical Solid State Letters*, *3*, 546.

Murphy J. F. (1967). Practical implications of research on anodic coatings on aluminum. *Plating*, *54*, 1241-1245.

Nayeb-Hashemi, A.A., & Clark J. B. (1988). *Phase diagrams of binary magnesium alloys.* ASM International, Metals Park, Ohio.

Patermaeakis G., & Kerassovito P. (1992). Study on the mechanism of oxide hydration and oxide pore closure during hydrothermal treatment of porous anodic Al_2O_3 films. *Electrochimica Acta*, *37*, 125-131.

Phani A., Gammel F., Hack T., & Haefke H. (2005). Enhanced corrosion resistance by sol-gel based ZrO_2-CeO_2 coating on magnesium alloys. *Materials and Corrosion*, *56,* 77-82.

Pilling N.B., & Bedworth R. E. (1923). The Oxidation of Metals at High Temperatures. *Journal of Institute Metals, 29*, 529-591

Polmear, I. J. (1995). *Light Metals Metallurgy of the Light Metals.* Wiley, New York

Potzies C., & Kainer U K**.** **(**2004). Fatigue of magnesium alloys. *Advanced Engineering Materials*, *6,* (5), 281-289.

Rakoch A. G., Khokhlov V. V., Bautin V. A., Lebedeva N. A., Magurova V., & Bardin I. V. (2006). Model Concepts on the Mechanism of Microarc Oxidation of Metal Materials and the Control over This Process. *Protection of Metals, 42,* 158–169.

Reichek K.N., Clark K.J., & Hillis J.E. (1985). Controlling the salt water corrosion performance of magnesium AZ91 alloy. *SAE technical paper*, 850417, 1-12.

Rudd A., Breslin C., & Mansfeld F. (2000). The corrosion protection afforded by rare-earth conversion coatings applied to magnesium. *Corrosion Science*, *42,* 275 288.

Rudnev V. S, Boguta D. L., Nedozorov P. M., & Kaidalova T. A. (2006). Anodic layers formed in polyphosphate electrolytes on rectifying metals. *Russian Journal of Applied Chemistry, 79*, 257–263.

Schumann S. & Friedrich H. (2006). Engineering Requirements, Strategies and Examples. In H.E. Friedrich and B.L. Mordike (Ed.). *Magnesium Technology* Springer-Verlag Berlin Heidelberg.

Sharma A.K. (1988). Electrodeposition of Gold on Magnesium-Lithium Alloys. *Metal Finishing 86,* (12), 33-34.

Sharma A.K. (1989). Chromate conversions coatings for magnesium—lithium alloys. *Metal Finishing, 87,* (2), 73-81.

Sharma A.K., Suresh M., Narayanmurthy H., & Sahu P. (1998). Electroless Nickel plating on magnesium alloy. *Metal Finishing*, *96*, 10-18.

Shatrov A. S., & Samsonov V. I. (2002). US Patent 6.896.785.

Shi Z., Song G., & Atrens A. (2005). Influence of the β phase on the corrosion performance of anodised coatings on magnesium–aluminium alloys. *Corrosion Science, 47,* (11), 2760-2777.

Shrestha, S., Merstllinger A., Sickert D., & Dunn B.D. (2003). Some Preliminary Evaluations of Black Coating on Aluminium AA2219 Alloy Produced by Plasma Electrolytic Oxidation (PEO) Process for Space Applications. In 9th International Symposium on Materials in a Space Environment, Noordwijk, The Netherlands.

Skar J I. (1999). Corrosion and corrosion prevention of magnesium alloys. *Materials and Corrosion*, *50*, 2-6.

Sluginov, N.P. (1880). *Journal of Russian Physical and Chemical Society*, *12,* 193.

Song G., & Atrens A. (1999). Corrosion mechanism of magnesium alloys. *Advanced Engineering Materials*, *1,* 11-33.

Song G., & Atrens A. (2003). Understanding Magnesium Corrosion - A Framework for Improved Alloy Performance. *Advanced Engineering Materials 5,* (12), 837-858.

Song G., Atrens A., & Dargush M. (1999). Influence of microstructure on the corrosion of die cast AZ91D. *Corrosion Science*, *41*, 249-273.

Song G., & StJohn D. (2002). The effect of zirconium grain refinement on the corrosion behavior of magnesium–rare earth alloy MEZ. *Journal of Light Metals 2,* 1-16.

Song G., Atrens A., Wu X., & Zhang B. (1998). Corrosion behavior of AZ21, AZ501 and AZ91 in NaCl. *Corrosion Science*, *40,* 1769-1791.

Song G., Atrens A., StJohn D., Nairn J., & Li Y. (2004). The electrochemical corrosion of pure magnesium in 1N NaCl. *Corrosion Science, 39,* 855-875.

Song G., Atrens A., StJohn D., Wu X., & Nairn J. (1997). The anodic dissolution of magnesium in chloride and sulphate solutions. *Corrosion Science, 39,*1981-2004.

Song Y.L.', Liu Y.H., Yu S.R., Zhu X.Y., & Wang Q. (2008). Plasma electrolytic oxidation coating on AZ91 magnesium alloy modified by neodymium and its corrosion resistance. *Applied Surface Science, 254,* (10), 3014-3020

Staiger M.P., Pietak A.M., Huadmai J., & Dias G. (2006). Magnesium and its alloys as orthopedic biomaterials: A review. *Biomaterials, 27,* 1728-1734.

Staroselsky A., & Anand L. (2003). A constitutive model for hcp materials deforming by slip and twinning: Application to magnesium alloy AZ31B. *International Journal of Plasticity, 19,* (10), 1843–1864.

Stephens R.I, Schrader C.D., & Lease K.B. (1995).Corrosion fatigue of AZ91E-T6 cast magnesium alloy in a 3.5 percent NaCl aqueous environment. *Journal of Engineering Material and Technology, 117*, (7), 293-298.

Sundararajan, G. and L.R. Krishna, (2003),"Mechanisms Underlying the Formation of Thick Alumina Coatings through the MAO Coating Technology". *Surface and Coating Technology*, 167, 269-277.

Tamar Y. and Mandler D., (2008),"Corrosion inhibition of magnesium by combined zirconia silica sol–gel films", *Electrochimica Acta* 53, (16), 5118–5127.

Tchevryakov V., Gao G., Bomback J., Pchelnikov A.P., & Cole G. (2000). Magnesium Technology 2000. *The Minerals, Metals and Materials Society*, 143.

Tomashow, N.D. (1966). *Theory of corrosion and protection of metals*. Macmillian Publishing Company, New York.

Umehara H., Takaya M., & Tsukuba T.I. (1999). Corrosion resistance of the die casting AZ91D magnesium alloys with paint finishing. *Aluminium,* 75, (7), 634 – 641.

Unger, R.H. (1987). Thermal spray coatings In *ASM Handbook Corrosion Volume 13*. (459). ASM International,USA.

Xue W., Deng Z., Lai Y., & Chen R. (1998). Analysis of Phase Distribution for Ceramic Coatings Formed by Microarc Oxidation on Aluminum Alloy. *Journal of American Ceramic Society, 81*, 1365-1368.

Yamauchi N., Demizu K., Ueda N., Cuong T., Sone T., & Hirose Y. (2005). Friction and wear of DLC films on Magnesium Alloy. *Surface and Coating Technology*, *175*, 107-111.

Yerokhin A. (2007). Preface. *Surface and Coatings Technology, 201*, 8659–8660.

Yerokhin A.L, Nie X, Leyland A., Matthews A., & Dowey S.J. (1999). Plasma electrolysis for surface engineering. *Surface & Coating Technology, 122*, 73-93.

Yerokhin, A.L., Nie X., Leyland A., & Matthews A. (2000).Characterisation of Oxide Films produced by Plasma Electrolytic Oxidation of a Ti-6Al-4V alloy". *Surface and Coating Technology*, *130,* 195-206.

Yerokhin A.L., Shatrov A., Samsonov V., Shashkov P., Leyland A., & Matthews A. (2004). Fatigue properties of Keronite coatings on a magnesium alloy. *Surface and Coatings Technology, 182*, 78–84.

Yerokhin, A.L., Snizhko L.O., Gurevina N.L., Leyland A., Pilkington A., & Matthews A. (2003). Discharge characterisation in plasma electrolytic oxidation of aluminium. *Journal of Physics*, *36,* 2110-2120.

Yin D., Zhang E., & Zeng S. (2008). Effect of Zn on mechanical property and corrosion property of extruded Mg-Zn-Mn alloy. *Transactions Nonferrous Metals Society, 18,* 763-768.

Yue T.M, Ha H.U., & Musson N.J. (1995). Grain size effects on the mechanical properties of some squeeze cast light alloys. *Journal of Material Science, 3,* 2277-2283.

Van, T.B., Brown S.D., & Wirtz G.P. (1977). Mechanism of Anodic Spark Deposition. *American Ceramic Society Bulletin*, *56,* 563-566.

Weiss D., & Robison S.T. (2005). Magnesium driving to permanent mold. *Modern Casting, 95,* (9), 26–29.

Westengen H., Bakke P., & Albright, D. (2005). Advances in Magnesium Alloy Development. *Die Casting Engineer, 49,* (6), 26–32.

Winzer N., Atrens A., Song G., Ghali E., Dietzel W., Kainer K.U., Hort N., & Blawert C. (2005). A critical review of the stress corrosion cracking (SCC) of magnesium alloys. *Advanced Engineering Materials*, *7* (8), 659-693.

Zeng R., Zhou W., Han E., & Ke W. (2005). Effect of pH value on corrosion of as-extruded AM60 magnesium alloy. *Acta Metallurgica*, *44* (3), 307-311.

Zhang Y., Yan C., Wang F., Luo H., & Cao C. (2002). Study on the environmentally friendly anodizing of AZ91D magnesium alloy. *Surface and coating Technology, 161*, 36-43.

Zhao M., Liu M., Song G., & Atrens A. (2008). Influence of the β-phase morphology on the corrosion of the Mg alloy AZ91. *Corrosion Science, 50,* (7), 1939-1953.